UNIVERSITÀ DEGLI STUDI DI MILANO
Facoltà di Medicina e Chirurgia
Dipartimento di Biologia e Genetica per le Scienze Mediche

DOTTORATO DI RICERCA IN
BIOTECNOLOGIE APPLICATE ALLE SCIENZE MEDICHE - CICLO XXIV
Scuola di Dottorato in Scienze Biomediche Cliniche e Sperimentali

TESI DI DOTTORATO DI RICERCA

PRECLINICAL RATIONALE FOR THE USE OF THE AKT INHIBITOR PERIFOSINE IN COMBINATION WITH THE MULTIKINASE INHIBITOR SORAFENIB IN HODGKIN LYMPHOMA

Settore BIO/13 – Biologia Applicata

DOTTORANDO
Dott.ssa Silvia Laura Locatelli
Matr. R08060

RELATORE
Prof. Carmelo Carlo-Stella

CORRELATORE
Dott. Andrea Anichini

Anno Accademico 2010/2011

To my family,

TABLE OF CONTENTS

AP-1	Activator protein 1
APRIL	A proliferation-inducing ligand
ATM	Ataxia telangiectasia mutated
ATR	Aataxia telangiectasia related
BAD	BCL2-associated agonist of cell death
BAFF	B-cell activating factor
BCMA	B-cell maturation antigen
BH	BCR homology domain
BLC	B lymphocyte chemoattractant
c-MET	Mesenchymal epithelial transition factor
C2	Protein kinase C homology domain 2
cHL	Classical Hodgkin lymphoma
DDR	Discoidin domain receptor tyrosine kinase
DNA-PKcs	DNA-dependent protein kinase
DNMT	DNA methytransferases
DSB	Double strand break
EBV	Epstein-Barr virus
EGF	Epidermal growth factor
ERK	Extracellular Related Kinase
FASL	Fas ligand
FBS	Fetal bovine serum
FGF	Fibroblast growth factor
Gal-1	Galectin-1
GC	Germinal centre
GM-CSF	Granulocyte macrophage colony-stimulating factor
GRB2	Growth factor receptor–bound protein 2
GSK3α	Glycogen synthase kinase-3α
HDAC	Histone deacetylase
HER	Membrane-bound human epidermal growth factor receptors
HGF	Hepatocyte growth factor
HIF-1α	Hypoxia inducible factor-1α
HL	Hodgkin lymphoma
HRS	Hodgkin Reed-Sternberg
IFN-γ	Interferon gamma
Ig	Immunoglobulin
IGF	Insulin growth factors
IGF-1R	Insulin-like growth factor 1 receptor
IKK	Inhibitor of k kinase
IL	Interleukin
IP	intraperitoneal
iSH2	Inter-SH2
IV	intravenously
LDHL	Lymphocyte-depleted Hodgkin lymphoma
LRCHL	Lymphocyte-rich classical Hodgkin lymphoma
LT-α	Lymphotoxin α
MAP3K	Mitogenactivated protein 3 kinase
MAPK	Mitogen-activated protein kinase

MAPKK	MAPK kinase
MAPKKK	MAPK kinase kinase
MCHL	Mixed cellularity Hodgkin lymphoma
MDC	Macrophage-derived chemokine
MDM	Mouse double minute
MEC	Mucosae-associated epithelial chemokine
MEK	MAPK/Extracellular signal-regulated kinase
mTOR	Mammalian target of rapamycin
NFkB	Nuclear factor kappa B
NGF	Nerve growth factor
NK	Natural killer
NLPHL	Nodular lymphocyte-predominant Hodgkin lymphoma
NOD/SCID	non-obese diabetic/severe combined immunodeficient
NSHL	Nodular sclerosis Hodgkin lymphoma
P	Proline-rich region
p70S6K	Ribosomal protein S6 kinase
PCR	Polymerase chain reaction
PDK	3-phosphoinositide–dependant protein kinase
PDK1	Phosphoinositide-dependent kinase 1
PDL	Programmed cell death 1 ligand
PH	Pleckstrin-homology
PI	Propidium Iodide
PI3K	Phosphoinositide 3-kinase
PKB	Pprotein kinase B
PO	per os
PX	Phox
RANKL	Receptor activator of NFkB ligand
RAPTOR	Regulatory-associated protein of TOR
RCC	Renal cell carcinoma
REAL	Revised European-American Classification of Lymphoid Neoplasms
RICTOR	Rapamycin-insensitive companion of TOR
RIP	Receptor-interacting protein
RS	Reed-Sternberg
RTKs	Receptor tyrosine kinases
SC	subcutaneous
SCID	Severe combined immunodeficiency
SCT	Stem Cell Transplantation
SHM	Ssomatic hypermutation
SHP2	Src homology 2 domain–containing tyrosine phosphatase
SOS	Son of sevenless homolog 1 (Drosophila)
TACI	Transmembrane activator and CAML interactor
TARC	Thymus and activation-regulated chemokine
TCR	T-cell receptor
TGF-β	Transforming growth factor β
TH	T helper cell
TNF-α	Tumor necrosis factor α

TNFR	Tumor necrosis factor receptor
TRAF	TNF receptor–associated factor 1
Treg	T regulatory cell
TRKA	Tyrosine kinase receptor A
TRRAP	Tansformation/transcription domain-associated protein
TSC2	Tuberous sclerosis complex-2
TYK2	Tyrosine kinase 2
VEGF	Vascular endothelial growth factor
Vps34p	Vacuolar protein sorting mutant 34 protein
WHO	World Health Organisation
4E-BP1	Elongation-initiation factor 4E-binding protein

ABSTRACT

INTRODUCTION: A significant proportion of Hodgkin lymphoma (HL) patients refractory to first-line chemotherapy or relapsing after autologous transplantation are not cured with currently available treatments and require new treatments. The PI3K/AKT and RAF/MEK/ERK pathways are constitutively activated in the majority of HL. These pathways can be targeted using the AKT inhibitor perifosine (Æterna Zentaris GmBH, Germany, EU), and the RAF/MEK/ERK inhibitor sorafenib (Nexavar®, Bayer, Germany, EU). We hypothesized that perifosine in combination with sorafenib might have a therapeutic activity in HL by overcoming the cytoprotective and anti-apoptotic effects of PI3K/Akt and RAF/MEK/ERK pathways. Since preclinical evidence supporting the anti-lymphoma effects of the perifosine/sorafenib combination are still lacking, the present study aimed at investigating in vitro and in vivo the activity and mechanism(s) of action of this two-drug combination.

METHODS: Three HL cell lines (HD-MyZ, L-540 and HDLM-2) were used to investigate the effects of perifosine and sorafenib using in vitro assays analyzing cell growth, cell cycle distribution, gene expression profiling (GEP), and apoptosis. Western blotting (WB) experiments were performed to determine whether the two-drug combination affected MAPK and PI3K/AKT pathways as well as apoptosis. Additionally, the antitumor efficacy and mechanism of action of perifosine/sorafenib combination were investigated in vivo in nonobese diabetic/severe combined immune-deficient (NOD/SCID) mice using tumor growth rates and survival as endpoints.

RESULTS: While perifosine and sorafenib as single agents exerted a limited activity against HL cells, exposure of HD-MyZ and L-540 cell lines, but not HDLM-2 cells, to perifosine/sorafenib combination resulted in synergistic cell growth inhibition (40% to 80%) and cell cycle arrest. Upon perifosine/sorafenib exposure, L-540 cell line showed significant levels of apoptosis (up to 70%, $P \leq .0001$) associated with severe mitochondrial dysfunction (cytochrome c, apoptosis-inducing factor release and marked conformational change of Bax accompanied by membrane translocation). Apoptosis induced by perifosine/sorafenib combination did not result in processing of caspase-8, -9, -3, or cleavage of PARP, and was not reversed by the pan-caspase inhibitor Z-VADfmk, supporting a caspase-independent mechanism of apoptosis. In responsive cell lines, WB analysis showed that anti-proliferative events were associated with dephosphorylation of MAPK and PI3K/Akt pathways. GEP analysis of HD-MyZ and L-540 cell lines, but not HDLM-2 cells indicated that perifosine/sorafenib treatment induced upregulation of genes involved in amino acid metabolism and downregulation of genes regulating cell cycle, DNA replication and cell death. In addition, in responsive cell lines, perifosine/sorafenib combination strikingly induced the expression of tribbles homologues 3 (TRIB3) both in vitro and in vivo. Silencing of TRIB3 prevented cell growth reduction induced by perifosine/sorafenib treatment. In vivo, the combined perifosine/sorafenib treatment significantly increased the median survival of NOD/SCID mice xenografted with HD-MyZ cell line as compared to controls (81 vs 45 days, $P \leq .0001$) as well as mice receiving perifosine alone (49 days, $P \leq .03$) or sorafenib alone (54 days, $P \leq .007$). In addition, perifosine/sorafenib treatment had no

effect on HDLM-2 nodules, but significantly reduced L-540 nodules with 50% tumor growth inhibition ($P \leq .0001$), compared to controls. In mice bearing subcutaneous nodules generated by HD-MyZ and L-540 cell lines but not HDLM-2 cell line, perifosine/sorafenib treatment induced significantly increased levels of apoptosis (2- to 2.5-fold, $P \leq .0001$) and necrosis (2- to 8-fold, $P \leq .0001$), as compared to controls or treatment with single agents.

CONCLUSIONS: Perifosine/sorafenib combination resulted in potent anti-HL activity both in vitro and in vivo. These results warrant clinical evaluation in HL patients.

1. INTRODUCTION

1.1 HODGKIN LYMPHOMA

Hodgkin lymphoma (HL), more commonly known as Hodgkin disease, is an uncommon neoplasm arising from B lymphocytes with an estimated 8490 new cases in the United States in 2010.[1] It was first described by Thomas Hodgkin in 1831. HL accounts for approximately 15% of all lymphomas and is common in young adults. The overall incidence rate has been steady since the 1970s. The outcome of patients with all stages of HL has improved dramatically during the past few decades mainly because of the use of intensive combination chemotherapy agents and involved-field radiation therapy. HL is one the most treatable and curable lymphomas. The challenges for the primary care providers are to monitor the long-term side effects of the intensive treatments and to improve patient's quality of life. The majority of HL patients present with lymphoadenopathy, typically in the supraclavicular or lower cervical region. In the absence of treatment, the disease follows a predictable course spreading from one group of lymph nodes to those adjacent in a systematic process. Mediastinal masses are frequent and patients often present with chest discomfort and coughing or breathlessness. Approximately a quarter of HL cases manifest systemic B symptoms including fatigue, weight loss, intermittent fevers and itchy skin associated with night sweats. Diagnosis is usually made by histological examination of an excisional biopsy of an enlargened lymph node.

The disease is then staged using the Ann Arbor staging system (Table 1.1) developed in 1971[2] and modified in 1989.[3] This system defines the extent of disease progression and helps predict prognosis and direct treatment. Four stages are described followed by the letter A or B, indicating the absence (A) or presence (B) of B symptoms.

Table 1.1 The Ann Arbor staging system for HL.

STAGE	SYMPTOMS
1	Involvement of one lymph nodes or lymphoid structure
2	Involvement of two or more lymph nodes on the same side of the diaphragm
3	Involvement of lymph nodes on both sides of the diaphragm
4	Involvement of extranodal site(s), with or without associated lymph node involvement

Treatment is by chemotherapy, radiotherapy or a combination of both. High-dose myeloablative chemotherapy followed by autologous stem cell transplantation (SCT) has an established role in the management of patients with relapsed HL. Autologous SCT has significantly increased the survival of patients with relapsed HL.[4,5] However, a significant proportion of relapsed HL (50 – 60%) patients are not cured with currently available therapeutic strategies, thus the development of new drugs will address a significant unmet medical need.[6,7]

Diagnosis rests on the identification of typical large multinucleated cells, the Reed-Sternberg (RS) cells, surrounded by a heterogeneous cellular infiltrate composed of lymphocytes, histiocytes, eosinophils, plasma cells and polymorphonuclear leukocytes. RS cells measure 20 – 60 μm in diameter and have at least two nuclei with prominent acidophilic or amphophilic nucleoli (Figure

1.1).[8] Hodgkin (H) mononuclear cells display similar cytological features to RS cells, and these cells are collectively referred to as HRS cells.[8] Cells with morphology similar to RS cells have been identified in both infectious mononucleosis and non-Hodgkin's Lymphoma, but the presence of the specific heterogeneous cellular background is unique to HL. Unusually for human lymphomas, the neoplastic cells make up a very low proportion (<1%) of the tumour cell population and this, in the past, has restricted a detailed investigation of these cells.[9,10]

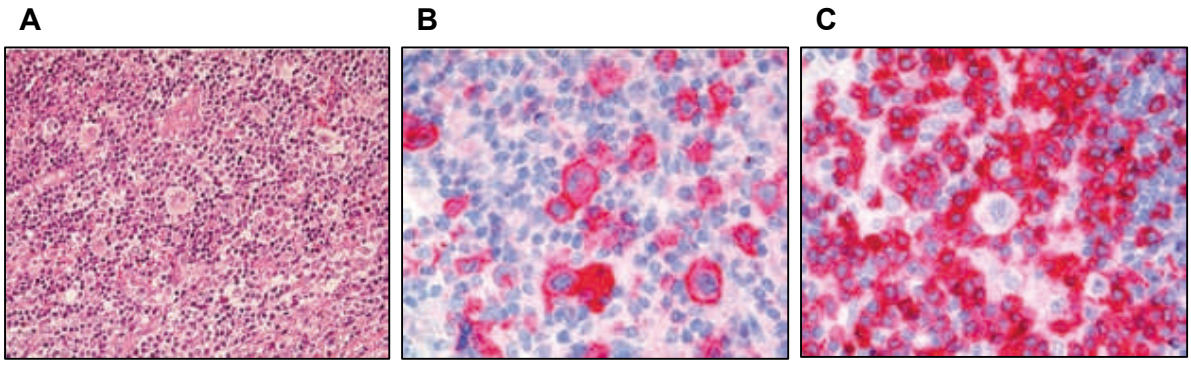

Figure 1.1: Hodgkin and Reed–Sternberg (HRS) cells in their microenvironment. This figure illustrates the typical histological and immunohistochemical picture seen in classical Hodgkin's lymphoma. (**A**) Haematoxylin and eosin staining of a case of nodular sclerosis Hodgkin's lymphoma. Several large HRS cells are visible, one of them in the centre of the picture. (**B**) CD30 immunostaining (red) highlighting several large $CD30^+$ HRS cells. (**C**) CD3 staining showing the dominant T-cell infiltrate and a ring of T cells around an HRS cell in the centre.

1.2 CROSSTALK BETWEEN CELLS: THE IMPORTANCE OF CYTOKINES AND CHEMOKINES IN HL

Cytokines and chemokines are low–molecular weight proteins with a wide variety of functions that work either in a paracrine manner to modulate the activity of surrounding cells or in an autocrine fashion to directly affect the cells that produce them. Specifically, these autocrine and paracrine interactions lead to the particular cellular composition found in HL and contribute to the proliferation and antiapoptotic phenotype of HRS cells (Figure 1.2). Although the cytokine and chemokine milieu in HL tissues is complex and interactive, a clear understanding of this biology will be clinically relevant in the future as therapies are developed that disrupt the crosstalk between malignant cells and the microenvironment. Hence, improved insight into the biology will be critical to introducing these novel biologic treatments into clinical practice. This section focuses on the involvement of cytokines in the formation of the microenvironment and highlights how, in return, HRS cells receive signals from the microenvironment through surface receptors. The clinical and pathologic features of HL reflect an abnormal immune response that is thought to be the result of expression of a variety of cytokines and chemokines by the HRS cells, altering the composition and function of the cells in the surrounding microenvironment and shaping the specific histopathologic appearance of the lymph node.[11] Moreover, the reactive cells in the microenvironment produce specific cytokines and chemokines that help maintain and even amplify the intense inflammatory

reaction.[12] In addition to the variability of cytokine expression in the different HL subtypes, Epstein-Barr virus (EBV) positivity also influences the relative expression of certain cytokines (eg, CXCL10, CXCL9, CCL5, and CCL3).[13]

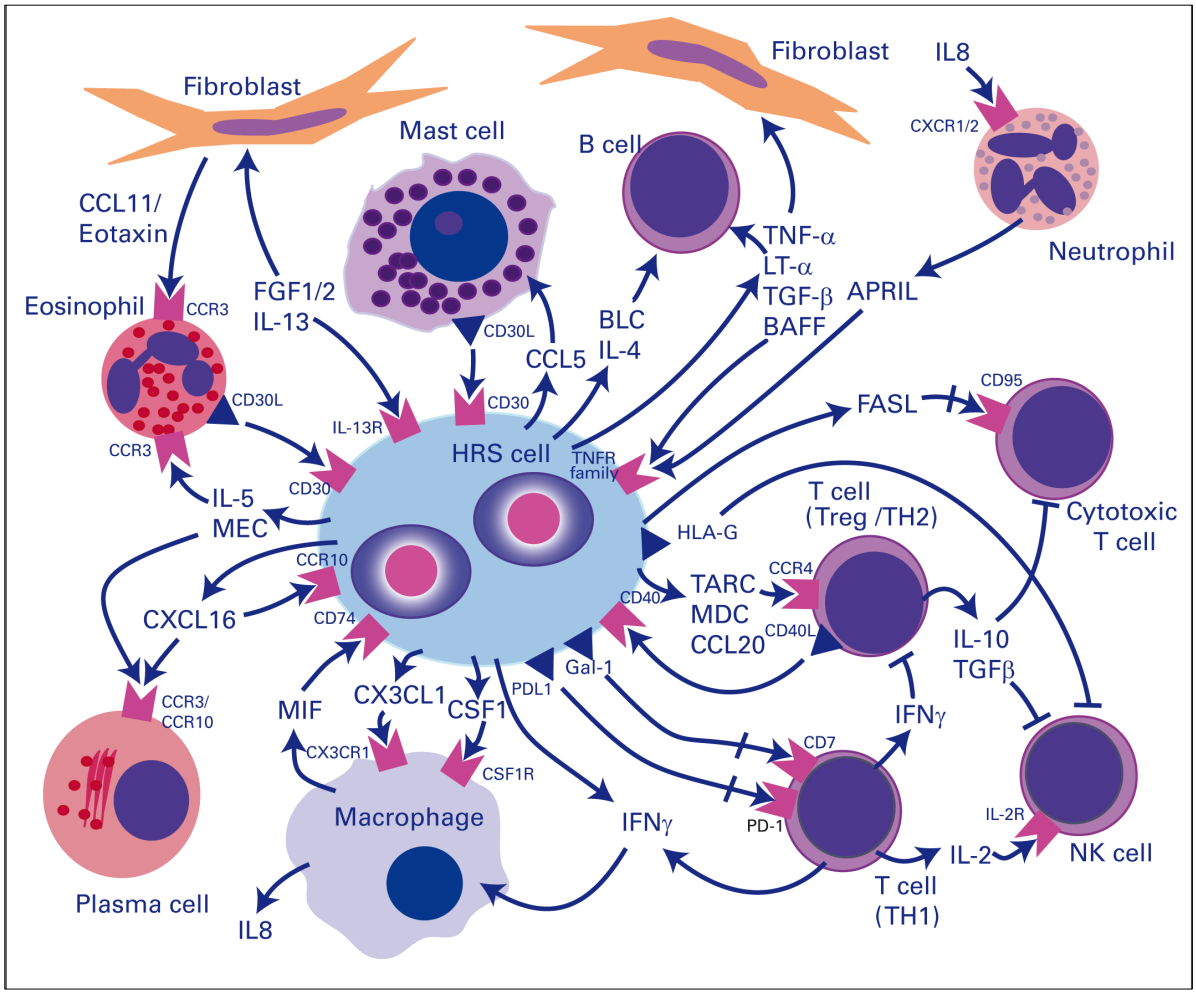

Figure 1.2: Schematic of the crosstalk between malignant Hodgkin Reed-Sternberg (HRS) cells and the tumor microenvironment in classical Hodgkin's lymphoma. In the center, a bi-nucleated HRS cell is shown expressing characteristic surface molecules as well as secreted cytokines and chemokines. Surrounding the HRS cells are cell types representative of the non-neoplastic cells attracted and activated by these molecules. The cells in the microenvironment themselves express a variety of chemokines and cytokines that further shape the reactive infiltrate and provide signaling for HRS cells. Only the main activating and inhibitory functions (arrows) of predominantly membrane-bound (purple triangles) and secreted molecules mediated by surface receptors (pink) are illustrated; other interactions exist. IL, interleukin; FGF, fibroblast growth factor; TNF-α, tumor necrosis factor α; LT-α, lymphotoxin α; TGF-β, transforming growth factor β; BAFF, B-cell activating factor; APRIL, a proliferation-inducing ligand; BLC, B lymphocyte chemoattractant; TNFR, tumor necrosis factor receptor; FASL, Fas ligand; MEC, mucosae-associated epithelial chemokine; Treg, T regulatory cell; TH, T helper cell; MDC, macrophage-derived chemokine; Gal-1, galectin-1; PDL, programmed cell death 1 ligand; IFN-γ, interferon gamma; NK, natural killer.

1.3 CLASSIFICATION OF HODGKIN LYMPHOMA

The first comprehensive classification of HL, then known as Hodgkin's disease, was the Rye Classification.[14] The proportion of HRS cells in the tumour cell population and the nature of the infiltrate allowed four HL subgroups to be identified: nodular sclerosis (NSHL), mixed cellularity (MCHL), lymphocyte-depleted (LDHL) and lymphocyte-predominant HL. The International Lymphoma Study Group was founded in Berlin in 1990 and published the Revised European-American Classification of Lymphoid Neoplasms (REAL) in 1994.[15] This system took into account the morphological, immunological, molecular and genetic components of lymphomas and leukaemias and also recognised entities commonly diagnosed in routine practice. The three major classified groups were HL, B-cell lymphomas/leukaemias and T-cell lymphomas/leukaemias. Diseases were initially classified by their cell of origin and then further subdivided by their histological grade. This classification was expanded upon by the Society for Hematopathology and the European Association of Hematopathologists for the World Health Organisation (WHO).[16] The WHO classification encompasses haematopoietic and lymphoid neoplasms and is in global use. Two distinct groups of HL are characterised in this classification, classical HL (cHL) and nodular lymphocyte-predominant HL (NLPHL), with the former being further subdivided into NSHL, MCHL, LDHL and lymphocyte-rich classical HL (LRCHL). NLPHL and cHL differ in the origin of their tumour cells, their clinical behaviour and their immunophenotype.[17] Immunophenotyping is an important diagnostic tool for differentiating between these two HL groups. In cHL, HRS cells are usually positive for CD15 and CD30, and either positive or negative for CD20.[18] In NLPHL cells are usually negative for CD15 and CD30, but positive for CD20.[19]

1.4 ORIGIN AND CLONALITY OF HRS CELLS

1.4.1 cHL-derived cell lines

The establishment of permanent cell lines has allowed the biological characterisation of many human neoplasms, but only a few cell lines have been derived from cHL cases: CO, HDLM-2, HD-MyZ, Ho, KM-H2, L-1236, L-428, L-540 and L-591. The origins of some are, however, dubious (eg, HD-MyZ) and some (eg, CO) have been reported to have been cross-contaminated with the T-cell acute lymphoblastic leukaemia cell line, CCRF-CEM.[20,21] The remainder have generally been derived from body fluids extracted from patients with end-stage disease. Only the L-1236 cell line has been shown to definitely be derived from HRS cells.[22]

1.4.2 The origin of HRS cells

Analysis of established cHL-derived cell lines has shown that HRS cells do not display specific lineage markers, and often coexpress markers typical for a number of different hematopoietic cell types. Developments in micromanipulation and microdissection procedures, coupled with single cell polymerase chain reaction (PCR) assays for immunoglobulin (Ig) gene rearrangements, have enabled the characterisation of single HRS cells. Ig gene rearrangements involve variable, diversity and joining regions and are unique to B-cells. These rearrangements are therefore distinct markers

which can be used to determine the origin of B lineage cells and assess clonality. Several studies have identified Ig gene rearrangments within HRS cells, micromanipulated from cHL cases, which indicates that these cells originate from B-cells.[23-25] Germinal centres (GCs) are specialised microanatomical structures, within secondary lymphoid follicles, which develop from antigen-specific B-cells that have clonally expanded during immune responses.[26] Upon entering the GC, B-cells automatically begin the cell death program and are only able to escape this process if they display key positive selection signals. They undergo several rounds of proliferation, somatic hypermutation (SHM) and selection in order to develop high affinity antigen receptors (Figure 1.3). The process of SHM is known to take place in secondary lymphoid organs, within the dark zone of the GC, during T-cell-dependent immune responses (Figure 1.3). SHMs are detectable in the majority of Ig gene rearrangements. Non-functional gene rearrangements, resulting from SHM, were identified within HRS cells micromanipulated from approximately 25% of cHL cases.[23] Any GC B-cells acquiring non-functional gene rearrangements within the GC undergo apoptosis instead of differentiation, and do not develop into memory B-cells or plasma cells. The presence of SHMs in HRS cells suggested, therefore, that these cells may derive from preapoptotic B-cells that have gained crippling mutations preventing them from undergoing antigenic selection. The expression of T-cell markers in a small proportion of HL cases suggested that some HRS cells could originate from T-cells.[25,27,28] In one study HRS cells with a cytotoxic T-cell phenotype were isolated from 3 cHL cases.[29] Germline configuration of IgH and T-cell receptor (TCR)-loci, and both Ig and TCR-gene rearrangements were investigated. In two of the HL cases, cytotoxic T-cell markers were identified in the HRS cells and the authors suggested that these cells were derived from mature GC B cells that aberrantly express T-cell markers. In the third HL case a typical T-cell gene rearrangement pattern was observed in the HRS cells indicating these cells were of T-cell origin. TCR gene rearrangements were detected in 2 of 13 T-cell marker-expressing HL cases in a separate study.[25,28] The remaining 11 HL cases in this study were of B-cell in origin. This demonstrated that it is possible for HRS cells with a T-cell phenotype to have a B cell genotype, and that in the vast majority of cases HRS cells are derived from B-cells.

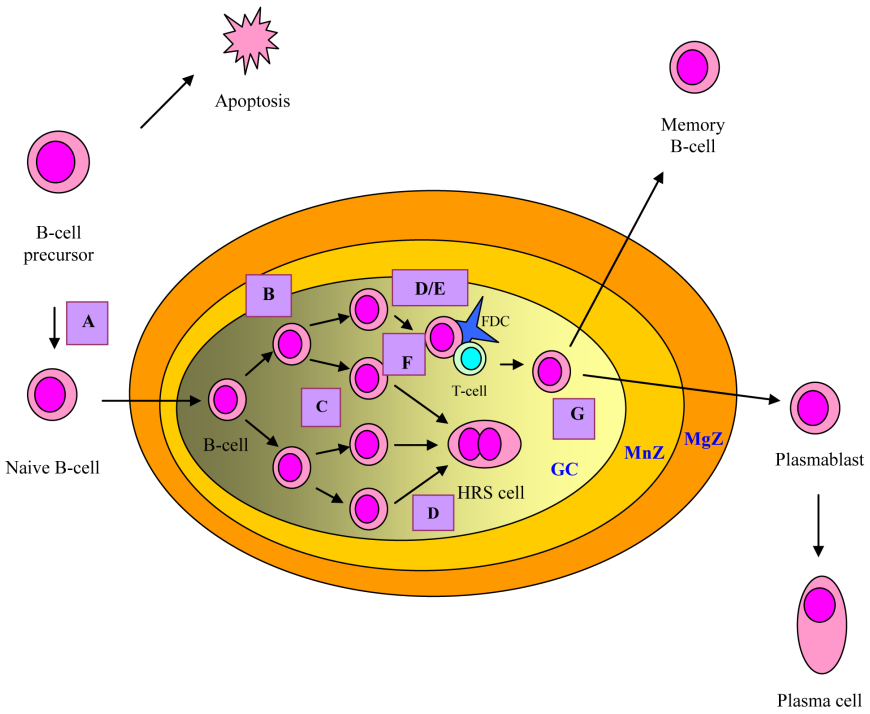

Figure 1.3: Cellular origin and B-cell differentiation within secondary lymphoid organs eg lymph nodes and spleen.[30] The marginal zone (MgZ) contains post-germinal centre (GC) B-cells and naïve B-cells. The mantle zone (MnZ) is formed by naive B-cells, which are replaced by proliferating B-cells and displaced to the outside of the primary B-cell follicle. Naive antigen-activated B-cells are transferred into primary B-cell follicles in lymph nodes, known as GC, where they become proliferating GC B-cells within the dark zone. A – V-region gene recombination in the bone marrow; B – clonal expansion; C – somatic hypermutation; D – mutations increasing antigen affinity; E – class switching; F – selection; G – differentiation.

From the unique morphology and the frequent identification of additional chromosomal copies in both the multinucleated RS and the mononucleated H cells, it was proposed that these cells may arise from fusion between a B-lymphocyte and a dendritic cell. A study of 5 cases of HL with two known rearranged IgH alleles sought to investigate this theory.[31] The majority of B-cells carry two rearranged IgH alleles whereas IgH alleles in non-B-cells show a germline configuration. The presence of additional IgH alleles in a germline configuration would therefore be consistent with a cell fusion between a B-cell and a non-B-cell. Single HRS cells were micromanipulated from selected HL cases and amplification reactions were performed to identify rearranged alleles in IgH and T-cell receptor VDJ and DJ genes. None of the cases showed evidence of additional IgH or TCR alleles to those already identified indicating that HRS cells do not represent fusions of B-cells.

1.4.3 The phenotype of HRS cells

HRS cells have a unique phenotype unrelated to any hematopoietic cell type. They usually expre some T-cell markers, dendritic cell markers (eg, fascin, thymus and activation-regulated chemokine (TARC)), myeloid cell markers (eg, CD15), plasma cell markers (eg, CD138) and some B-cell markers

(eg, Pax-5). Other B-cell markers (eg, CD20 and Oct-2) and B-cell receptors are rarely identified on HRS cells. Hence, the revelation that HRS cells originated from B-cells prompted a large gene expression study comparing gene expression profiles of HL-derived cell lines and normal B-cells.[32] A global downregulation of B-cell specific genes within HRS cells was revealed. It was suggested that the loss of B-cell gene expression could result in these cells not being recognised as B-cells and failing, therefore, to be identified for apoptosis, the mechanism within the GC by which defective B-cells are normally apoptosed.

1.5 SIGNALING PATHWAYS ACTIVE IN HRS CELLS

Cancer cell proliferation, apoptosis, angiogenesis, invasion, and metastasis are regulated by an interconnecting network of cellular signaling pathways involving extracellular ligands, transmembrane receptors, intracellular signaling protein kinases, and transcription factors.[33] These intracellular signaling effectors are modulated by external factors, such as epigenetic changes, oncogenic mutations, molecular chaperones, and ubiquitin-proteasome pathways. Insights into these complicated intracellular processes have exposed many novel cancer targets for which chemotherapeutic agents may be developed (Figure 1.4).

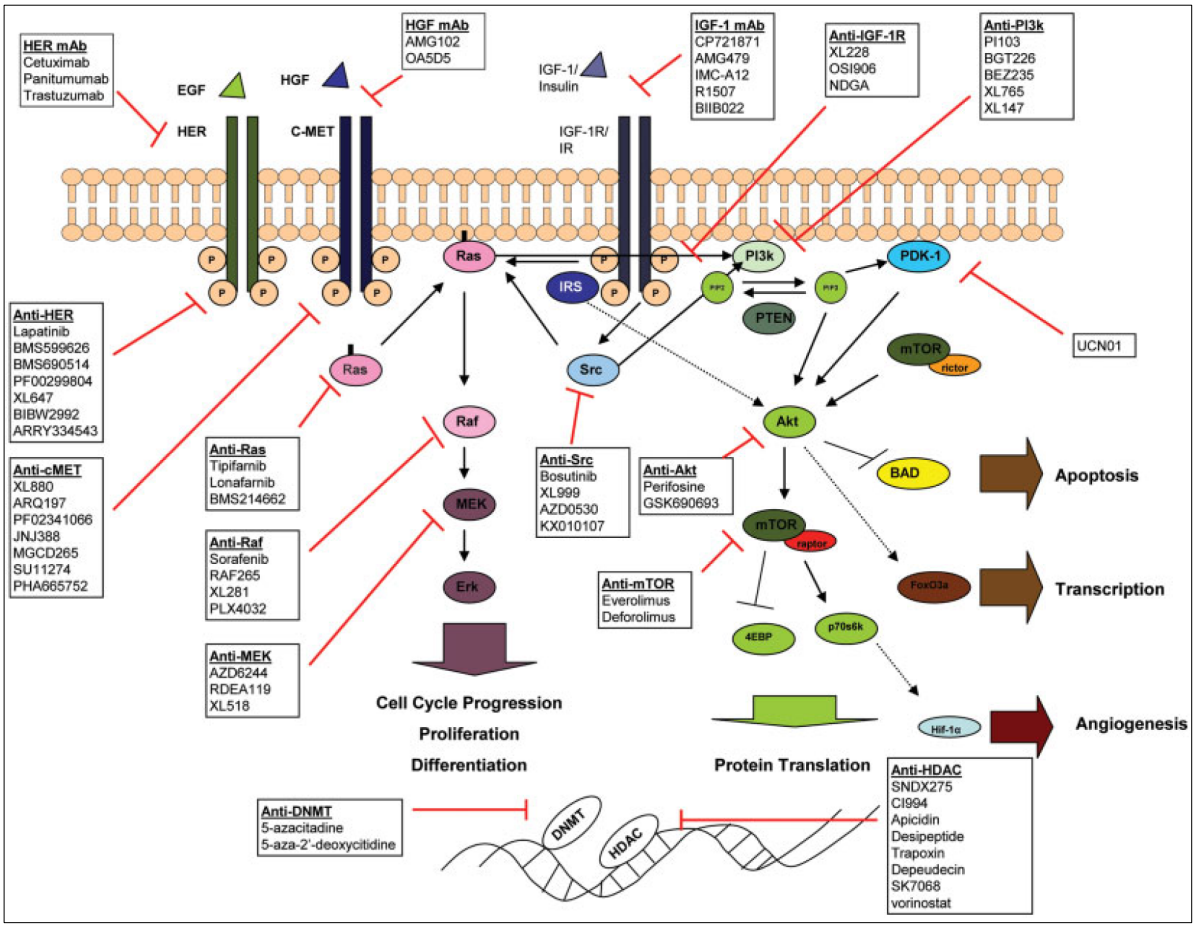

Figure 1.4: Signaling pathways involved in the proliferation, angiogenesis, and differentiation in neoplasms with the targets amenable to therapeutic interventions in cancer therapy. Membrane-bound human epidermal growth factor receptors (HER), c-MET, and insulin-like growth factor 1 receptor (IGF-1R) mediate mitogenic

signals from extracellular ligands, such as epidermal growth factor (EGF), hepatocyte growth factor (HGF), and insulin growth factors (IGF), respectively. The Ras/Raf/MEK/Erk (mitogen-activated protein kinase, MAPK) and PI3k/Akt/mTOR pathways are major intracellular axes that regulate intracellular signaling traffic. DNA methytransferases (DNMT) and histone deacetylases (HDAC) are "epigenetic switches" that modulate the expression of oncogenes and tumor suppressor genes. The agents targeting the signaling proteins are indicated in boxes.

The heterodimeric Nuclear factor kappa B (NFkB) is a key transcription factor involved in many inflammatory and immunologic processes. Activation of several cell-surface receptors (eg, CD40) leads to degradation of the NFkB inhibitor IkBα or other members of the IkB family, that normally bind to NFkB and prevent its translocation into the cell nucleus. Inactivation of IkB is mediated by IkB kinases, which phosphorylate IkB and cause its ubiquitination and degradation. Upon degradation of IkB, NFkB can move into the nucleus and activate expression of multiple genes. NFkB (p65/RelA) was first described in 1996 to be constitutively active in Hodgkin lymphoma cell lines[34] and to be critical for HRS cell survival in vivo in Severe combined immunodeficiency (SCID) mice.[35] NFkB has been shown to mediate both proliferative and anti-apoptotic gene expression programmes in HRS cells.[36] Inhibition of NFkB activity and induction of spontaneous cell death in HL cell line by overexpression of an IkBα superrepressor has provided further evidence that NFkB is critical for HRS cell surivival.[36] NFkB therefore might be regarded as a transforming master switch for HRS cells in HL, although constitutive NFkB activation is not a specific feature of HRS cells but is also characteristic for inflammatory disease and other lymphomas, such as a subset of diffuse large B-cell lymphomas. There are various explanations for NFkB up-regulation in HRS cells: gene amplification of c-rel;[37,38] activation of cell-surface receptors such as CD30,[39] CD40,[40] RANK,[41] or Notch1;[42] expression of viral latent membrane proteins 1 and LMP2a in EBV-positive cases; or loss-of-function mutations of the NFkB suppressor IMBN or IMBP.

Upon TNFR ligation, NFkB activation is induced via TRAF signaling[39,43] and the mitogen-activated protein kinase (MAPK) pathway.[44] It has been shown that activation of the MAPK/Extracellular signal-regulated kinase (MEK) leads to phosphorylation of downstream ERK in HRS cells, thus promoting cell survival.[44] Inhibition of Extracellular Related Kinase (ERK) phosphorylation was efficient ininhibiting ligand-induced cell survival in HRS cell lines. Of note, CD30 signaling has recently been linked to the non-canonical NFkB activation pathway involving RelB/p52 in HRS cells.[45]

Analysis of the Phosphoinositide 3-kinase (PI3K)/AKT signaling cascade revealed constitutive activity of this pathway in HRS cell lines, which has been linked to IL6 secretion and expression of EHG homeobox gene HLXB9 of HRS cells in vitro.[46] It has been demonstrated that targeting of the PI3K/AKT pathway with small molecule inhibitors might be of potential use for future treatment strategies in patients with Hodgkin lymphoma (Table 1.2).[47]

The activator protein 1 (AP-1) complex is formed by hetero or homodimers of jun, Fos, and ATF family proteins. In Hodgkin lymphoma and also in anaplastic large-cell lymphoma but not in other

lymphoma entities, c-jun and junB have been decribed to be aberrantly expressed in the malignant cell population.[48] C-jun seems to be the major transactivating force of the constitutive AP-1 complex. Its activity in HRS cells is independent of JNK but relies on an unknown autoregulatory mechanism, whereas junB activity is NFkB dependent. Both c-jun and junB support proliferation of HRS cells, possibly via induction of cyclin D2 and c-MET expression.[48]

Notch1 is a cell transmembrane receptor that upon ligand binding is cleaved, so that the intracellular domain can translocate into the nucleus and function as a transcription factor.[49] Notch1 signaling plays an important role in various cell fate decisions, including B- and T-cell development. In Notch1 expressing lymphoid precursors B-cell development is suppressed and T-cell differentiation is promoted.[49] With this background, it was surprising that strong Notch1 expression was detected in B-cell-derived HRS cells.[42] The Notch1 ligand Jagged1 is expressed in HRS cells and also in other cells in the tumor tissue, suggesting that Notch1 is activated and functioning in HRS cells.[42] This is supported by studies with HL cell lines, which showed that activation of Notch1 promotes cell proliferation and survival,[42] although another study could not verify the growth-promoting effect of Notch1 activation in a HL line.[50] The aberrant expression of Notch1 in HRS cells may also contribute to the lost B-cell phenotype of HRS cells discussed above, although the B-cell-specific target genes inhibited by Notch1 are still largely unknown.

Many cytokines signal through the Jak/STAT pathway. Upon cytokine receptor activation, Jak kinases become activated, and these can then phosphorylate members of the STAT family of transcription factors. Posphorylated STATs can enter the cell nucleus and activate transcription of target genes. In HRS cells, STAT3, STAT5a, and STAT6 are expressed and constitutively activated.[51,52] The activation of STAT6 is likely mediated by an autocrine stimulation loop, because this factor is activated by IL13R signaling, and HRS cells express both IL13 and the IL13R.[11,52] For STAT5a, it has been shown that both its expression as well as its activation is positively regulated by NFkB activitiy in HRS cells.[51] STAT signaling is presumably important for HRS cell proliferation, because inhibition of IL13 signaling or STAT3 activity in HL cell lines inhibits cell proliferation.[53,54] Once again, this probable oncogenic addiction of cHL to the members of the JAK-STAT cascade makes it an additional, crucial, targetable pathway (Table 1.2).

Based on gene expression profiling studies, aberrant expression of multiple receptor tyrosine kinases, which are not normally expressed by B-cells, was recently identified in Hodgkin lymphoma.[55] The coexpression of several receptor tyrosine kinases, including PDGFRA, DDR2, EPHB1, RON, TRKA, and TRKB, was most pronounced in cHL, but was also identified in lymphocyte-predominant HL. Activation of these tyrosine kinases was implicated by the phosphorylation of several kinases themselves and by an elevated phospho-tyrosine content of the HRS cells in a considerable fraction of cases.[55] The receptor tyrosine kinase activity seems not to be due to somatic mutations, but to ligand-induced activation, as the ligands for several of the tyrosine kinases were detected in the cells surrounding the HRS cells or in the HRS cells themselves, indicating both paracrine and autocrine activation mechanisms.[55] A coexpression and activation of

multiple receptor tyrosine kinases appears to be unique to HL among lymphoid malignancies and suggests that this activation may play a central role in HL pathogenesis. However, the critical downstream targets of the kinase activities remain to be identified.

In summary, multiple signaling pathways are aberrantly activated in HRS cells in vitro and in vivo and critically contribute to the proliferation and survival of the HRS cells (Figure 1.5). For some of the signaling pathways mechanisms for their aberrant and constitutive activation were elucidated in recent years. Future functional studies using knockdown experiments such as RNA interference technology might help to clarify the relative contribution of each of the mentioned pathways for the pathogenesis of Hodgkin lymphoma.

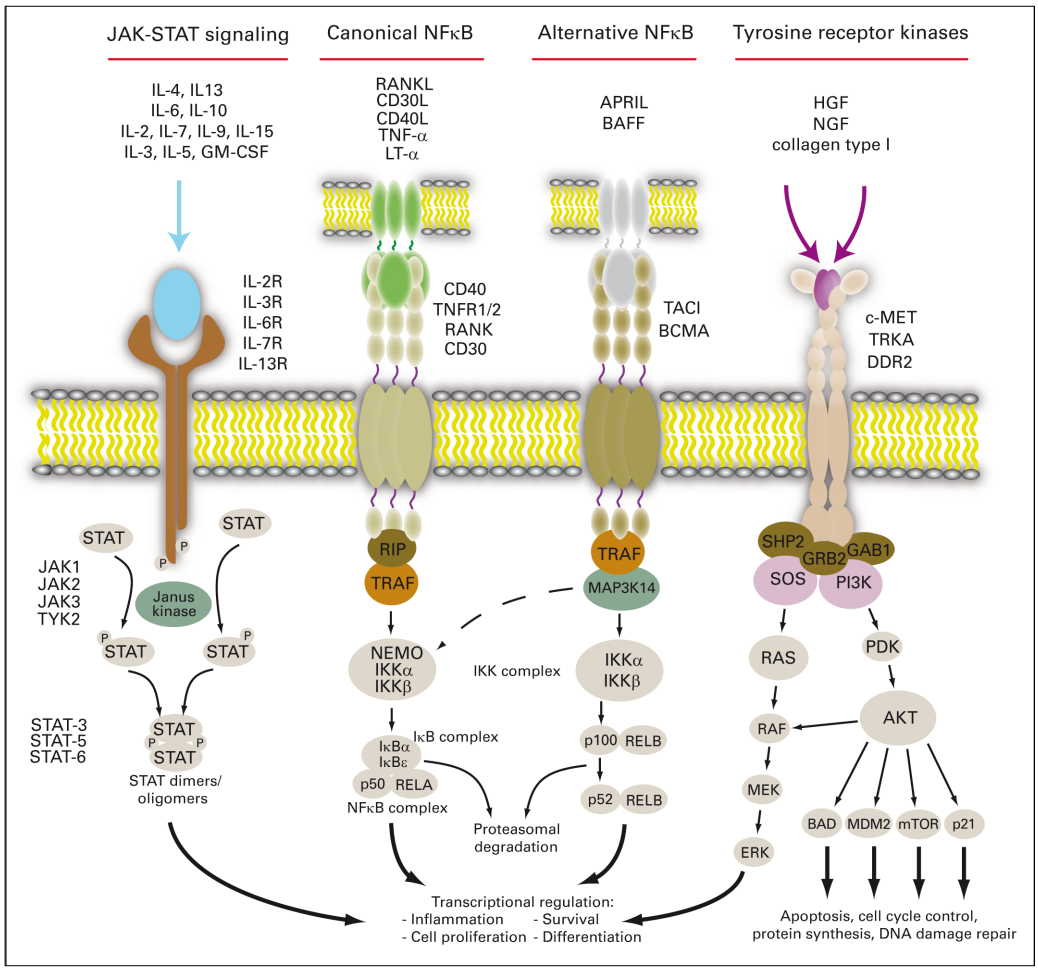

Figure 1.5: Pathway activation in HRS cells through signaling from the microenvironment. Soluble and membrane-bound signaling molecules produced by reactive cells (paracrine activation) activate the Janus kinase–signal transducer and activator of transcription signaling (JAK-STAT) and canonical and alternative NFkB pathways and receptor tyrosine kinases. For the JAK-STAT signaling pathway, the most commonly expressed ILs, IL receptors, and activated STATs are shown. For the NFkB pathway, only the principal activation cascades are shown, and inhibitor of k kinase (IKK) complex activation by other kinases are described. Downstream signaling of receptor tyrosine kinases is shown using the example of tyrosine kinase receptor A (TRKA) and illustrating the Ras and Akt pathways; other signal transduction pathways exist. GM-CSF, granulocyte macrophage colony-stimulating factor; RANKL, receptor activator of NFkB ligand; TNF-α,

tumor necrosis factor α; LT-α, lymphotoxin α; APRIL, a proliferation-inducing ligand; BAFF, B-cell activating factor; HGF, hepatocyte growth factor; NGF, nerve growth factor; TACI, transmembrane activator and CAML interactor; BCMA, B-cell maturation antigen; c-MET, mesenchymal epithelial transition factor; DDR, discoidin domain receptor tyrosine kinase; TYK2, tyrosine kinase 2; RIP, receptor-interacting protein; TRAF, TNF receptor–associated factor 1; MAP3K, mitogenactivated protein 3 kinase; SHP2, Src homology 2 domain–containing tyrosine phosphatase; SOS, son of sevenless homolog 1 (Drosophila); GRB2, growth factor receptor–bound protein 2; PI3K, phosphoinositide 3-kinase; ERK, extracellular signal-regulated kinase; MEK, MAP-ERK kinase; PDK, 3-phosphoinositide–dependant protein kinase; BAD, BCL2-associated agonist of cell death; MDM, mouse double minute; mTOR, mammalian target of rapamycin.

Table 1.2: Overview of selected novel targeted therapeutic strategies being studied for the treatment of classical Hodgkin lymphoma

TARGETS	AGENTS	MECHANISM OF ACTION
CD20	Rituximab Ibritumomab tiuxetan	Antibody-dependent cytotoxicity (ADCC) Radioimmunotherapy Apoptosis facilitation through opening of store-operated Ca++ channels cHL stem cell depletion?
CD25 (IL2Rα)	^{90}Y-Daclizumab DAB486IL-2 RFT5-SMPT-dgA	Radioimmunotherapy Cytotoxin delivery
CD30	MDX-060 SGN-30 MDX-1401 SGN-35 H22xKi-4 ^{131}I-Ki-4 Ki-4.dgA	ADCC Radioimmunotherapy Cytotoxin delivery
CD40	SGN-40 Chir12.12	ADCC Abolishment of CD40 signaling
CD80	Galximab	ADCC
EBV	EBV-specific cytotoxic lymphocytes	Cytotoxicity against virus infected HRSC?
HSP90	7-allylamino-17-demethoxy-geldanamycin (17-AAG)	Abolishment of NF-kB, Akt and Jak stabilization by HSP90
IkBα	Bortezomib	Blocking IkBα degradation → decreased NF-kB signaling Blocking anti-apoptotic mechanisms
Inhibitor of NF-kB kinase (IKK)	As_2O_3	Inhibition of IKK → decreased NF-kB signaling
IL13	TNX-650 CAT-354	Abolishment of growth promoting loops
IL4R	IL4-cytotoxin	Cytotoxin delivery
JAK-STAT	17-AAG Tyrphostin AG17 ISIS 345794	Abolishment of stimulating signaling pathways by inhibiting STAT phosphorylation or abolishment of Jak stabilization by HSP90
mTOR/Raptor	Sirolimus Everolimus	Stabilization of IkBα → decreased NF-kB signaling Inhibition of angiogenesis
PI3K	LY294002 QLT394	Abolishment of the PI3K/Akt survival pathway
VEGF	Bevacizumab	Abolishment of VEGF-VEGFR2 growth promoting loops Inhibition of angiogenesis

1.6 PI3K/AKT PATHWAY

1.6.1 Phosphoinositide 3-kinase (PI3K) family

PI3Ks are a family of enzymes, which phosphorylate the 3'-OH position of the inositol ring of phosphoinositides. They have been divided into three classes on the basis of structural features and in vitro lipid substrate specificity (Figure 1.6).[56-58]

Class I PI3Ks form heterodimers, which consist of one of the four closely related ~110 kDa catalytic subunits, and an associated regulatory subunit belonging to two distinct families. In vitro they are capable to convert PtdIns to PtdIns-3-P, PtdIns-4-P to PtdIns(3,4)P_2, and PtdIns(4,5)P_2 to PtdIns(3,4,5)P_3, but the in vivo substrate is PtdIns(4,5)P_2.[59] Class I PI3Ks are activated by a large variety of cell-surface receptors, comprising growth factor receptors as well as G protein-coupled receptors.[60]

Class II PI3Ks are capable to phosphorylate PtdIns and PtdIns-4-P in vitro, but their relevant in vivo substrates are still under investigation. This class of large (170–200 kDa) enzymes has three members, all characterized by a C-terminal C2 homology domain, which is Ca^{2+}-insensitive due to the lack of a conserved aspartate residue.[61] No adaptor molecules for class II PI3Ks have been identified so far. Although class II PI3Ks have been localized to the trans-Golgi network and low-density microsomes, their mode of action is still poorly understood. Mainly the PI3KC2α isoform has been reported to associate with clathrin and has been attributed a role in clathrin assembly and clathrin-mediated vesicular trafficking.[62,63] A growing list of stimuli was described to activate class II PI3Ks, including chemokines (MCP-1), cytokines (leptin and TNFα), LPA, insulin, and other data show association of the class II enzymes with EGF-, PDGF- and SCF-receptors. Recently, it was demonstrated that PI3KC2β might be involved in LPA-induced cell migration of ovarian and cervical cancer cells.[64]

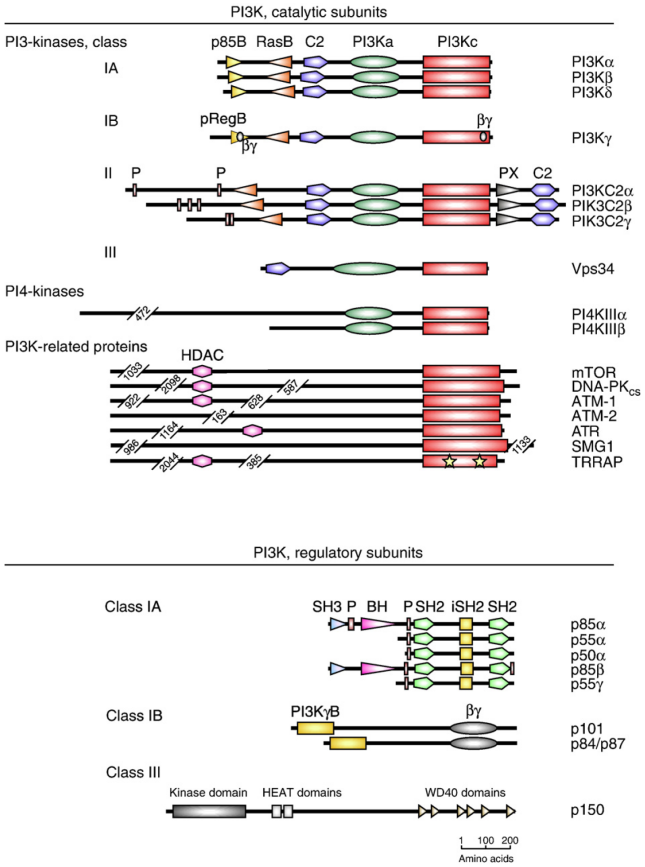

Figure 1.6: Domain structure of phosphoinositide 3-kinases (PI3Ks), PI4Ks and PI3K-related proteins' catalytic and regulatory subunits. All catalytic subunits of the depicted kinases share a core catalytic domain (PI3Kc), which contains the ATP-binding site. In the case of TRRAP this domain has no kinase activity due to mutations in conserved residues (shown as stars). At their N-terminus, the catalytic domains of PI3K class I have a regulatory subunit binding domain (p85B binds p85/55/50 regulatory subunits; pRegB binds p101 and p84/87PIKAP proteins), followed by a Ras-binding domain (RasB), a C2 domain (protein kinase C homology domain 2) and a PI3K accessory (helical) domain (PI3Ka). PI3Kγ contains interaction sites for βγ subunits of trimeric G proteins in the pRegB and the PI3Kc domains. PI3Ks of the class II do not have a known adaptor subunit-binding site in front of their RasB site, but display two to three proline-rich (P) stretches, as well as a PX (phox) and an additional C2 domain at the C-terminus. The catalytic subunit of the class III enzyme Vps34 is composed only of the C2, PI3Ka and PI3Kc domains. The PI3K-related proteins are large enzymes sharing only the PI3Kc domain with PI3Ks and PI4Ks. Some members of this class contain also an HDAC (histone deacetylase) domain. The regulatory subunits of class IA PI3Ks contain a proline-rich region, two SH2 (Src-homology 2) domains, as well as an iSH2 region (with a coiled-coil structure), which interacts with the catalytic subunit. p85α and p85β have at the N-terminus an additional SH3 (Src-homology 3) and BH (BCR homology) domain. The structure of p101 and p84/87PIKAP is not well explored. The N-terminus is required for association with PI3Kγ, and Gβγ interaction is mediated by the C-terminal part of these adaptors. The adaptor of the class III PI3K Vps34 is the Ser/Thr protein kinase p150 (hVps15). Besides the kinase domain, this protein contains HEAT (Huntington, Elongation Factor 3, PR65/A, TOR) domains and a series of WD40 repeats. In the case of the PI4K and the PI3K-related proteins, only part of the protein is depicted here, and the number of excised amino acids is displayed. ATM, ataxia telangiectasia mutated; ATR, ataxia telangiectasia-related; DNA-PKcs, catalytic subunit of DNA-dependent protein kinase; HEAT, Huntington, Elongation Factor 3, PR65/A, TOR; iSH2, inter-SH2; mTOR, mammalian target of rapamycin; P, proline-rich region; PX, phox; TRRAP, transformation/transcription domain-associated protein.

Class III PI3Ks are solely able to phosphorylate PtdIns, and thus generate only PtdIns-3-P. The single member of this class is Vps34, of which the S. cerevisiae Vps34p (vacuolar protein sorting mutant 34 protein) is the prototype, and has been shown to play an essential role in trafficking of newly synthesized proteins from the Golgi to the yeast vacuole, an organelle equivalent to lysosomes in mammals.[65] In S. cerevisiae, Vps34p forms a complex with the N-terminal myristoylated Ser/Thr protein kinase Vps15p, which is required for activation and recruitment of Vps34p to Golgi membranes.[66] In mammals, Vps34p is associated with the orthologue of yeast Vps15p, p150 (also called hVps15), which targets hVps34p to Rab5-positive endosomes. Therefore, it appears that hVps34p is also central to endocytosis and vesicular trafficking.[67] As it has been demonstrated in yeast, Vps34p forms two distinct complexes with Vps15p, Atg6/Vps30p and either Atg14 or Vps38.[68] Interestingly, deletion of Atg14 leads to defects in autophagy, while deletion of Vps38 causes a vacuolar-sorting defect. Mammalian orthologues of Atg14 and Vps38 have not been identified yet. The mammalian orthologue of Atg6/Vps30p is Beclin-1, which is capable to bind hVps34p directly. Down regulation of Beclin-1 in cells leads to minimal defects in autophagy and vesicular trafficking.[69] Mice heterozygous for Beclin-1 (Beclin-$1^{+/-}$) show decreased autophagy and enhanced tumor formation.[70] In the last years, a lot of attention was given to the requirement of Vps34p in the induction of autophagy in nutrient, amino acid, as well as glucose-deprived cells. Recent data suggest a role of Vps34p in the activation of mammalian target of rapamycin (mTOR) downstream of amino acids, resulting in mTOR-dependent phosphorylation of ribosomal protein S6 kinase (p70S6K1) and elongation-initiation factor 4E-binding protein (4E-BP1).[71]

Class IV PI3Ks consists of high molecular weight enzymes with a catalytic core similar to PI3Ks and PI4Ks (Fiure 1.6), and include mTOR, DNA-dependent protein kinase (DNA-PK_{cs}), the ataxia telangiectasia mutated gene product (ATM), ataxia telangiectasia related (ATR), SMG-1 and transformation/transcription domain-associated protein. The first five members are active protein serine-threonine kinases that are involved in cell growth control and genome/transcriptome surveillance.[72,73] DNA-PK_{cs}, ATM, ATR and SMG-1 are involved in DNA-damage responses. The first two are primarily responsible for double strand break (DSB) repair, whereas ATR and SMG-1 respond to ultraviolet-induced stress as well as DSB.[74] SMG-1 is involved also in mRNA surveillance mechanisms.[75] The only active kinase not involved in DNA-damage is mTOR, which is regulated by growth factors and nutrient availability, and coordinates protein synthesis, cell growth and proliferation.[76]

1.6.2 PI3K class I activation and signaling

The PI3K pathway is a key signaling transduction cascade controlling the regulation of cell growth, proliferation, survival as well as cell migration. PI3Ks are activated by a wide variety of different stimuli including growth factors, inflammatory mediators, hormones, neurotransmitters, and immunoglobulins and antigens.[60,77] The class IA PI3K isoforms PI3Kα, β and δ, are all bound to one of the p85/p55/p50 regulatory subunits, which all harbor two SH2 domains that bind with high affinity to phosphorylated Tyr-X-X-Met motifs. These motifs are present in activated growth factor receptors, their substrates and numerous adaptor proteins (Figure 1.7). PI3Kγ, the only class IB

PI3K, associates with the adaptor proteins p101 or p84/p87[PIKAP], and is activated and translocated to the plasma membrane by βγ subunits of trimeric G proteins (Figure 1.7). Activation of class I PI3Ks leads to the production of PtdIns(3,4,5)P_3, which recruits adaptor and effector proteins containing pleckstrin-homology-(PH)domains, eg, protein kinase B (PKB/Akt). Once at the membrane, PKB/Akt is phosphorylated at Thr308 by phosphoinositide-dependent kinase 1 (PDK1). Full activation of PKB/Akt is achieved by phosphorylation of Ser473 within the hydrophobic motif by socalled PDK2 kinases, of which the mTOR complex 2[78] and DNA-PK_{cs}[79,80] seem to be the most relevant ones at present. Once activated, PKB/Akt phosphorylates a plethora of proteins, regulating their activity either in a positive or negative manner.[78] These target molecules are involved in many different cellular outputs, which span from cell cycle progression to cell survival, degranulation, metabolism, ribosome biogenesis, translation, transcription, and cell motility (Figure 1.8).[81] The activation of the PI3K pathway is negatively regulated by the action of two phosphoinositide phosphatases. The SH2 domain-containing inositol phosphatase has a 5′-phosphoinositide phosphatase activity which converts PtdIns(3,4,5)P_3 to PtdIns(3,4)P_2.[82,83] The other phosphatase is the phosphatase and tensin homolog deleted in chromosome ten (PTEN; also MMAC for mutated in multiple advanced cancers; or TEP1, TGF-β-regulated and epithelial cell enriched phosphatase 1), which hydrolyzes PtdIns(3,4,5)P_3 to PtdIns (4,5)P_2.[84] PTEN is often mutated, deleted or down-regulated in various tumors, which leads to a constitutive activation of the PI3K pathway.[85,86]

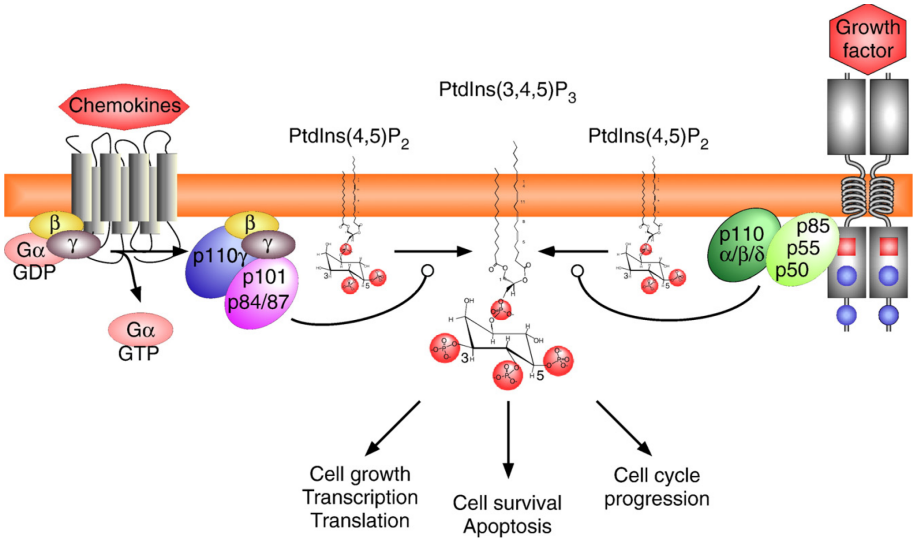

Figure 1.7: Simplified activation scheme of class I PI3Ks. Heterodimeric PI3Kα, PI3Kβ, and PI3Kδ complexes are activated downstream of growth factors, cytokine receptors and their substrates, whereas PI3Kγ activation is triggered downstream of G protein-coupled receptors (GPCRs). Binding of growth factors to their cognate receptor leads to receptor dimerisation and auto-phosphorylation of multiple tyrosines (pY, blue circle), which can be located in pYxxM motifs (blue squares). These act as docking sites for the SH2 domains present in the PI3K regulatory subunits p85, p55, and p50. This translocates the catalytic PI3K subunit to the plasma membrane to initiate the conversion of PtdIns(4,5)P_2 to PtdIns(3,4,5)P_3. PtdIns(3,4,5)P_3 then recruits proteins with a pleckstrin homology (PH) domain and amplifies the growth factor signaling cascade. In the case of PI3Kγ, binding of chemokines to GPCRs induces the dissociation of heterotrimeric G_i-proteins. Free $G_{\beta\gamma}$ subunits interact with PI3Kγ and the adaptor proteins p101 and p84/87[PIKAP], usually triggering transient, high amplitude signals of PtdIns(3,4,5)P_3.

1.6.3 Cellular functions of AKT

The activated Akt regulates a wide range of target proteins, and has multiple cellular functions including cell survival, cell cycle progression, and cell growth. The aberrant activation of Akt signaling has been widely implicated in many human cancers. Major functions of the Akt pathway involved in human cancers are summarized in Figure 1.8.

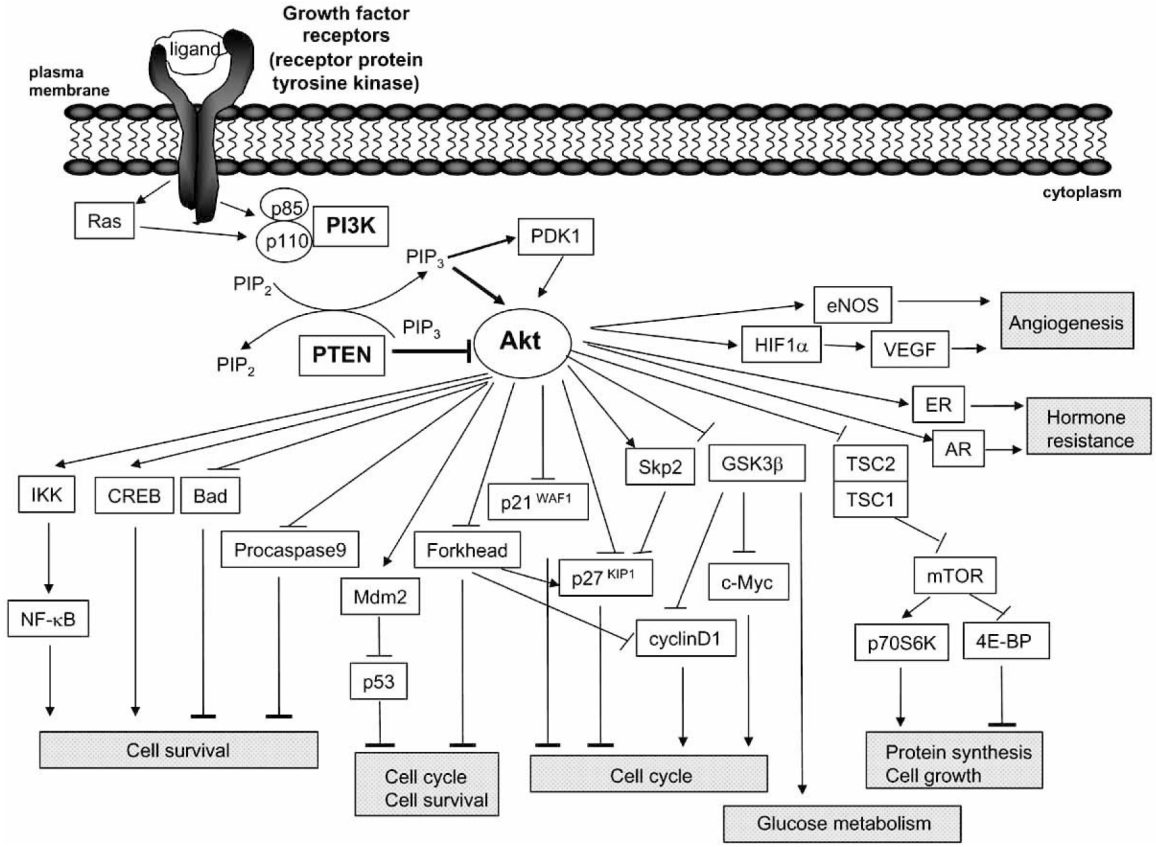

Figure 1.8: Schematic signaling of the Akt pathway involved in human cancers. The activation of Akt signaling pathway results from various mechanisms, including PI3K activation via receptor tyrosine kinase activation and loss of PTEN function. Once activated, Akt regulates a wide range of target proteins and has multiple cellular functions including cell survival, cell cycle progression, and cell growth.

1.6.3.1 Cell cycle progression, and Cell Proliferation

PI3K/Akt pathway has been shown to be activated during the G1/S transition and to play a key role in cell cycle progression.[87] Akt phosphorylates many kinds of proteins involved in protein synthesis and cell cycle regulation. These proteins include glycogen synthase kinase-3α (GSK3α), the forkhead transcription factors, cyclindependent kinase inhibitors $p21^{WAF1}$ and $p27^{KIP1}$ and mTOR.[88] GSK3α phosphorylates cyclin D1 and c-Myc, which play distinct roles in cell cycle progression through G1 phase,[89] and promotes their degradation.[90,91] Akt phosphorylates and inhibits GSK3α, thereby contributing to the stabilization of cyclin D1 and c-Myc. The forkhhead transcription factors repress cyclin D1 expression while enhancing expression of the cell cycle inhibitors $p27^{KIP1}$ and p130Rb2.[92]

Akt phosphorylates the forkhead transcription factors, then promotes the cyclin D1 expression and inhibits the expression of $p27^{KIP1}$ and p130Rb2. Recent studies suggest that Akt also regulates $p27^{KIP1}$ stability,[93,94] possibly through an upregulation of Skp2.[95,96] Akt also directly phosphorylate $p21^{WAF1}$[97,98] and $p27^{KIP1}$,[93,99] thus leading to their cytoplasmic mislocalization and cell cycle progression. p53 is probably the best characterized tumor suppressor, which regulates cell cycle and apoptosis.[100] Akt can promote p53 degradation by phosphorylating and activating its negative regulator Mdm2.[101,102]

1.6.3.2 Cell survival and apoptosis

The activation of the PI3K/PKB pathway has an antiapoptotic effect. Here, PKB/Akt phosphorylates and inhibits caspase 9, a protease crucial in the initiation of the apoptotic cascade.[103] PKB/Akt also phosphorylates the death promoter BAD at Ser136, and thus releases the anti-apoptotic proteins Bcl-2 and Bcl-XL.[104] PKB/Akt can also activate and phosphorylate I-kB kinase. This kinase in turn phosphorylates and inactivates the inhibitor I-kB, which then releases the transcription factor NF-kB. As a consequence, the latter translocates to the nucleus and activates transcription of anti-apoptotic proteins such as Bcl-2 and Bcl-XL.[105] Finally, inactivation and cytosolic retention of FOXO as mentioned above, leads to a block in transcription of FasL, and thus intercepts ligand-induced apoptosis.

1.6.3.3 Cell growth, transcription, and translation

mTOR participates in the regulation of the initiation of mRNA transcription and protein translation in response to the nutrient availability and growth factor stimuli.[106] mTOR is phosphorylated and activated downstream of PI3K/Akt, and plays an important role in stimulating cell proliferation.[107] mTOR controls cell growth by activating p70S6K and inhibiting 4E-BP1, two events which stimulate protein translation.[107] The PI3K/Akt pathway has recently been shown to activate mTOR, at least in part, through the pathway involving Akt's phosphorylation and inhibition of the tuberous sclerosis complex-2 (TSC2) gene product tuberin.[108-110] TSC2 is one of the two genes found mutated in the tuberous sclerosis complex disease. The other one is TSC1, which encodes the protein hamartin, an obligatory binding partner of tuberin. Hamartin/tuberin complex inhibits p70S6K and activates 4E-BP1. Akt directly phosphorylates tuberin and inhibits the formation of this complex. mTOR exists in mutually exclusive complexes with raptor (regulatory-associated protein of TOR) or rictor (rapamycin-insensitive companion of TOR).[111,112] Recent studies have shown that mTOR is not only a major downstream target of Akt but also a critical activator of Akt by forming complex with rictor.[112] Importantly, the raptor-mTOR complex is rapamycin sensitive and is responsible for phosphorylation of p70S6K and 4E-BP1, whereas the rictor-mTOR complex is rapamycin insensitive and is one of the enzymes that can catalyze the activating phosphorylation of Akt at Ser473 and facilitate Thr308 phosphorylation by PDK1 (Figure 1.9).

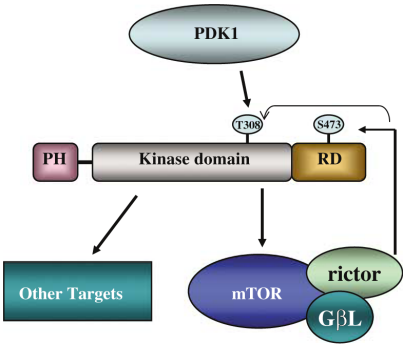

Figure 1.9: Schematic diagram of feedback regulation of Akt by rictor-mTOR.

1.6.3.4 Angiogenesis

The activation of the Akt signaling pathway appears to play an important role in the angiogenesis. Akt, activated in response to proangiogenic factors such as vascular endothelial growth factor (VEGF), prevents endothelial cell apoptosis.[113] Akt also phosphorylates and activates endothelial nitric oxide synthase and allows for neovascularization and VEGF-mediated cell migration.[114] Forced expression of Akt induces angiogenesis,[115] suggesting the direct and sufficient role of Akt in regulating angiogenesis. Hypoxia inducible factor-1α (HIF-1α) is activated by hypoxia and induces the transcription of various genes involved in angiogenesis, including VEGF.[116] Increase of PI3K and Akt or decrease of PTEN activity induces HIF-1α expression in cancer cells, leading to upregulation of VEGF and angiogenesis.[117] Recently, an increased PI3K activity and Akt1 phosphorylation has been shown to be required for the HIF-1α expression in invasive breast carcinoma.[118] In addition, a recent study showed that Akt can induce the HIF-1α expression independent of hypoxia.[119]

1.6.4 ACTIVATION OF AKT IN HUMAN CANCER

In addition to preclinical studies, many clinical observations support targeting the PI3K/Akt/mTOR pathway in human cancer. The frequent activation of Akt has been reported in many human cancers, including carcinomas of breast, prostate, gastric, lung, ovary, pancreas, and thyroid, as well as in glioblastoma and various hematological malignancies.[120] Numerous studies have shown the associations between Akt activation and the clinicopathological characteristics, such as advanced stage, poor prognosis and histological grade.[120] Akt activation in human cancer is caused by various mechanisms which are described below.

1.6.4.1 Alterations Related to AKT Activation in Human Cancer

Alterations of PI3K

The gene PIK3CA, which encodes the p110α catalytic subunit of PI3K, is frequently amplified in some human cancers. In ovarian cancer, an increased copy number of PIK3CA has been shown in approximately 40% cases with increased PI3K activity.[121] Increased PIK3CA gene copy number was also reported in primary gastric carcinomas,[122] head and neck squamous cell carcinomas,[123] uterine

cervical carcinoma.[124] Similar to ovarian cancer cell lines, PIK3CA gene amplification in gastric cell lines has been shown to be strongly associated with the increased expression of PIK3CA and an elevated Akt activity.[122] Somatic mutations of the PIK3CA gene have been reported in gastric, colorectal, breast, and endometrial carcinomas and certain brain tumors.[72,125] A mutation of the PIK3R1 gene, which encodes the p85α regulatory subunit of PI3K, has been shown in human T-cell lymphoma cell line from a patient with Hodgkin's disease.[126] The mutant protein contributes to a constitutively active form of PI3K. Compared to PIK3CA, mutation of the PIK3R1 gene is an infrequent event in human cancer.

Alterations of PTEN

PTEN is a tumor suppressor, which negatively regulates Akt pathway. Loss of PTEN function leads to an elevated concentration of the PIP3 substrate, and consequent constitutive activation of downstream components of the PI3K pathway, including the Akt and mTOR.[84] The loss of the PTEN function via gene mutation, deletion, or promoter methylation has been reported in some types of tumors, including endometrial carcinoma, glioblastoma multiforme, anaplastic astrocytoma, prostate, ovarian and thyroid carcinoma, and hepatocellular carcinoma, breast, lung, renal cell carcinoma and melanoma, microsatellite-high colorectal carcinoma and gastric carcinoma.[127] Decreased expression of PTEN has been reported to be associated with lymph node metastasis and poor prognosis and to be predictive of the failure of tamoxifen treatment.[128] We recently reported that loss of heterozigosity at the PTEN gene locus was associated with Akt activation and resulted in chemoresistance in gastric carcinomas[129] and associated with negative progesterone receptor expression in breast carcinomas.[130]

Alterations of Akt

Akt2 gene amplification is considered to be a frequent event in various human cancers. Akt2 gene amplifications have been reported in ovarian, pancreatic, breast, and gastric cancer and head and neck squamous cell carcinomas.[123,131,132] In contrast to Akt2, Akt1 gene amplification is not a frequent event in any tumor types. Recently, Akt1 gene amplification with Akt1 overexpression has been reported in a single case of gliosarcoma.[133] Although Akt1 gene amplification is a rare event, Akt1 overexpression has been reported in breast and colorectal cancers.[134,135] Akt3 gene amplification has not been reported so far.

1.6.5 PI3K/Akt/mTOR PATHWAY AND CHEMOTHERAPEUTIC RESISTENCE

The rationale for targeting the PI3K/Akt/mTOR pathway in combination therapy comes from data describing constitutive or residual pathway activation in cells that have developed resistance to conventional chemotherapy and radiation,[136] as well as to other targeted therapies such as EGFR antagonism. In these cases, combining chemotherapy or radiation with a pathway inhibitor can overcome acquired resistance to EGFR tyrosine kinase inhibitors. Some standard chemotherapeutic agents appear to directly inhibit Akt in vitro, and the cytotoxicity may be a direct consequence of

inhibition of Akt signaling.[137,138] Because Akt is integrally involved in cellular survival, many groups have investigated the effects of combining chemotherapy with pathway inhibitors.

1.6.6 THERAPEUTIC APPROACHES OF TARGETING THE AKT PATHWAY IN CANCER

The PI3K/Akt signaling pathway has become an attractive target for cancer drug development for some reason. As abovementioned, this pathway inhibits many proteins that are related to apoptosis and which regulate cell cycle progression and promote cell proliferation and growth. It is expected that inhibition of this pathway might therefore inhibit cell growth and proliferation, and reverse the repression of apoptosis and resistance to cytotoxic agents in cancer cells. In addition, many components of the PI3K/Akt pathway are kinases which are ideal for the development of small molecule inhibitors. Moreover, the hyperactivation of the PI3K/Akt pathway is found in a wide range of tumors and numerous studies have shown that drugs inhibiting this pathway are likely to be used for treating various types of cancer. However, based on the complexity of the PI3K/Akt signaling and crosstalk with multiple pathways, combined with its importance in multiple physiological functions, it is very important to confirm efficacy and safety in the development of the target therapies for this pathway (Figure 1.10). A number of inhibitors of proteins involved in PI3K/Akt signaling pathway have been under development, and some agents have now entered clinical trials or been approved for clinical practice. These agents include inhibitors, which directly inhibit the PI3K/Akt/mTOR pathway and indirectly inhibit this pathway by inhibiting the upstream regulators of PI3K/Akt, such as membrane growth factor receptors. Ongoing clinical trials are expected to show the efficacy of these agents while also revealing the mechanisms of sensitivity or resistance to those agents by accompanying translational research.

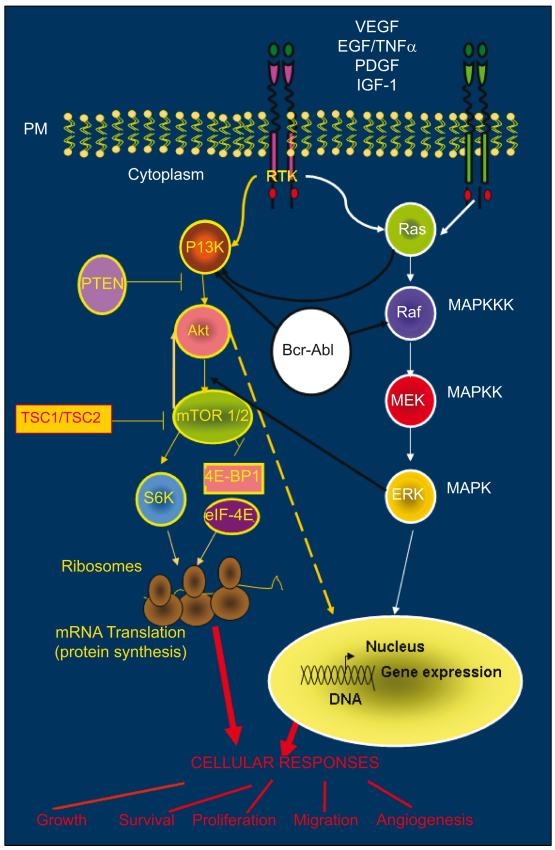

Figure 1.10: PI3K-Akt-mTOR pathway and cross-talk with other signaling cascades: (Ras/Raf/MAPK and BCR-ABL). PI3K-Akt and Ras/Raf/MAPK pathways are common routes that control key cellular responses. The large amount of cross-talk between these pathways is often responsible for treatment resistance.

1.6.6.1 Akt inhibitors

As we described above, PI3K/Akt/mTOR pathway plays a critical role in proliferation and survival in tumor cells and is also linked with resistance to radiotherapy, chemotherapy, endocrine therapy and novel anticancer therapies.[139] In this setting, this pathway seems to bring together all the characteristics of a good target for the treatment of cancer. Currently, clinical trials with inhibitors of the PI3K/Akt pathway in monotherapy or in combination with other anti cancer drugs are underway in cancer patients. In addition, these novel inhibitors are being also tested in chemo- and hormonal-therapy refractory patients.[140,141] Although we will focus on inhibitors of Akt, currently PI3K and mTOR inhibitors are more advanced in their development than Akt inhibitors. During recent years, intense efforts made in the search for Akt inhibitors have yielded several promising candidates, such as lipid-based inhibitors that compete with PIP3 to bind the PH domain of Akt, ATP-competitive inhibitors, small molecule inhibitors, and peptide-based inhibitors reviewed elsewhere.[142] The lipid-based inhibitors include perifosine, an orally active membrane-permeable ether lipid with a single long alkyl chain (Figure 1.11).

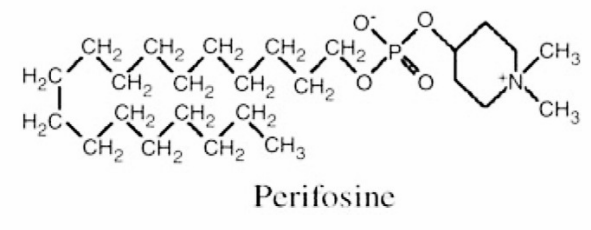

Figure 1.11: Compound structure for Perifosine.

In vitro, perifosine inhibits translocation of Akt to the cell membrane, and inhibits the growth of melanoma, lung, prostate, colon, and breast cancer cells in association with inhibition of Akt activity.[143,144] Additional in vitro data demonstrates synergistic effects of perifosine and traditional chemotherapeutic agents such as etoposide in leukemia cells,[145] doxorubicin in multiple myeloma cells,[146] and temozolomide in glioma cells.[147] Perifosine has also been found to sensitize cancer cells to apoptosis and cell cycle arrest induced by radiation in vitro and in vivo.[148,149] Perifosine has also shown efficacy and tolerability in phase I clinical trials.[150] However, given the limited efficacy of perifosine monotherapy in a variety of solid malignancies in phase II trials, an alternative strategy would be to combine perifosine with chemotherapy, radiation therapy and targeted agents in an attempt to enhance cytotoxicity and overcome chemotherapeutic resistance through inhibition of the Akt pathway. These data have prompted several phase I combination studies with perifosine including evaluation of perifosine combined with lenalidomide,[151] sorafenib, sunitinib, docetaxel, paclitaxel, imatinib, or gemcitabine. In addition, a phase I trial combining perifosine and radiotherapy in advanced solid tumors demonstrated that perifosine could be safely utilized as a radiation sensitizer, and phase II trials with this strategy are in development.[152]

1.6.6.2 Combining pathway inhibitors with other targeted therapies

The concept of "oncogene addiction" asserts that some cancers depend on one gene or a few genes for their survival and maintenance of the malignant phenotype. Although PI3K/Akt/mTOR pathway activation is required for the development and/or maintenance of certain stages of cancer, tumor heterogeneity and clinical experience suggest that combination therapy will be required to achieve remission or cure in most patients. Because signaling of multiple receptor tyrosine kinases (RTKs) is propagated through Akt, simultaneous inhibition of RTKs such as IGF-IR or erbB family members with pathway components such as Akt or mTOR may circumvent feedback activation seen with either approach alone. Such an approach can be considered proximal and distal signaling inhibition (Figure 1.12, left panel). Based on the observed feedback activation of Akt by mTOR inhibitors, it is possible that they might be most effective when combined with proximal pathway inhibitors. For example, synergistic effects between rapamycin and LY294002, an upstream inhibitor of PI3K, are commonly observed in vitro.[153-155] Most recently, Fan *et al* showed that a dual inhibitor of PI3Kα and mTOR, PI-103, was able to inhibit Akt activity as well as proliferation in glioma cells, regardless of PTEN or EGFR status.[156] PI-103 was effective in inhibiting the growth of glioma xenografts in the absence of toxicity, most likely through a cytostatic mechanism.

Another possible approach is to combine inhibition of the PI3K/Akt/mTOR pathway with inhibition of a parallel pro-survival signaling pathway such as the MEK/ERK pathway (Figure 1.12, middle panel).[157] This approach abrogates compensatory activation of other pro-survival pathways when the PI3K/Akt/mTOR pathway is inhibited. For example, combining an inhibitor of PI3K with an inhibitor of MEK causes a synergistic increase in apoptosis in both PTEN mutant and wild-type cells.[158]

In addition to combining PI3K/Akt/mTOR inhibitors with agents that inhibit either the same or parallel pro-survival signaling pathways, PI3K/Akt/mTOR inhibitors have also been combined with targeted agents that defy easy categorization such as imatinib and those that do not directly affecting signaling pathways, eg, histone deacetylase (HDAC) inhibitors and proteasome inhibitors (Figure 1.12, right panel).[159] Although the mechanisms behind the efficacy of these combinations are not completely understood, they represent potentially useful combinations for patients whose tumors do not respond to more conventional therapy regimens.

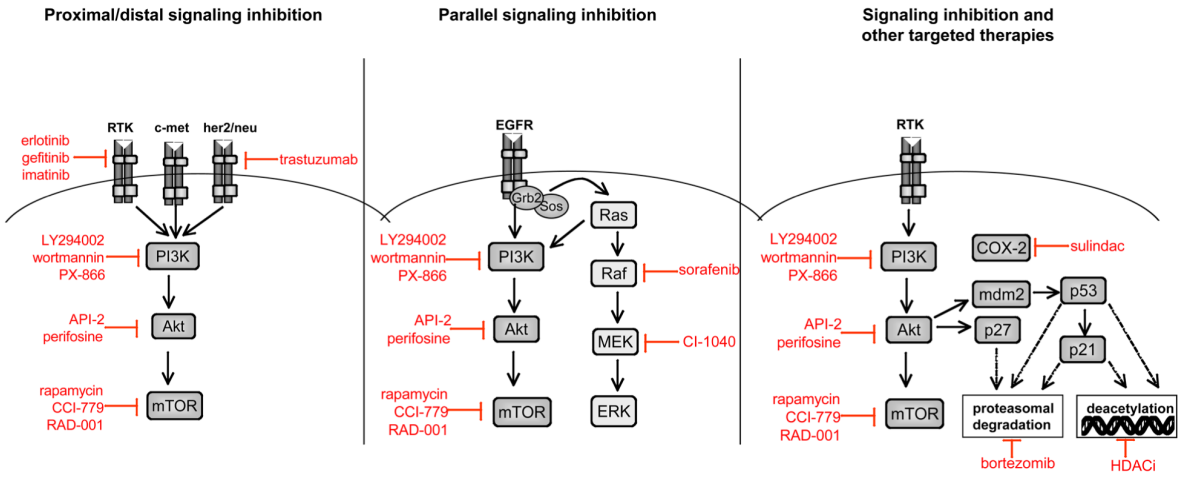

Figure 1.12: Combinatorial approaches with inhibitors of the PI3K/Akt/mTOR pathway. Several approaches can be employed when combining pathway inhibitors with other targeted therapies. Inhibition of proximal pathway components, such as RTKs and oncogenes, combined with distal inhibition of Akt or mTOR may be an effective approach to circumvent feedback activation that could occur with distal inhibition alone (left panel). Alternatively, dual inhibition of parallel signaling pathways prevents compensatory activation of redundant pro-survival pathways (middle panel). Finally, pathway inhibition can be combined with several other types of targeted therapies, including inhibition of HDAC complexes, the proteasome and cyclooxygenase-2 (COX-2) (right panel).

1.7 THE MITOGEN-ACTIVATED PROTEIN KINASE (MAPK) PATHWAY

Human tumorigenesis is a multistep process during which accumulation of genetic and epigenetic alterations leads to the progressive transformation of a normal cell into a malignant cancer cell. During this process, cancer cells acquire new capabilities (hallmarks) that enable them to escape from normal homeostatic regulatory defense mechanisms. These hallmarks are defined as: self-

sufficiency in growth signals, insensitivity to antiproliferative signals, evasion from apoptosis, limitless replicative potential, sustained angiogenesis, and increased motility and invasiveness.[160] While the mechanisms by which cancer cells acquire these capabilities vary considerably between tumors of different types, most if not all of these physiological changes involve alteration of signal transduction pathways. Among the signaling pathways most frequently dysregulated in human cancer is the Ras-Raf-MEK-ERK1/2 pathway. The Ras-dependent ERK1/2 MAPK pathway is one of the best-studied signal transduction pathways. Mammalian cells possess four well characterized and widely studied MAPKs (Figure 1.13). These cascades are comprised of three protein kinases that act as a signaling relay controlled, in part, by protein phosphorylation: a MAPK kinase kinase (MAPKKK), a MAPK kinase (MAPKK) and a MAPK.[161] The terminal serine/threonine kinases (MAPKs) are the ERK1/2, the c-Jun amino-terminal kinases (JNK12/3; also called SAPKs), p38 kinases (p38α/β/γ/δ) and ERK5. Generally, the ERK pathway is activated by growth factor-stimulated cell surface receptors, whereas the JNK, p38 and ERK5 pathways are activated by stress and growth factors.

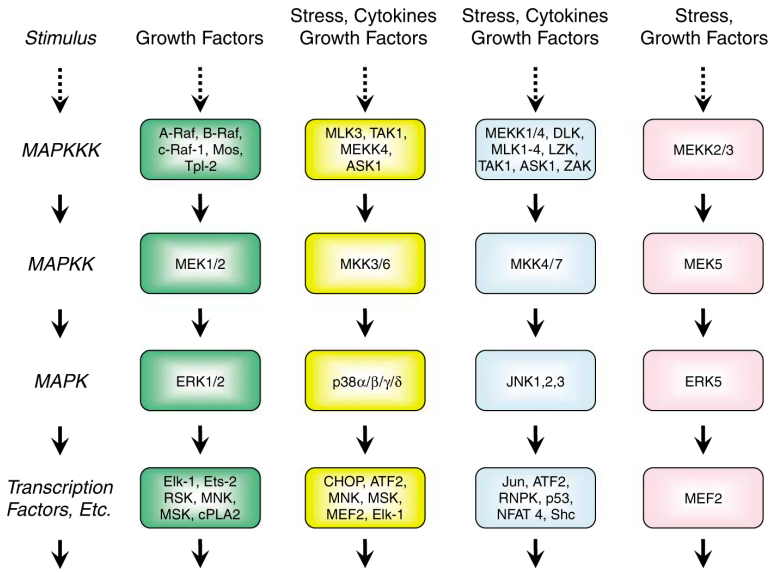

Figure 1.13: Mammalian MAPK cacades. There are four major mammalian MAPKKK–MAPKK–MAPK protein kinase cascades. Many of the substrates for MAPKs are nuclear transcription factors. Interactions and substrates were compiled from information from STKE (http://stke.sciencemag.org/index.dtl).

ERK1/2 MAP kinases are activated by virtually all growth factors and cytokines acting through receptor tyrosine kinases, cytokine receptors or G protein-coupled receptors (Figure 1.14). Typically, ligand binding to receptor tyrosine kinases induces dimerization of the receptor and autophosphorylation of specific tyrosine residues in the C-terminal region. This generates binding sites for adaptor proteins, such as growth factor receptor-bound protein 2 (GRB2), which recruit the guanine nucleotide exchange factor Sos at the plasma membrane. Sos activates the membrane-bound Ras by catalyzing the replacement of GDP with GTP. In its GTP-bound form, Ras recruits Raf kinases (ARAF, BRAF and CRAF) to the plasma membrane, where they become activated by a complex interplay of phosphorylation events and protein-protein interactions. Raf acts as a

MAPKKK and activates the MAPKKs MEK1 and MEK2, which, in turn, catalyze the activation of the effector MAP kinases ERK1 and ERK2.[162] Once activated, ERK1/ERK2 phosphorylate a panoply of nuclear and cytoplasmic substrates involved in diverse cellular responses, such as cell proliferation, survival, differentiation, motility, and angiogenesis.[163]

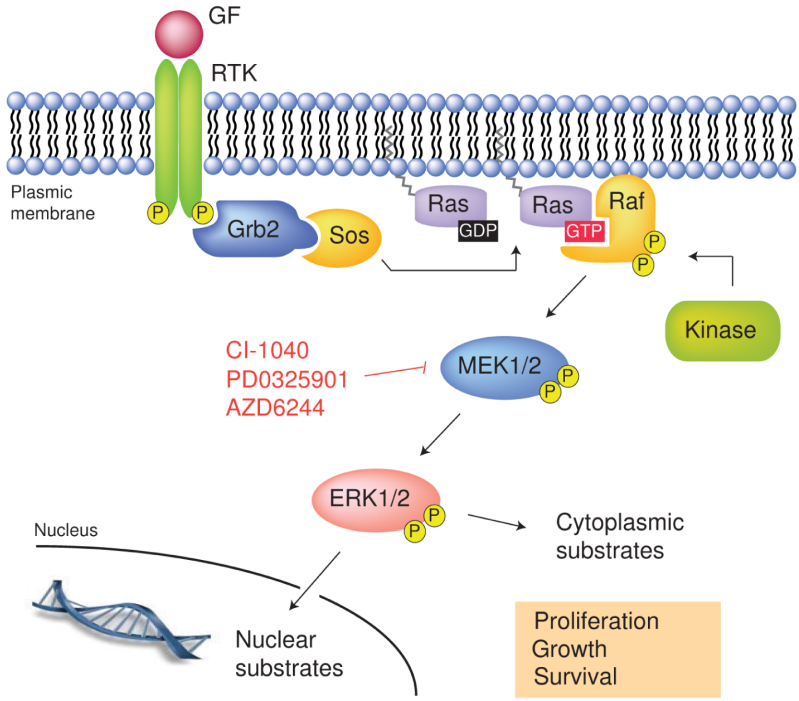

Figure 1.14: Schematic representation of the Ras-Raf-MEK-ERK1/2 MAP kinase pathway. The figure shows the cascade of activation of the MAP kinases ERK1/ERK2 mediated by growth factor binding to receptor tyrosine kinases. See text for details. GF, growth factor; RTK, receptor tyrosine kinase.

1.7.1 The ERK1/2 MAP kinase pathway is a key regulator of cell proliferation and survival

Multiple lines of evidence have implicated the ERK1/2 MAP kinase pathway in the control of cell proliferation.[164] ERK1 and ERK2 are activated in response to virtually all mitogenic factors. Several studies have reported that the mitogenic response to growth factors is correlated with their ability to induce sustained ERK1/2 activity.[165] These early findings were confirmed by subsequent RNA interference-based studies showing that silencing of ERK1/ERK2 expression inhibits the proliferation of various cell types.[166,167] Treatment with small molecule inhibitors of MEK1/MEK2 was reported to inhibit the proliferation of a variety of cell types.[168] Reciprocally, expression of constitutively-active forms of MEK1 was sufficient to stimulate cell proliferation and relax growth factor dependency.[169] ERK1/2 signaling is required for the progression of cells from the G0/G1 to S phase.[164,170] Activation of the ERK1/2 pathway is associated with induction of the positive cell cycle regulators cyclin D1[171] and c-Myc,[172] and with down-regulation of anti-proliferative proteins such as Tob1,[173] Foxo3a[174] and p21.[175] In addition to its direct role in the cell division cycle, the ERK1/2 MAP kinase pathway also regulates cell growth by stimulating protein and nucleotide biosynthesis.[176] One mechanism by which the ERK1/2 pathway increases global protein translation is through

phosphorylation and inactivation of tuberin (also known as TSC2), a negative regulator of mTOR, resulting in increased mTOR signaling.[177] Studies in several experimental systems have highlighted the important role of the Raf-MEK-ERK1/2 MAP kinase pathway in the control of cell survival.[178,179] Early studies have shown that activation of the ERK1/2 pathway prevents apoptosis induced by growth factor withdrawal, loss of matrix attachment or cytoskeletal disruption in cultured cells.[180,181] These findings were reinforced by genetic studies showing that loss of ERK1/ERK2 or MEK1/MEK2 induces cell death in various mouse tissues.[182] ERK1/2 signaling promotes cell survival by repressing the expression or activity of pro-apoptotic Bcl-2 family proteins, such as Bim and Bad, and by inducing the expression of prosurvival members like Bcl-2 and Mcl-1.[179]

1.7.2 Hyperactivation of the ERK1/2 MAP kinase pathway in cancer

Given the central role of the Raf-MEK-ERK1/2 signaling pathway in cell proliferation and survival signaling, it is therefore not surprising that alterations in this pathway are highly prevalent in human cancer. Multiple genetic changes can lead to hyperactivation of the ERK1/2 pathway in cancer. Aberrant activation of receptor tyrosine kinases such as the epidermal growth factor (EGF) receptor, as a result of gene amplification or gain of function mutations, is frequently observed in carcinomas and brain tumors.[183] Activating mutations in RAS genes, most often in KRAS, are found in ~30% of cancers and are generally acquired early in the tumorigenic process.[184] More recently, large-scale resequencing studies have revealed that BRAF is mutated in ~20% of all cancers and in more than 40% of melanomas.[185] The majority of these mutations are clustered in the kinase domain of B-Raf and lead to the stimulation of ERK1/2 activity in cells.[186] It is noteworthy that RAS and BRAF mutations are generally mutually exclusive in tumors, suggesting an epistatic relationship. Also, activating mutations in MEK1 gene are found at low prevalence in lung carcinomas, melanomas and colon carcinomas.[187,188] However, no mutation in the ERK1 or ERK2 gene has been reported to date in tumors. Consistent with these observations, numerous studies using clinical specimens have documented the hyperactivation of MEK1/MEK2 and ERK1/ERK2 in solid tumor and hematological malignancies.[189,190] Preclinical pharmacological studies have demonstrated that blockade of the ERK1/2 pathway with small-molecule MEK1/2 inhibitors markedly restrains the proliferation of various carcinoma and leukemic cell lines by inducing cell cycle arrest and apoptosis.[191] In vivo studies further established that administration of orally available MEK1/2 inhibitors elicits significant tumor regression in mouse xenograft models.[192] The strategic position of MEK1 and MEK2 in the Ras-dependent ERK1/2 pathway in conjunction with a promising preclinical profile have provided strong rationale for the development of small molecule inhibitors of MEK1/2 for chemotherapeutic intervention in cancer.[190]

1.7.3 Raf inhibitors

Therapeutic strategies that target Raf seem ideally suited to address the high percentage of human cancers displaying constitutive activation of the MAP kinase pathway. Therapeutic approaches include inhibitors of chaperone proteins, eg, Hsp90, which act to indirectly inhibit Raf by destabilization of the protein leading subsequently to its degradation. The impressive efficacy of

geldanamycin analogs, which are naturally occurring antibiotics, is well documented but likely results from their broader pleiotropic effects.[193] Few small-molecule Raf kinase inhibitors have been reported. Both L-779450 and SB203580 have been shown to be more effective at inhibiting c-Raf than B-Raf.[194,195]

To date, the most successful anti-Raf inhibitor has been sorafenib (BAY 43-9006; Nexavar), an orally available compound that received FDA approval in 2005 for the use in advanced renal cell carcinoma (RCC). Sorafenib is a bi-aryl urea compound[196] that was originally developed as an inhibitor of Raf-1.[197] Subsequent analysis revealed that sorafenib was a potent inhibitor of both wild-type and mutant (eg, V600E, the most frequent mutation found in human cancers) B-Raf kinases in vitro. Crystallographic analyses of sorafenib complexed with the kinase domain of B-Raf showed that the inhibitor bound to the ATP-binding pocket and prevented kinase activation, thus preventing substrate binding and phosphorylation (Figure 1.15).[198] Shortly after clinical analyses begin, it was revealed that sorafenib also showed very potent activity for other protein kinases in vitro and in vivo, in particular, for the proangiogenic RTKs such as VEGFR-2, VEGFR-3, PDGFR-β, Flt-3, c-Kit and FGFR-1.[199] In cell culture and mouse models representing a wide range of tumor cell types, sorafenib exhibited broad antitumor activity and was associated with reduced MEK and ERK activation, supporting the possibility that its antitumor activity involves, in part, inhibition of Raf.[199] However, despite its association with reduced ERK activation, sorafenib antitumor activity must also be a consequence of its ability to inhibit angiogenesis-related kinases as well as other non-Raf kinases. This possibility is supported by the potent antitumor activity that was independent of Ras or B-Raf mutation status that was seen with sorafenib in xenograft studies

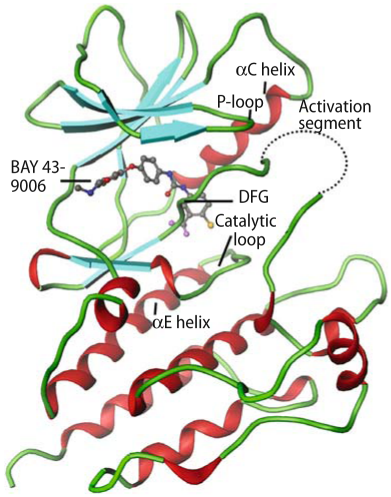

Figure 1.15: Ribbon diagram of the B-Raf kinase domain bound to BAY43-9006. The amino terminus lobe is composed primarily of anti-parallel β-strands, including the phosphate binding loop (P-loop) responsible for functional binding of ATP. The kinase activation segment contains the Raf family conserved phosphorylation sites, T491 and S494. In this crystal structure, the Raf activation segment is disordered and indicated here with a dotted line. The carboxyl-terminal lobe is primarily composed of α-helices. The α-helix E (αE helix) functions to position the C-terminal catalytic residues in the proper orientation for the binding of MEK substrate and the phosphotransfer reaction. The Raf inhibitor BAY43-9006 is shown here binding in the kinase active site located between the two lobes.

Phase I clinical trials established sorafenib as a safe and well-tolerated oral agent with skin rash and diarrhea as the most common adverse effects.[200] Results from phase I clinical trials suggested clinical activity in several patients with RCC, resulting in subsequent clinical trials focused on RCC. In addition, several single agent and combination clinical studies are ongoing in hepatocelluar carcinoma, non-small-cell lung cancer, prostate cancer, breast cancer, ovarian cancer, pancreatic cancer, melanoma and hematological malignancies.[201] The results of clinical trial analyses of sorafenib have not provided sufficient information to conclude that inhibition of Raf provides a clinical value. Although preclinical cell culture and mouse model analyses showed that continued expression of mutant B-Raf is critical for melanoma growth and tumorigenicity, phase II clinical trial analyses with sorafenib observed little or no antitumor activity when evaluated as monotherapy for advanced melanomas.[202] Some clinical efficacy had been seen for melanomas when sorafenib was used in combination, with clinical trials ongoing for advanced melanomas with sorafenib combination with bevacizumab or carboplatin and paclitaxel. The clinical success of sorafenib has prompted a debate regarding the advantages and disadvantages of highly specific versus broad specificity inhibitors.[203] As cancer is a multistep process, requiring multiple alterations, it is expected that effective cancer treatment requires concurrent activities that target different defects.[160] The greater success of combination chemotherapy is consistent with this premise. The ability to optimize the pharmacokinetics and pharmacodynamic properties of a single agent with multiple activities is also a great advantage for the successful clinical development of a drug. In the development of sorafenib, the intention was the identification of a Raf inhibitor, with the activity against other protein kinases fortuitous and unplanned. Hence, this has complicated a full understanding of the mechanism of action of sorafenib and the importance of its anti-Raf activities for its clinical efficacy. Therefore, whether blocking Raf will be a clinically effective approach will require future clinical evaluation of more specific and potent Raf kinase inhibitors. The clinical success of highly selective protein kinase inhibitors, in particular monoclonal antibody (mAb)-based drugs (eg, trastuzumab, bevacizumab), demonstrates that there is clinical value for both highly selective and multitargeted inhibitors.

2. OBJECTIVES

A significant proportion of Hodgkin lymphoma (HL) patients refractory to first-line chemotherapy or relapsing after autologous transplantation are not cured with currently available therapies. Phosphoinositide 3-Kinase/Akt (PI3K/Akt) and mitogen activated protein kinase (MAPK) signaling pathways regulate many cellular processes, and dysregulation of these signaling cascades is often found in HL. These pathways can be targeted using the AKT inhibitor perifosine (Æterna Zentaris GmBH, Germany, EU), and the RAF/MEK/ERK inhibitor sorafenib (Nexavar, Bayer, Germany, EU).

We hypothesized that perifosine in combination with sorafenib might have a therapeutic activity in HL. The proposed project was aimed at investigating in vitro and in vivo the activity and mechanism(s) of action of perifosine in combination with sorafenib by using three HL cell lines (HD-MyZ, L-540, HDLM-2).

- The effects of perifosine and sorafenib on cell growth and survival, used as single agents or in combination, were evaluated in vitro in HL cell lines. Tumor cells were exposed to increasing concentrations of each agent and the combined treatment. At the end of the incubation, viable cell countings and apoptosis assays were carried out. To investigate the mechanism(s) of action of perifosine/sorafenib, Western blot, mitochondrial depolarization, protein arrays, cell cycle and gene expression profiling analysis were assessed.

- Additionally, the antitumor efficacy and mechanism(s) of action of perifosine/sorafenib were investigated in vivo in nonobese diabetic/severe combined immunodeficient (NOD/SCID) mice. The antitumor activity were evaluated by comparing the survival (Logrank test) of treated mice with those of mice treated with the drug solvent. Furthermore, tumor-bearing NOD/SCID mice were treated with perifosine and sorafenib alone or in combination. Subsequently, tumor nodules were excised and tumor cells were analyzed by means of the appropriate immunohistochemical procedures. Apoptosis and necrosis were evaluated by the TdT-mediated dUTP nick and labeling (TUNEL) staining method. Image analysis were carried out using the open source ImageJ software.

3. MATERIAL AND METHODS

3.1 REAGENTS

Sorafenib (BAY43-9006) was purchased from Bayer Schering Pharma (Berlin,Germany, EU). Perifosine was obtained from Aeterna Zentaris (Frankfurt, Germany, EU). The pan-caspase inhibitor Z-VADfmk was purchased from R&D Systems (Minneapolis, USA). Tetramethylrhodamine ethyl ester (TMRE) were purchased from Invitrogen (Milan, Italy, EU). All reagents were formulated as recommended by their suppliers.

3.2 CELL LINES

HD-MyZ, HDLM-2 and L-540 HL cell lines were purchased from the German Collection of Microorganisms and Cell Cultures (DSMZ, Braunschweig, Germany, EU). Cell lines were cultured in RPMI-1640 (Lonza, Basel, Switzerland) supplemented with 10-20% (v/v) inactivated fetal bovine serum (FBS) (Lonza), 1% (v/v) L-glutamine (Lonza) in a humidified chamber (95% air, 5% CO_2) at 37°C. All cell lines were regularly screened to ensure absence of mycoplasma contamination by MycoAlert® Mycoplasma Detection Kit (Lonza), according to the manufacturer's instructions.

3.3 EXPERIMENTAL FORMAT

The proposed project is aimed at investigating in preclinical models, in vitro and in vivo, the anti-lymphoma activity of combination of perifosine and sorafenib. This is expected to provide a clear rationale to early-phase clinical trials using lymphoma-eradicating combinations of targeted agents. The aim of the project was pursued through the following phases:

- **Phase 1 - In vitro anti-lymphoma effects and mechanism(s) of action of perifosine and sorafenib used as single agent or in combination.** Three HL cell lines (HD-MyZ, HDLM-2 and L-540) were used to investigate the effects of perifosine and/or sorafenib on cell growth and survival. Firstly, tumor cells were exposed to increasing concentrations of each agent (0 – 10 μM) for dose-response assay, secondly HD-MyZ cell line was exposed to (2.5 μM) perifosine and/or (2.5 μM) sorafenib, whereas L-540 and HDLM-2 cell lines were treated with (5 μM) perifosine and/or (5 μM) sorafenib for proliferation and viability assays. To perform the different experiments, an appropriate number of cells according to the type of experiments were seeded in culture plates or flask (Costar, Corning Incorporated, NY, USA). Next day, drugs were added every 24 hours to the media at the concentrations indicated in each experiment. HD-MyZ and HDLM-2 cells were simultaneously treated with the indicated drug concentrations; L-540 cells were sequentially treated with perifosine for 24 hours followed by sorafenib for an additional 24 and 48 hours. At the end of the incubation, viable cell countings and apoptosis assays were carried out. To investigate the mechanism(s) of action of targeted agents, cell cycle analysis, caspase activation assays, mitochondrial membrane depolarization ($\Delta\Psi_m$), Western blot analysis, protein arrays, and gene expression profiling were used.

- **Phase 2 - In vivo anti-lymphoma activity of perifosine in combination with sorafenib**. For testing the antitumor activity of the compounds, the best route of administration and the maximal tolerated doses of the compounds as single agents and in combination, were first chosen. The compounds were administered, according to the selected doses and schedules, to mice with advanced lymphomas (start of treatment when subcutaneous (SC) tumors were palpable or a 3 days after IV tumor injection). The antitumor activity was evaluated by comparing the weight of tumors (Student's t test) and the survival (logrank test) of treated mice with those of mice treated with the drug solvent. Five mice per group were treated and each experiment was performed at least twice.
- **Phase 3 - In vivo anti-lymphoma mechanism(s) of action perifosine/sorafenib.** Tumor-bearing NOD/SCID mice were treated with the appropriate combination of targeted agents as established in Phase 2. Subsequently, 5 days following treatment, tumor nodules were excised and tumor cells were analyzed by means of the appropriate immunohistochemical procedures. Apoptosis and necrosis were evaluated by the TdT-mediated dUTP nick end labeling (TUNEL) staining method. Images of tissue sections were acquired at 2 – 20x magnification with an automatic high-resolution scanner (dotSlide System, Olympus, Tokio, Japan) and subdivided in a collection of non-overlapping RGB images in TIFF format. Image analysis will be carried out using the open source ImageJ software (Rasband, W.S., ImageJ, U.S. National Institutes of Health, Bethesda, MD, USA, http://rsb.info.nih.gov/ij/).

3.4 PROLIFERATION AND VIABILITY ASSAYS

3.4.1 Viable cell counting

HD-MyZ, L-540 e HDLM-2 cell lines ($0.2 – 0.4 \times 10^6$/mL) resuspended in FBS-supplemented culture medium were exposed to perifosine, sorafenib or control vehicle for 48 – 72 hours. At the end of incubation, viable and dead cells were identified by Annexin-V/Propidium Iodide (PI) staining and flow cytometry analysis. To obtain absolute cell counts, cell samples were supplemented with Flow-Count beads (Beckman Coulter, Milan, Italy, EU) and stained with PI. Cell counts per μl were calculated by the following equation: viable cells (Annexin-V^-/PI^-) × total beads/counted beads.

3.4.2 Assesment of apoptosis

The Annexin-V–fluorescein isothiocyanate (FITC) assay (Immunostep, Salamanca, SP, EU) was used to detect cell death by apoptosis or necrosis after 48 – 72 hours exposure to perifosine and sorafefenib used as single agent or in combination. Briefly, cells were washed twice with cold phosphate-buffered saline (PBS) (BioWhittaker, Lonza, Verviers, Belgio, EU), resuspended in binding buffer (10 mM HEPES, 140 mM NaCl, 5 mM $CaCl_2$, pH 7.4), and incubated with Annexin-V–FITC. At the end of the incubation, PI was added. Samples were acquired by setting photomultiplier tubes on the autofluorescence of the related negative control. All plots were gated on high Forward Scatter (FSC) and low Side Scatter (SSC) to exclude cell debris. A minimum of 50,000-gated events was collected per sample. Data were acquired on a BD fluorescence-activated cell sorting

(FACS)Calibur using BD CellQuest software version 3.3 (Becton Dickinson, Lincoln Park, NJ) and analyszed by FlowJo 8.7.1 software version for Macintosh (Tree Star, Inc. Ashland,OR). Annexin-V/PI double staining allows quantification of early (Annexin-V^+/PI^-) and late (Annexin-V^+/PI^+) apoptotic cells, as well as necrotic cells (Annexin-V^-/PI^+).

3.4.3 Cell cycle analysis

Cell cycle distribution was analyzed by DNA staining with the fluorescent dye Propidium Iodide (PI) and measured by flow cytometry. HD-MyZ, L-540 e HDLM-2 cell lines (1×10^6) were cultured in the absence or in the presence of perifosine and sorafenib used as single agents or in combination for 48 hours. All cells were washed with PBS and fixed in 70% ethanol and kept at 4°C before DNA staining with PI. Fixed cells were washed with PBS to remove ethanol, stained with 2.5 μg/ml PI (Calbiochem, Darmstadt, Germany) in the presence of 12.5 μg/ml RNAse (Sigma-tau, Rome, Italy), and incubated overnight at 4°C before analysis. The number of cells at different cell cycles was measured by a (FACS)Calibur flow cytometry system (B-D). The histograms were analyzed with FlowJo software (Tree Star).

3.4.4 Measurement of mitochondrial membrane depolarization ($\Delta\Psi_m$)

Mitochondrial membrane depolarization ($\Delta\Psi_m$) was determined by using the fluorescent probe TMRE (Invitrogen, Oregon, USA).[204,205] Briefly, cells (1×10^6/mL) were incubated with 50 nM TMRE (37°C, 10 minutes) in the dark and analyzed by flow cytometry using a (FACS)Calibur flow cytometry system (B-D). The fluorescent dye TMRE is accumulated by mitochondria and as a results of mitochondrial membrane depolarization, a shift to the left in the emission spectrum by apoptotic cells can be detected. Percentual of $TMRE^-$ cells were analyzed with FlowJo software (Tree Star).

3.4.5 Caspase inhibition assay

To gain a better understanding of the mechanism of apoptosis potentiated by perifosine and sorafenib, effects of these agents alone or in combination on caspase-dependent and -independent apoptosis were investigated. L-540 cell line were coltured in the presence or absence of the pan-caspase inhibitor, Z-VADfmk (50 μM) (R&D Systems, Abingdon, UK, EU) administered 1 hour prior to treatment with perifosine and sorafenib used alone or in combination. After 48 – 72 hours exposure to perifosine and sorafenib dead cells and mitochondrial membrane depolarization were analyzed by flow cytometry for staining with Annexin-V/PI and TMRE (see paragraphs 3.4.2, 3.4.4).

3.5 SUBCELLULAR FRACTIONS AND WESTERN BLOT ANALYSIS

Total proteins were extracted from 5×10^6 HD-MyZ, L-540 and HDLM-2 cells cultured without or with perifosine, sorafenib or perifosine/sorafenib. At different time points, cells were collected, washed in ice-cold PBS (Lonza), and homogenized in NP-40 lysis buffer (1% NP-40, 20 mM Tris-HCl pH 8, 137 mM NaCl, 10% glycerol, 2 mM EDTA, 1 mM sodium orthovanadate, 10 μg/mL aprotinin, 10 μg/mL leupeptin). Mitochondrial/Cytosolic fractions were obtained with a

Mitochondria/Cytosol Fractionation Kit (Biovision, CA, USA) according to the manufacturer's instructions. The purity of mitochondrial and cytosolic fractions was determined by Western blot analysis using anti-HSP60 antibody (Cell Signaling, Danvers, MA, USA). Protein concentrations were determined using the Bradford protein assay (Bio-Rad Laboratories, Milano, Italy, EU). Cell lysates (40 μg) were resolved by electrophoresis on 10 – 12% precast polyacrylamide gels (Bio-Rad) and transferred to nitrocellulose membranes (Amersham, Pittsburgh, PA). After the membranes were blocked in Tris-buffered saline solution (0.1% Tween-20 (TBS-T), 1% bovine serum albumin (BSA) and 3% ovalbumin) (Sigma-Aldrich, Milano, Italy, EU), blots were hybridized overnight with the appropriate primary antibody. After hybridization with horseradish peroxidase (HRP)-conjugated secondary antibody, immunocomplexes were visualized using an enhanced chemiluminescence Western blotting detection system (Amersham Biosciences, Milan, Italy, EU). Blotting analysis was performed using anti- AIF, -Cytochrome c, -Mcl-1, anti-phospho-MEK, -ERK, -AKT(T308), -S6, anti-p38α and anti-caspase-8 antibodies (Cell Signaling), anti-caspase-3 antibody (Santa Cruz, San Diego, CA, USA), anti-caspase-9, anti-poly(ADP-ribose)polymerase (PARP) antibodies (B-D) and anti-TRIB3 (Sigma-Aldrich) antibody. To normalize the amount of loaded protein, all blots were stripped and reprobed with rabbit polyclonal antibody anti-β-actin (Amersham Biosciences). Full-range Rainbow molecular marker (12-225 kDa, Amersham, GE Healthcare) was run in parallel in each sodium dodecyl sulphate - polyAcrylamide gel electrophoresis (SDS-PAGE) analyses. Images were acquired on ArtixScan F1 scanner (Microtek International Inc., Hsin-Chu, Taiwan) using SilverFast Launcher software (MicrotekSDK) and processed with Photoshop CS4 software (Adobe Systems Incorporated, San Jose, CA). Quantitation was done using ImageJ software (NIH). The values indicated above each protein band represent densitometric ratios of cells treated with perifosine, sorafenib or the combination and the control vehicle-treated cells, normalized to β-actin.

3.6 PHOSPHO-KINASE PROTEOME PROFILER ARRAY

To assess the basal phosphorylation levels of serine/threonine/tyrosine kinases in the PI3K/Akt signaling pathways of HD-MyZ, L-540 and HDLM-2 cell lines, we used the human phospho-Kinase proteome profiler array (R&D Systems, Minneapolis, MN, USA) in accordance with the manufacturer's protocol. Briefly, exponentially growing cell lines (10^7 cells) were washed with ice-cold DPBS and solubilized in NP-40 lysis buffer (1% NP-40, 20 mM Tris-HCl pH 8, 137 mM NaCl, 10% glycerol, 2 mM EDTA, 1 mM sodium orthovanadate, 10 μg/mL aprotinin, 10 μg/mL leupeptin) by gently rocking the lysates (30 minutes, 4°C). Cell lysates were then centrifuged (14,000 rpm, 5 minutes, 4°C), and supernatants were transferred into a clean test tube to determine protein concentrations using the Bradford protein assay (Bio-Rad Laboratories), followed by storage at -80°C until use. According to the manufacturer's instructions, equal amounts of proteins (200 μg) from basal control cells were incubated with the human phospho-Kinase array kit. The following kinases were detected: Akt (S473), Akt (T308), TOR (S2448), GSK-3α/β (S21/S9), p70S6Kinase (T229), p70S6Kinase (T389), p70S6Kinase (T421/S424). Phospho-Kinase array data developed on X-ray films (Amersham Biosciences) following exposure to chemiluminescent reagents were scanned

and analyzed using the open source imaging software ImageJ (NIH). The assays were conducted in duplicate, using samples from independent experiments, and produced similar results. A background value was determined for each array, using negative controls and empty spots positioned in clear areas. This average background signal was subtracted from each spot to normalize the values obtained.

3.6.1 Densitometric analysis

Autoradiography protein array films were scanned by ArtixScan F1 scanner (Microtek International Inc.) to quantitative Akt (S473), Akt (T308), TOR (S2448), GSK-3α/β (S21/S9), p70S6Kinase (T229), p70S6Kinase (T389), and p70S6Kinase (T421/S424) expression, and the images were quantified using ImageJ software (NIH). Below there is a brief schematic representation of how to analyze proteome profiler array using ImageJ software. After selecting each lane with a rectangular selection (Figure 3.1, Step 1), ImageJ generates the lane profile plots (Figure 3.1, Step 2) where each peak of interest refers to the expression intensity of the respective dot blot. Then the software labels each measured peak with its size as a percent of the total size of the measured peaks (Figure 3.1, Step 3).

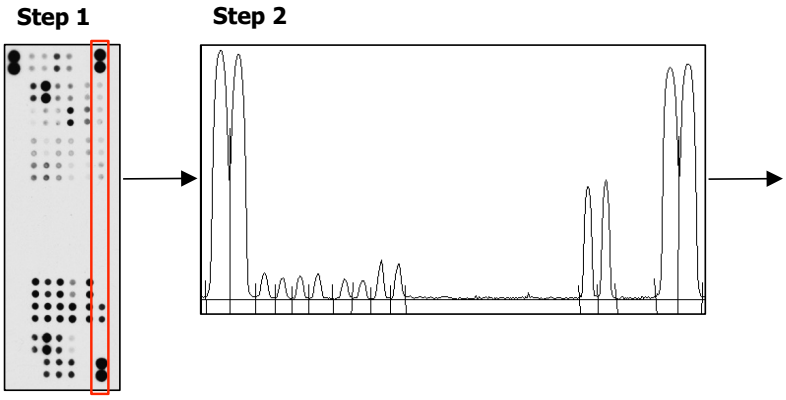

TARGET	Peak Area pixel	AVERAGE
Positive Control	3931.385 3571.385	3751.39
p38alfa	220.728 164.314	192.52
ERK1/2	174.899 197.607	186.25
JNK pan	154.607 147.899	151.25
GSK-3alfa/beta	254.607 252.607	253.61
p53 (S392)	936.435 951.728	944.08
Positive Control	3471.092 3775.385	3623.24
MEK1/2	287.021 282.314	284.67
MSK1/2	576.021 552.021	564.02
AMPKalfa1	277.314 322.021	299.67
Akt (S473)	99.607 101.314	100.46
Akt (T308)	1438.435 1415.728	1427.08
p53 (S46)	1292.849 1242.021	1267.44
TOR	409.435 413.021	411.23
Positive Control	3931.385 3571.385	3751.39

Figure 3.1: Schematic representation of ImageJ densitometric analysis.

3.7 GENOME-WIDE EXPRESSION PROFILING OF HODGKIN LYMPHOMA LINES TREATED WITH PERIFOSINE, SORAFENIB AND THEIR COMBINATION

Cells from three HL cell lines (HD-MyZ, L-540 and HDLM-2) were treated with perifosine (10 μM), sorafenib (5 μM), or their combination for 24 hours. Three biological replicates of untreated and drug-treated cells were set up. Total RNA was isolated using TriZol (Invitrogen) reagent, according to the manufacturer's instructions. After a clean-up treatment with RNAeasy kit following the

manufacture's recommendations (Qiagen, Milano, Italy, EU) and with RNase-free DNase to remove contaminating genomic DNA, RNA integrity and purity was assessed by Bioanalyzer (Agilent). Single-color hybridization of RNAs was performed on Illumina Bead Chip HumanHT-12_v3 Microarrays (Illumina San Diego, CA) containing more than 48,000 transcript probes. The expression profiles have been deposited in NCBI's Gene Expression Omnibus (GEO) with GSE accession number GSE31060. Background correction, filtering of data, and quantile normalization were done using the BeadStudio Illumina software. The BRB-array Tools (Vers.4.2.0) software was used to identify genes significantly modulated by any of the drug treatments. To this end, we carried out Class Comparison with a random-variance F-test analysis carried out at $P = .005$. Permutation P values for significant genes were computed based on 10,000 random permutations. Pairwise comparison for differential modulation of each gene by any two treatments was carried out at $P = .01$. Clustering of significantly modulated genes was done by Cluster 3.0 software using centered correlation as distance metric and complete linkage clustering. Heat maps were visualized by Java Treeview software. Ingenuity Pathway Analysis (IPA 8.5, www.ingenuity.com) was used to analyze the network connections, functions and canonical pathways of the identified genes.

3.8 REAL-TIME REVERSE TRANSCRIPTASE-PCR (RT-PCR)

Total RNA (1 μg) used for microarray experiments (for cell lines, independent RNA preparations were used) was reverse-transcribed using the High-Capacity cDNA Archive Kit (Applied Biosystems, Foster City, CA, USA). The expression of TRIB3, DDIT4, CCNE1, CDC25A, and PLEKHF1 genes was determined using a TaqMan based real-time PCR method. To analyze and quantify the levels of the TRIB3, DDIT4, CCNE1, CDC25A, and PLEKHF1 genes, we used a TaqMan isoform-specific probe (assay no. Hs01082394_m1; Hs01111686_g1; Hs01026536_m1; Hs00947994_m1; Hs00759096_s1, respectively) (Applied Biosystems). Amplification was performed using a total reaction volume of 25 μl in a MicroAmp Optical 96-well reaction plate. All real-time PCR reactions were carried out with TaqMan Universal Master Mix. Reactions were run on the ABI Prism 7000 sequence detection system (Applied Biosystems) using the following conditions: 50 °C for 2 min, 95 °C for 10 min, followed by 40 cycles of 95 °C for 15 s and 60 °C for 1 min. Quantification analysis was performed by the ΔΔCt method and statistically analyzed by GraphPad Prism software (GraphPad Software Inc., San Diego, CA, USA). Data were normalized to the expression levels of the housekeeping β2-microglobulina gene.

3.9 siRNA GENE SILENCING

L-540 cells were transfected with 100 nM Hs_TRIB3_5 FlexiTube siRNA premix-reagent or negative control siRNA premix-reagent (Qiagen, Milano, Italy, EU) following the instructions of the manufacturer. Cells (0.4×10^6/mL) were plated and transfected with the given siRNAs. After 24 hours, the cells were treated with perifosine and sorafenib as indicated. Gene silencing effects were evaluated by Western blot and Viable cell counting as described above after the indicated times of treatment.

3.10 IN VIVO EXPERIMENTAL MODEL

3.10.1 In vivo activity of perifosine/sorafenib in tumor-bearing non-obese diabetic/severe combined immunodeficient (NOD/SCID) mice

Six- to eight-week-old NOD/SCID mice with a body weight of 20 to 25 g were purchased from Charles River (Milano, Italy, EU) and xenografted with HD-MyZ, L-540, or HDLM-2 cell lines. Mice were housed under standard laboratory conditions according to our institutional guidelines. Animal experiments were performed according to the Italian laws (D.L. 116/92 and following additions), which enforce the EU 86/109 Directive, and were approved by the institutional Ethical Committee for Animal Experimentation. Mice were inoculated intravenously (IV) with HD-MyZ (1.8×10^6 cells/mouse). After 3 days HD-MyZ injection, mice were randomized in four groups (n=5/group, for a total of two different experiments) to receive per os (PO) injections of perifosine (7.5 mg/kg/mouse/5die/5weeks) and/or intraperitoneal (IP) injections of sorafenib (60 mg/kg/mouse/5die/5weeks), or control NaCl solution 0.9%. Endpoint of in vivo IV experiments was death.

HD-MyZ (5×10^6 cells/mouse), L-540 and HDLM-2 (25×10^6 cells/mouse) cells were inoculated subcutaneously (SC) in the right flank of each mouse. When tumor volume reached approximately 100 mg in weight (10 days after tumor inoculation), mice were randomly assigned to receive either a short- or long-term treatment with perifosine and/or sorafenib or control vehicle. The short-term treatment consisting of perifosine (30 mg/kg/mouse, PO) or sorafenib (90 mg/kg/mouse, IP) (alone or in combination) or control vehicle, for 5 days was used to assess necrotic and apoptotic areas.
For the long-term treatment 25×10^6 cells/mouse of L-540 and HDLM-2 cell lines were SC inoculated in the right flank of each mouse. After 7 and 11 days from tumor cells inoculum, mice were treated with perifosine (15 mg/Kg/mouse, PO) and/or sorafenib (30 mg/Kg/mouse, IP) or control vehicle 5 days per week for 3 weeks (days 7 – 25 from tumor inoculum for L-540 model; days 11 – 29 from tumor inoculum for HDLM-2 model). The endpoint of the long-term treatment was tumor weight. Mice were checked twice weekly for tumor appearance, body weight measurements and toxicity. The tumors were measured with calipers, and their weights were calculated using the formula: $(a \times b^2)/2$, where a and b represented the longest and shortest diameters, respectively. Antitumor efficacy was measured as tumor growth inhibition (TGI) defined as $[1 - (T/C) \times 100]$, where T and C are the mean tumor weight in the treated and untreated control groups, respectively. Each experiment was performed on at least two separate occasions, using five mice per treatment group.

3.10.2 Tumor sample processing

Paraffin-embedded tumor nodules were processed for immunohistochemistry and immunofluorescence analyis.
Tumor nodules were fixed in formalin (10% neutral buffered formalin) and embedded in paraffin under the following procedure.

Table 3.1: Tumor sample processing scheme.

REAGENT	ALTERNATING PRESSURE AND VACUUM	TIME (hours)	TEMPERATURE (°C)
Formalin	-	8	Room Temperature (RT)
Ethanol 70%	+	1	RT
Ethanol 95%	+	1,30	RT
Ethanol 95%	+	2	RT
Ethanol 100%	+	1	RT
Ethanol 100%	+	1,30	RT
Ethanol 100%	+	2	RT
Xylene	+	2	RT
Xylene	+	2	RT
Paraffin	+	1,30	60
Paraffin	+	1,30	60
Paraffin	+	2	60

Paraffin-embedded tumor nodules were cut in a microtome to the desired thickness (2 μm) and affixed onto the slide. Nodule sections were mounted on positively charged coated slides and dried (60°C for 1 hour) to remove any water that may be trapped under the section.

3.10.3 Histological analysis of tumor nodules

Sections from formalin-fixed, paraffin-embedded tumor nodules (thickness of 2 μm) were dewaxed, hydrated and stained with hematoxylin and eosin. Apoptosis and tumor necrosis were detected using TdT-mediated dUTP nick end-labeling (TUNEL) staining (Roche, Milano, Italy, EU) according to the manufacturer's instructions. Positive signal was revealed by 3,3'-diaminibenzidine staining and tumor sections were then counterstained with hematoxylin, rapidly dehydrated using graded ethanols to xylene, and mounted in a drop of fast-drying mounting medium.

3.10.4 Immunohistochemistry

Sections (2 μm thick) from formalin-fixed paraffin-embedded HL lymphonode blocks were dewaxed and hydrated. Epitope retrieval was performed with 2 mM EDTA pH 8 for 30 min at 95°C. Sections were then rinsed with PBS containing 0.05% Tween 20 and blocked with Ultra V Block (Thermo Scientific) for 10 minutes at RT. Rabbit anti-human phospho-S6 (1:80) (Cell Signaling), and rabbit anti-human phospho-ERK1/2 (1:60) (Cell Signaling) antibodies were incubated for 1 hour at RT. UltraVision LP detection system (Thermo Scientific) was used to reveal antigen positivity. Finally, after rinsing with PBS containing 0.05% Tween 20, sections were counterstained with hematoxylin, rapidly dehydrated using graded ethanols to xylene, and mounted in a drop of fast-drying mounting medium.

3.10.5 Immunofluorescence and confocal microscopy

Sections from formalin-fixed, paraffin-embedded tumor nodules (thickness of 2 μm) were dewaxed and hydrated. Epitope retrieval was performed with 10 mM Sodium Citrate buffer pH 6 for 10 min at 95°C. Sections were then rinsed with PBS containing 0.05% Tween 20 and blocked with Ultra V Block (Thermo Scientific) for 10 minutes at RT. Rabbit anti-human DDIT4 (1:50) (Sigma, St. Louis, MO, USA) and rabbit anti-human TRIB3 (1:100) (Sigma, St. Louis, MO, USA) antibodies were incubated for 1 hour at RT. After being washed in PBS containing 0.05% Tween 20, sections were incubated with the appropriate Alexa Fluor 568-conjugated secondary antibody (Invitrogen) for 30 minutes at RT. Finally, after rinsing with PBS containing 0.05% Tween 20, sections were incubated with TO-PRO-3 nuclear dye (1:10000) (Invitrogen) for 20 minutes at RT. After mounting in a drop of anti-bleaching mounting medium (Vectashield, Vector Laboratories, Burlingame, CA, USA), sections were examined under an epifluorescent microscope equipped with a laser confocal system (MRC-1024, Bio-Rad Laboratories, Milano, Italy, EU). Image processing was carried out using LaserSharp computer software (Bio-Rad Laboratories).

3.10.6 Analysis of stained sections

After TUNEL staining, entire tissue sections were acquired at 20× magnification with an automatic high-resolution scanner (dotSlide System, Olympus, Tokyo, Japan) and subdivided into a collection of non-overlapping red, green, and blue (RGB) images in TIFF format (final resolution 3.125 pixels/μm). For necrosis quantification images were acquired at 2x magnification without further subdivision. Image analysis was carried out using the open-source ImageJ software (http://rsb.info.nih.gov/ij/). Routines for image analysis were coded in ImageJ macro language and executed on RGB images without further treatment. Per each experimental condition, at least three sections from different tumor nodules were analyzed. The number of total and TUNEL+ cells per section was counted as follows. Briefly, the dynamic range of images was expanded to full by contrast enhancement, and cells were identified by appropriate filtering in the RGB channels. Resulting black and white images were combined to represent only pixels selected in every color channel. For each image, both total and TUNEL+ cells were counted by the ImageJ internal function for particle analysis. TUNEL-stained sections were also analyzed for the presence of necrotic areas. Images were at first treated for noise reduction by application of a median filter with a 1.5-pixel radius. Then, necrotic and total tissue areas were recognized using different filter values under direct human supervision. Black areas in the final binary images were quantified in terms of pixel counts to obtain a percent necrotic index expressed as (necrotic area)/(total tissue area) × 100. Per each parameter, the accuracy and appropriate cut-off levels were determined by comparing filtered, black and white images to the RGB originals. Automatic routines were validated by comparing results with those obtained by visual counting of up to 10% of the total images.

3.11 STATISTICAL ANALYSIS

Statistical analysis was performed with the statistical package Prism 5 (GraphPad Software, San Diego, CA, USA) run on a Macintosh Pro personal computer (Apple Computer Inc.). To test the probability of in vitro significant differences between untreated and treated samples, the two-way analysis of variance (ANOVA) was used, and individual group comparisons were evaluated by Bonferroni post-test. Survival curves were created using the product limit method of Kaplan-Meier and survival differences were compared using the logrank test. Tumour volume data from the in-vivo study were analysed with two-way analysis of variance (ANOVA), and individual group comparisons were evaluated by Bonferroni post-test. TUNEL staining data was statistically analyzed with one-way analysis of variance (ANOVA), and individual group comparisons were evaluated by Bonferroni post-test. Differences were considered significant if $P \leq .05$.

4. RESULTS

4.1 ACTIVATION OF THE MAPK AND PI3K/Akt SIGNALING PATHWAYS IN HODGKIN LYMPHOMA SAMPLES FROM HL PATIENTS

To examine activation of the MAPK and PI3K/Akt pathways in paraffin-embedded human Hodgkin lymphoma tissues, immunohistochemistry was performed on primary tumor samples from 2 HL patients using antibodies against phospho-ERK1/2 and phospho-S6.
For immunohistochemistry, staining of a nonmalignant reactive lymph node specimen was used as a positive control for phospho-ERK1/2 and phospho-S6 expression. Phosphorylation of phospho-ERK1/2 and phospho-S6 was detected in both HL lymphomas (Figure 4.1).

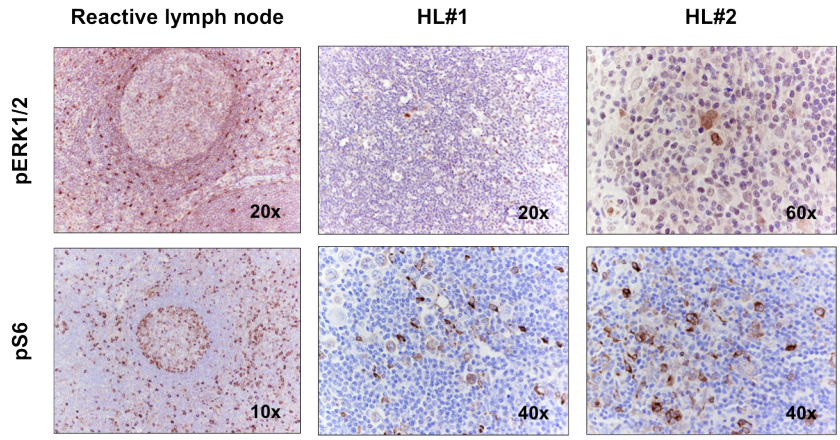

Figure 4.1: Activation of MAPK and PI3K/Akt signaling in HL. Constitutive activation of the MAPK and PI3K/Akt signaling pathways in patient samples of HL. Activation of ERK1/2 and S6 was assessed in HL tissue by immunohistochemistry with phosphospecific antibodies for ERK1/2 and S6. Shown is a section from a nonmalignant reactive lymph node and an example of two cases of classical HD.

4.2 BIOLOGICAL EFFECT OF PERIFOSINE AND SORAFENIB AS SINGLE AGENTS ON HL CELL LINES

To further characterize the in vitro effects of perifosine and sorafenib, we performed cell proliferation assays. To that end, we tested increasing concentrations of the drug in each cell line measuring cell proliferation by cell counting and viability experiments.

4.2.1 Growth inhibition by perifosine and sorafenib

The finding that the MAPK and PI3K/Akt signaling pathways are constitutively activated in primary HL tissue suggested that MAPK and PI3K/Akt dual-inhibition might inhibit growth of these cells. Three representative HL cell lines, HD-MyZ, L-540, and HDLM-2, were treated with increasing doses of perifosine and sorafenib (1 μM – 10 μM) for 48 and 72 hours and assessed for the effects on proliferation and survival (Figure 4.2A-B). We evaluated perifosine and sorafenib antitumor activity in term of annexin-V^-/PI^- cells after 48 – 72 hours. Whereas perifosine induced a dose- and time-dependent decrease of cell proliferation in two out of three cell lines, sorafenib reduced viable cell countings in all cell lines. The HD-MyZ cell line was the most sensitive to

perifosine, showing a 50% growth inhibition (IC_{50}) value of 6.1 μM after 72 hours (Figure 4.2A). The HDLM-2 cell line was the most resistant to perifosine, in which perifosine at 10 μM decreased cell survival by <20% at 72 hours without evidence of a dose-dependent effect (Figure 4.2A). All the tested cell lines exhibited moderate response to sorafenib with IC_{50}s ranging from 3 to 8 μM (Figure 4.2B) at 72 hours, which are within the clinically achievable and steady-state plasma levels of 15 to 20 μM.[200,206]

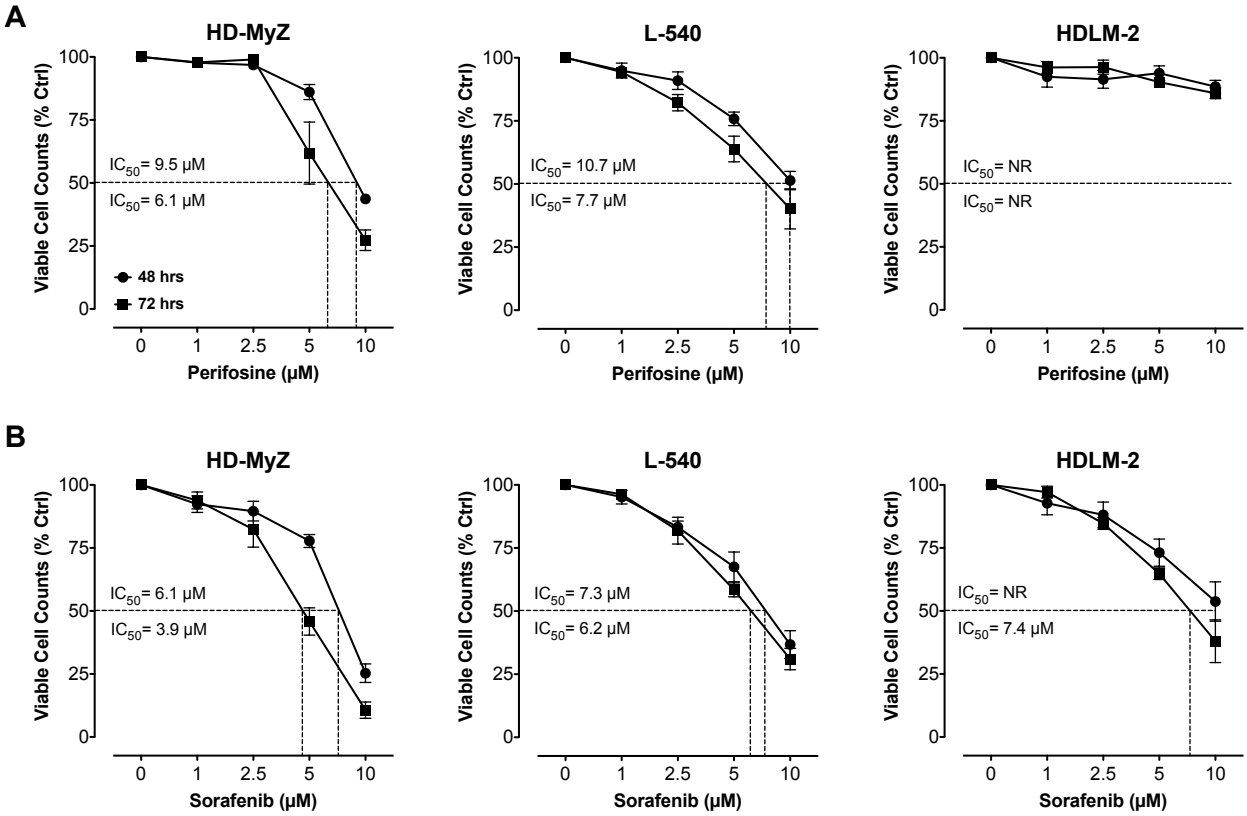

Figure 4.2: Effect of perifosine and sorafenib on growth of HD-MyZ, L-540 and HDLM-2 cells. HD-MyZ, L-540 and HDLM-2 cells were plated as described in "Materials and Methods" for the period indicated on the graph. Perifosine (**A**) or sorafenib (**B**) were added at increasing concentrations and compared with controls. After specified period of drug exposure (either 48 or 72 hours), absolute cell counts were obtained using Flow-Count beads and Annexin-V/Propidium Iodide (PI) staining. Viable cells are expressed as Annexin-V^-/PI^- cells. The fractions of viable cell counts in drug-treated cells are plotted against drug concentration. Each statistical error bar (± SEM) represents four independent experiments.

4.3 IN VITRO BIOLOGICAL EFFECT OF PERIFOSINE AND SORAFENIB AS COMBINED AGENTS IN HL CELL LINES

4.3.1 Perifosine and sorafenib combined treatment inhibit the growth of HL cells

To evaluate potential synergy, we used perifosine and sorafenib at concentrations below IC_{50} values. Both drugs were added simultaneously in the HD-MyZ and HDLM-2 cells, whereas with one drug preceding the other by 24 hours in L-540 cell line. As presented in Figure 4.3, the combination of

perifosine and sorafenib was more potent than each single agent alone in decreasing the survival of HD-MyZ and L-540 cells. Perifosine 2.5 μM and sorafenib 2.5 μM alone decreased the survival of HD-MyZ cells by less than 20%, whereas their combination decreased cell survival by greater than 40% at 72 hours (Figure 4.3). Viable cell counts was reduced by 50% following individual (5 μM) perifosine or (5 μM) sorafenib treatment and co-treatment further enhanced the reduction up to 74% in L-540 cell line at 72 hours (Figure 4.3). This enhanced effect was absent in HDLM-2 cells. This result further demonstrates that the combination of perifosine and sorafenib exhibits a more than additive (i.e., synergistic) effect on inhibition of cell growth.

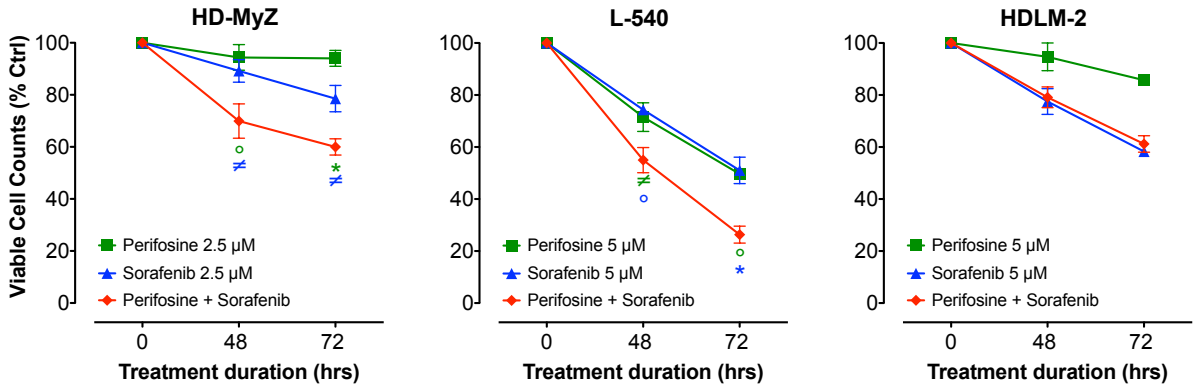

Figure 4.3: Coadministration of perifosine and sorafenib results in a marked cell growth reduction of Hodgkin lymphoma cells. HD-MyZ, L-540 and HDLM-2 cells were exposed to perifosine (■ green) and sorafenib (▲ blue) alone or in combination (u red) for 48 and 72 hours after which viable cell counts were obtained as described in Materials and Methods. Both drugs were added simultaneously in the HD-MyZ and HDLM-2 cells, whereas with perifosine preceding sorafenib by 24 hours in L-540 cell line. Mean (± SEM) values refer to three independent experiments. * P <.0001, ° P <.001, and ≠ P <.01, compared to single treatments (perifosine, green; sorafenib, blue).

4.3.2 Perifosine in combination with sorafenib enhances apoptosis in HL cells

We further examined if the cytotoxic effects of perifosine/sorafenib combined treatment were mediated through the induction of apoptotic cell death in HD-MyZ, L-540 and HDLM-2 cell lines. As shown in Figure 4.4, perifosine in combination with sorafenib induced a significant (P ≤.05 at least) increase in apoptotic cells only in L-540 cell line, compared to single treatments, as indicated by AnnexinV/PI staining. After 72 hours-exposure to concentrations of 5 μM perifosine and 5 μM sorafenib, the combination treatment induced cell death in 74% of L-540 cells, whereas apoptosis was induced only in 30% of the HDLM-2 cells, suggesting that the L-540 cells were more sensitive to perifosine/sorafenib-induced apoptosis (Figure 4.4). The HD-MyZ cells were resistent to perifosine and sorafenib-induced apoptosis both as single drugs and in combination.

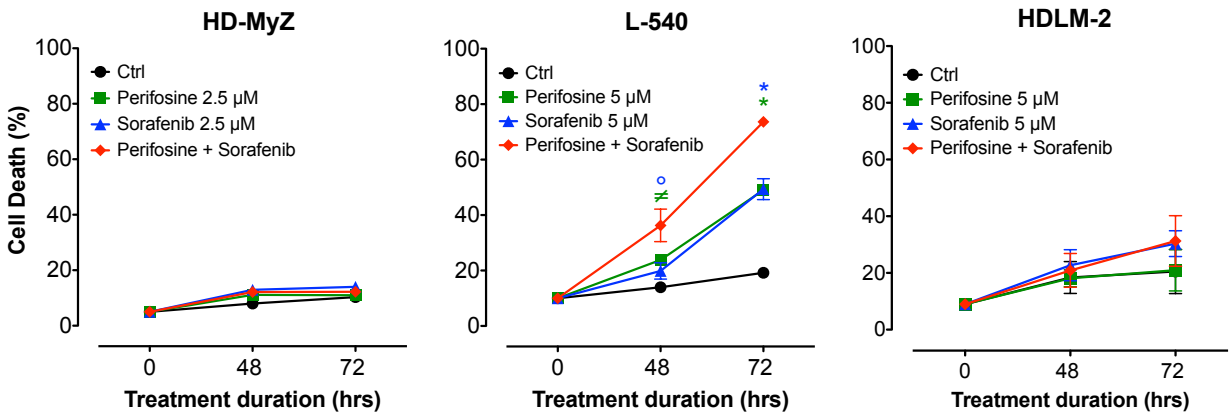

Figure 4.4: Coadministration of perifosine and sorafenib results in a striking increase in apoptosis of Hodgkin lymphoma cells. HD-MyZ, L-540 and HDLM-2 cells were exposed to perifosine (■ green) and sorafenib (▲ blue) alone or in combination (u red) for 48 and 72 hours after which the percentage of apoptotic cells was assessed by annexin-V/PI double staining and flow cytometry analysis as described in Materials and Methods. Both drugs were added simultaneously in the HD-MyZ and HDLM-2 cells, whereas with perifosine preceding sorafenib by 24 hours in L-540 cell line. Mean (± SEM) values refer to three independent experiments. * P <.0001, ° P <.001, and ≠ P <.01, compared to single treatments (perifosine, green; sorafenib, blue).

4.3.3 Effect of combined perifosine and sorafenib on cell cycle progression

Because perifosine in combination with sorafenib is effective in decreasing cell number in HD-MyZ and L-540 cells (Figure 4.3), we further examined cell cycle alteration in HD-MyZ, L-540 and HDLM-2 cell lines after exposure to perifosine and sorafenib used as single agents or in combination (Table 4.1).

Table 4.1: Modulation of the cell cycle profile by perifosine and sorafenib. Distribution of HL cells, cultured in the absence (Ctrl) or presence of perifosine and/or sorafenib, in the different phases of the cell cycle calculated from the flow cytograms after PI staining, and expressed as the percentage of the total population. Data are expressed as means ± SEM of results from three independent experiments. * P <.0001 and ≠ P <.05 compared to control, ° P <.01 and § P <.05 compared to single treatments.

CELLS	TREATMENT	sub-G0 (%)	G0/G1 (%)	S (%)	G2/M (%)
HD-MyZ	Ctlr	0.4 ± 0.01	34 ± 0.3	33 ± 1	32 ± 1
	Perifosine (2.5 μM)	0.5 ± 0.01	36 ± 0.6	29 ± 1	35 ± 1
	Sorafenib (2.5 μM)	0.6 ± 0.01	32 ± 0.4	33 ± 1	34 ± 1
	Perif/Soraf	1.7 ± 0.03	34 ± 2.6	**11 ± 2.5*≠**	**53 ± 3*≠**
L-540	Ctlr	4 ± 0.3	39 ± 4	37 ± 1	20 ± 6
	Perifosine (5 μM)	6 ± 0.8	33 ± 1	30 ± 2	30 ± 3
	Sorafenib (5 μM)	12 ± 0.3	35 ± 4	29 ± 0.5	24 ± 3
	Perif/Soraf	**18 ± 3≠**	51 ± 1	**15 ± 0.5*§**	15 ± 3
HDLM-2	Ctlr	3 ± 0.3	42 ± 0.7	35 ± 0.7	20 ± 0.1
	Perifosine (5 μM)	3 ± 0.6	35 ± 2.4	36 ± 0.2	25 ± 1.6
	Sorafenib (5 μM)	9 ± 0.9	50 ± 2.5	30 ± 0.5	10 ± 1.7
	Perif/Soraf	9 ± 1	46 ± 3.4	29 ± 1.5	14 ± 0.4

Cell cycle analysis revealed that perifosine/sorafenib treatment resulted in the accumulation of HD-MyZ-treated cells in the G2/M phase without induction of apoptosis (Figure 4.5). Proliferating control HD-MyZ cells yielded 34% cells in the G0/G1 phase, 33% cells in the S phase, and 32% cells in G2/M phase of cell cycle 48 hours after treatment. Concordant with the growth inhibition data (Figure 4.3), HD-MyZ cells were minimally perturbed by either 2.5 μM perifosine or 2.5 μM sorafenib, whereas the combination causes a consistent increase in G2/M (to 53%) along with virtual loss of the S-phase (11%) fraction, furthermore minimally increased the sub-G0 fraction, indicating that the perifosine/sorafenib-antiproliferative effect was predominantly due to a cytostatic, rather than a cytotoxic effect in the HD-MyZ cells (Figure 4.5). Similarly, cell cycle analysis of the L-540 cells (Figure 4.5) indicated that individual treatment of either perifosine or sorafenib (at 5 μM, respectively) had a marginal effect, whereas combined treatment of perifosine and sorafenib led also to virtual loss of the S-phase population and retention of G0/G1 populations after 48 hours. Therefore, we detected 38%, 33%, 35%, and 51% G0/G1 cells in L-540 cells treated with control vehicle, 5 μM perifosine, 5 μM sorafenib, and the combination treatment respectively, after 48 hours.

Interestingly, perifosine in combination with sorafenib significantly reduced the percentage of the cells in the S- and G0/G1-phases (15% and 51%, respectively) and strongly increased the sub-G0 fraction (18%) indicating that perifosine/sorafenib primarily decreases cell numbers in L-540 cells via cell cycle arrest with induction of apoptosis (Figure 4.5). No significant cell cycle alterations were assessed in HDLM-2 cell line, further supporting its resistance to perifosine/sorafenib-treatment (Figure 4.5). In the following studies, we focused on revealing the mechanisms underlying perifosine/sorafenib-induced apoptosis.

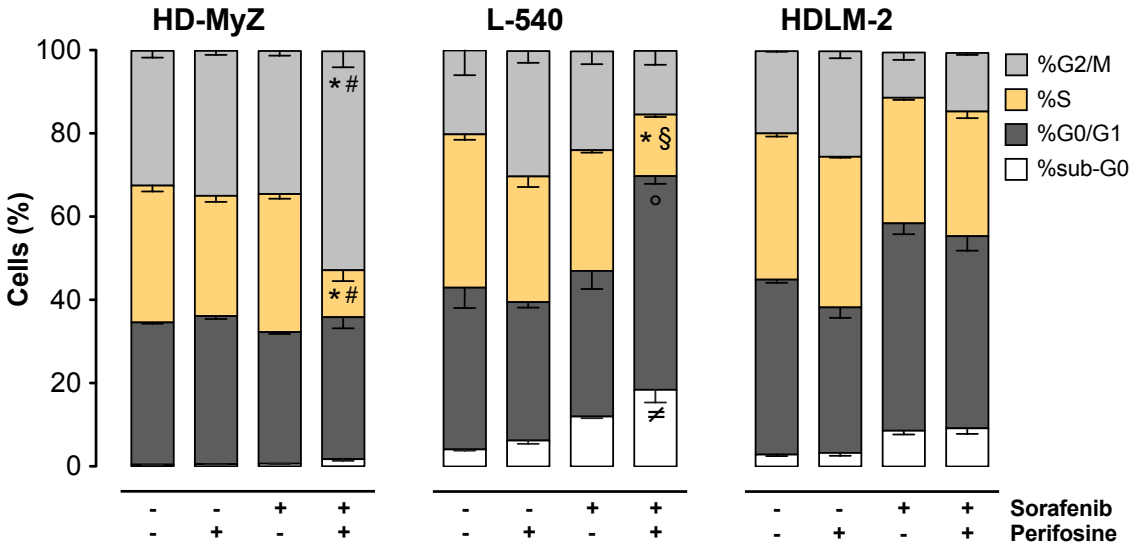

Figure 4.5: Perifosine/sorafenib treatment induced cell cycle arrest in HL cells. Cell cycle analysis of combined treatment of perifosine (2.5μM) and sorafenib (2.5μM) on HD-MyZ, and perifosine (5μM) and sorafenib (5μM) on L-540 and HDLM-2 cells after 48 hours. Flow cytometry was done to define the cell cycle distribution in comparison to untreated controls. Both drugs were added simultaneously in the HD-MyZ and HDLM-2 cells, whereas with perifosine preceding sorafenib by 24 hours in L-540 cell line. Mean (± SEM) values refer to three independent experiments. * P <.0001 and ≠ P <.05 compared to control, ° P <.01 and § P <.05 compared to single treatments.

4.4 MECHANISM OF PERIFOSINE/SORAFENIB-INDUCED CELL DEATH

4.4.1 Perifosine- and sorafenib-potentiated apoptosis was caspase-independent

Previous studies investigating the mechanism(s) of perifosine and sorafenib-induced apoptosis showed different pathways of cell death, involving both caspase-dependent[146,207] or caspase-independent[208,209] mechanisms. To gain a better understanding of the mechanism of apoptosis potentiated by perifosine and sorafenib in HL cells, effects of these agents alone or in combination on caspase-dependent and -independent apoptosis were investigated. Perifosine and sorafenib treatment had no marked effect on the activity of caspase 3, 8, 9 and PARP in HD-MyZ, L-540 and HDLM-2 cell lines at 48 hours (Figure 4.6).

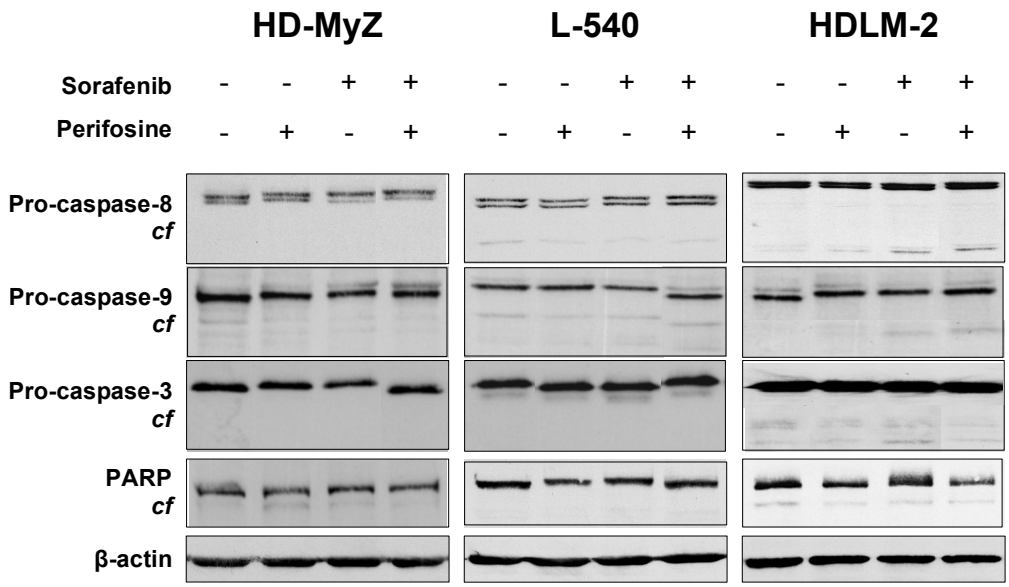

Figure 4.6: Perifosine in combination with sorafenib does not induce processing of the caspases or PARP. HD-MyZ, L-540 and HDLM-2 cells were treated with perifosine (5μM), sorafenib (5 μM) alone or in combination for 48 hours. Whole-cell lysates were obtained and Western blot analysis employed to monitor caspase cleavage/activation and PARP degradation. Equal protein loading was confirmed by blotting for β-actin. No processing of the caspases or PARP was observed. CF, indicates cleaved fragments.

The role of caspases in apoptosis potentiated by perifosine and sorafenib was further tested by pretreating L-540 cells with Z-VADfmk, a pan-caspase inhibitor. Consistent with its inhibition of caspase activity, Z-VADfmk significantly reduced the apoptosis induced by sTRAIL (10 ng/ml) from 47% to 16% (P <.0001) in KMS-11 cell line (data not shown); however, it had no apparent effect on apoptosis potentiated by the perifosine and sorafenib combination in L-540 cell line, further supporting that perifosine/sorafenib acts through a caspase-independent pathway (Figure 4.7).

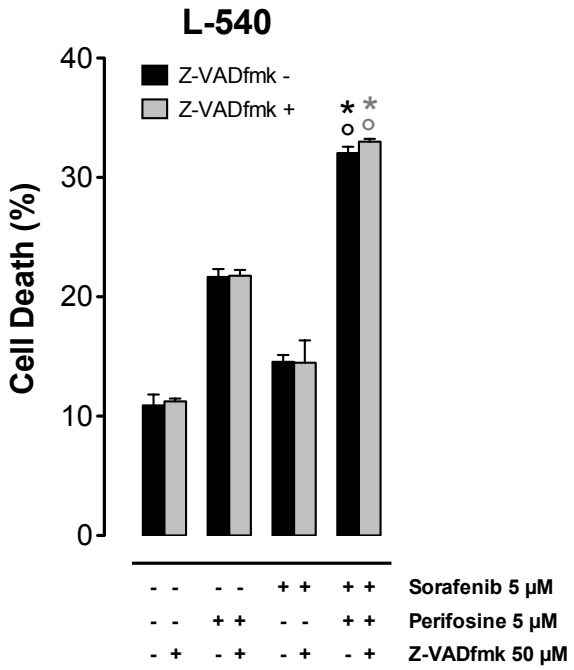

Figure 4.7: Combined exposure of HL cells to perifosine and sorafenib led to caspase-independent cell death. L-540 cells were pre-treated with 50 μM Z-VADfmk for 1 hours then treated with 5 μM perifosine ± 5 μM sorafenib for 48 hours. Following treatments, cell death was assayed by flow cytometry using the Annexin V/PI double staining. * P <.0001 compared to sorafenib alone, ° P <.001 compared to perifosine alone. Columns, mean; bars, SEM.

4.4.2 Cotreatment with perifosine and sorafenib results in a marked Bax conformational change and translocation to the mitochondrial fraction, and release of the mitochondrial cytochrome c and AIF

In general, apoptotic signals converge toward the multi-domain pro-apoptotic proteins Bax and Bak. While Bak is localized in the organelle membranes, particularly in the mitochondria where it undergoes conformational change upon apoptotic stimuli, Bax is primarily distributed in the cytosol in non-apoptotic cells. Upon diverse apoptotic stimuli, Bax undergoes conformational change, accompanied by translocation into the mitochondrial membrane, promoting the release of pro-apoptotic mitochondrial proteins (e.g., cytochrome c) into the cytosol and inducing apoptosis.[210] Therefore, the effects of combined ERK1/2 and PI3-K/Akt inhibition were examined in relation to Bak and Bax conformational change and intracellular Bax localization. Individual treatment (48 – 72 hours) with perifosine or sorafenib modestly induced Bax translocation, whereas combined treatment dramatically increased mitochondrial translocation (Figure 4.8). Consistent with these findings, combined treatment with perifosine and sorafenib (48 – 72 hours) resulted in a pronounced increase in AIF and cytochrome c cytosolic release whereas no effect were observed when perifosine or sorafenib were administered individually (Figure 4.8). These findings indicate that perifosine and sorafenib cooperate to promote Bax and Bak conformational change, Bax mitochondrial translocation, and AIF and cytochrome c cytosolic release.

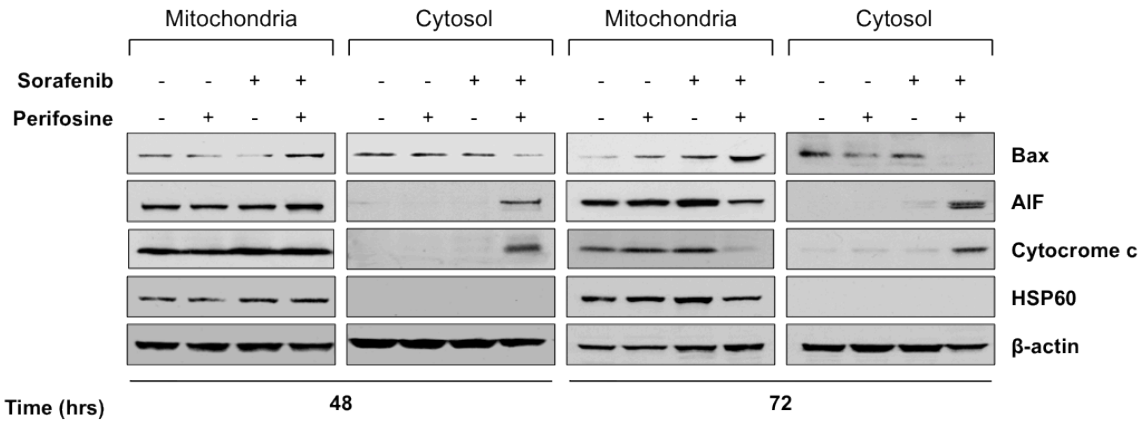

Figure 4.8: Perifosine/sorafenib combined treatment induces conformationale change of Bax, cytosolic release of cytochrome-c and AIF. L-540 cells were exposed to 5 μM sorafenib and 5 μM perifosine alone or in combination for 48–72 hours, after which mitochondrial and cytosolic fractions were obtained and subjected to Western blot analysis, as explained in Material and Methods section, to monitor conformationale change of Bax, release of cytochrome-c and apoptosis-inducing factor (AIF). The purity of mitochondrial and cytosolic fractions was determined by Western blot analysis using anti-HSP60 antibody. Equal protein loading was confirmed by blotting for β-actin.

4.4.3 Cotreatment with perifosine and sorafenib results in marked mitochondrial damage

To further examine the molecular mechanism(s) whereby perifosine/sorafenib triggers cell death, we investigated whether loss of mitochondrial potential was involved in perifosine/sorafenib-induced cell death in L-540 cell line. Treatment with perifosine/sorafenib induced a potent time-dependent mitochondrial membrane depolarization that could be detected in L-540 cell line (Figure 4.9), with loss of mitochondrial potential being detectable in 40% to 80% of perifosine/sorafenib-treated cells after 48- and 72-hours, respectively. In addition, perifosine/sorafenib can induce a severe mitochondrial injury both in Z-VADfmk pretreated and non-Z-VADfmk treated L-540 cells at similar levels further indicating that perifosine/sorafenib treatment can induce apoptosis by caspase-independent mechanisms (Figure 4.9).

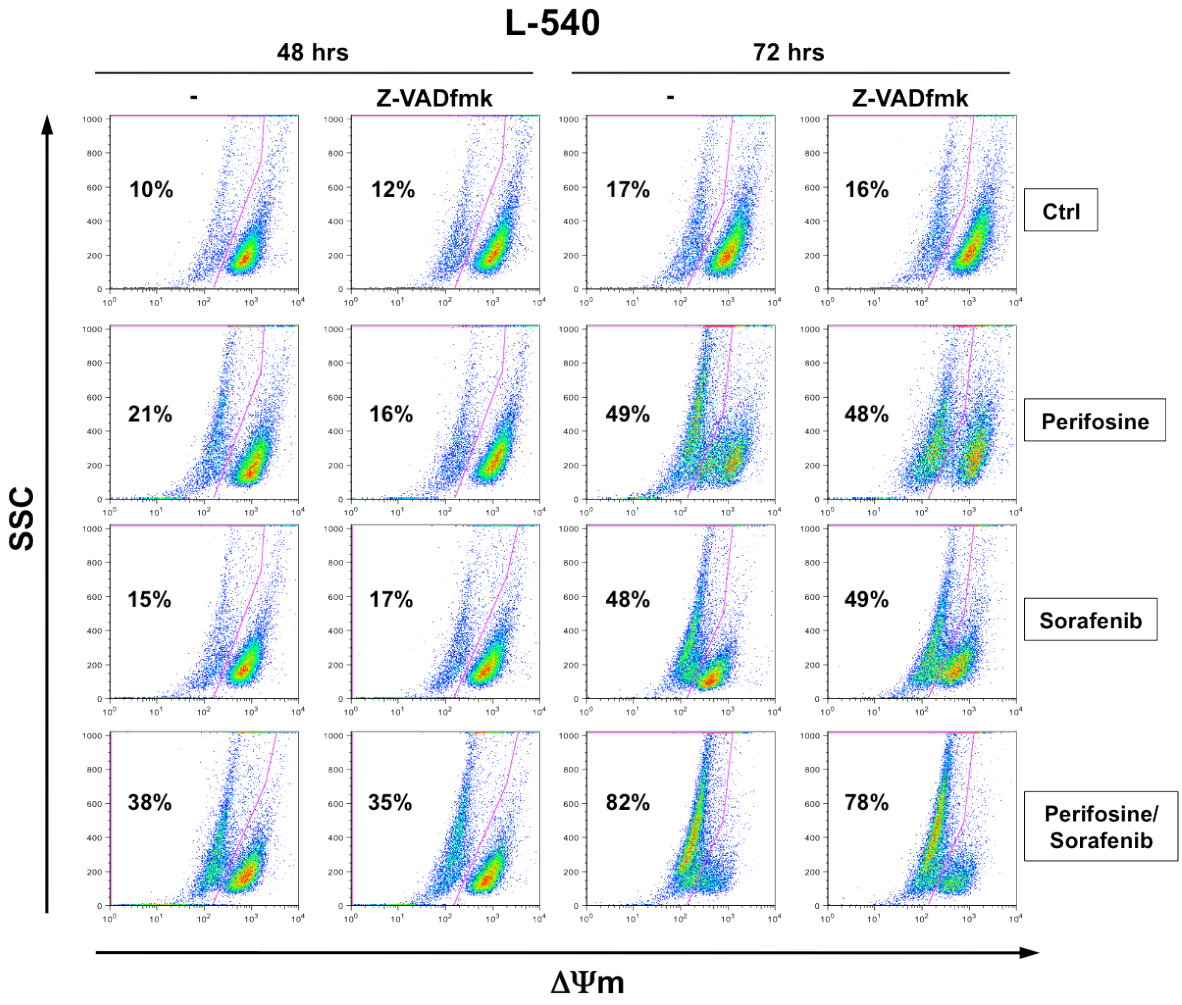

Figure 4.9: Combined exposure of HL cells to perifosine and sorafenib resulted in a marked increase in mitochondrial injury. L-540 cells were treated with perifosine (5 μM), sorafenib (5μM), or the combined treatment plus Z-VADfmk (50 μM). Treatment with the caspase inhibitor Z-VADfmk was started 1 hour before adding perifosine and sorafenib. At the indicated time points, loss of mitochondrial potential ($\Delta\Psi_m$) was measured using TMRE staining and flow cytometry. Shown representative dot plots of mitochondrial membrane depolarization.

4.5 PATHWAY INHIBITION IN RESPONSE TO PERIFOSINE AND SORAFENIB AS COMBINED AGENTS

Since perifosine has been shown to modulate Akt as well as other signaling pathways, including the JNK and MAPK pathways, and sorafenib affects the phosphorylation levels of key mediators of the RAF/MEK/ERK cascade, we examined whether perifosine in combination with sorafenib enhanced the modulation of similar signal transduction pathways in human HL cells.

4.5.1 Baseline phosphorylation of Akt and its downstream target in HL cells

We first examined baseline phosphorylation of Akt and the direct and indirect Akt targets GSK-3α/β and p70S6 kinase (p70S6K), in HD-MyZ, L-540 and HDLM-2 cell lines, using a sensitive and

semiquantitative human phospho-Kinase array kit (R&D Systems, Inc.) (Figure 4.10). In addition, by western blotting and densitometric scanning, we observed that HDLM-2 cells have very low basal levels of p-Akt, whereas both HD-MyZ and L-540 cells have much higher basal levels of p-Akt. When comparing the apoptosis results presented in Figure 4.4, it seems that low basal levels of p-Akt correlated with low sensitivity to perifosine-induced apoptosis.

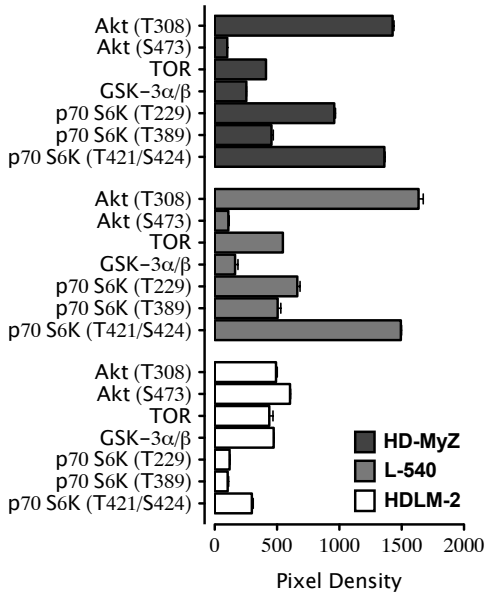

Figure 4.10: HD-MyZ, L-540 and HDLM-2 baseline phosphorylation levels of Akt and its downstream targets. Shown are data from one of two independent experiments in duplicate. The chemiluminescence signal intensity of individual spots was analyzed using the open source imaging software ImageJ (http://rsb.info.nih.gov/ij/).

4.5.2 Perifosine in combination with sorafenib significantly affects phosphorylation of MAPK and PI3-K/Akt pathways

HD-MyZ and L-540 responsive cell lines exhibited a significative decrease in p-Akt levels when exposed to perifosine/sorafenib (p-Akt levels were only detectable in HD-MyZ cells after 6-hours exposure), whereas in HDLM-2 cells, p-Akt levels were unaffected (Figure 4.11). We also detected, in HD-MyZ and L-540 cells, a 77-94% decrease, respectively, in the level of p-S6, a well-known substrate of Akt, furthering the notion that perifosine in combination with sorafenib inhibits Akt signaling in HL cells (Figure 4.11).

In examining MAPK signal transduction pathway, we observed inhibition of MEK1/2 and ERK1/2 phosphorilations up to 80% and 43%, respectively, 16 hours after perifosine/sorafenib-treatment in HD-MyZ cells. In accordance with results relative to phosphorylation reduction, amounts of p-MEK1/2 and p-ERK1/2 proteins were reduced to a larger extent (61% and 86%, respectively) in L-540 cells than in HD-MyZ cells. p-38α levels were reduced by 32% in HD-MyZ and by 75% in L-540 cells, whereas Mcl-1 amounts were reduced by 100% both in HD-MyZ and L-540 cell lines (Figure 4.11). Interestingly, perifosine/sorafenib combined treatment did not alter the levels of p-MEK1/2,

p-ERK1/2 and Mcl-1 but did decrease the levels of p-38α in HDLM-2 cell line (Figure 4.11). These results demonstrate that perifosine/sorafenib potently inhibit baseline phosphorylation of Akt and its downstream target proteins consistent with downmodulation of MEK, ERK and Mcl-1 phosphorylation. Furthermore, perifosine in combination with sorafenib downregulates the PI3-K/Akt and MAPK signaling pathways in a cell line-dependent fashion.

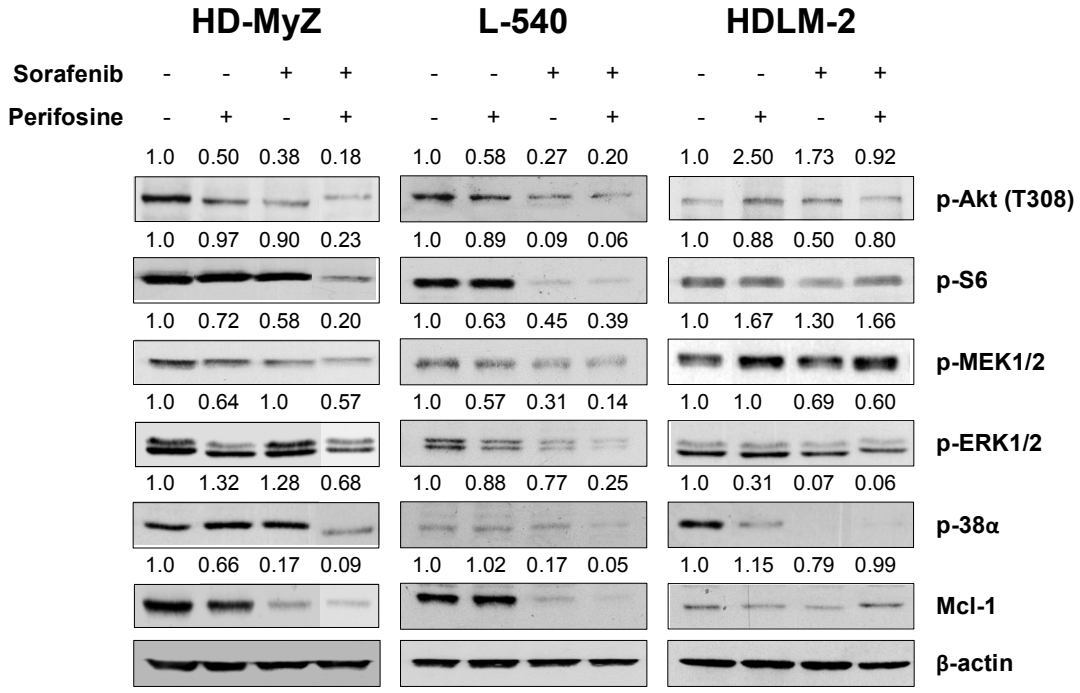

Figure 4.11: Perifosine/sorafenib treatment induced changes in survival signals in HL cells. Immunoblots of extracts from HD-MyZ, L-540 and HDLM-2 cells treated with perifosine (5 μM) and/or sorafenib (5 μM) for 16 hours. Equal protein loading was confirmed by blotting for β-actin. Quantitation was done using ImageJ software (NIH). The values indicated above each protein band represent densitometric ratios of cells treated with perifosine, sorafenib or the combination over the control vehicle-treated cells, normalized to β-actin. Representative blots are shown. Experiments were repeated twice with similar results.

4.6 MODULATION OF GENE EXPRESSION IN HODGKIN LYMPHOMA CELL LINES BY PERIFOSINE, SORAFENIB AND THEIR COMBINATION

To gain insight into the effects of perifosine and/or sorafenib on HL cell lines, we carried out genome-wide microarray analysis of HD-MyZ, L-540, and HDLM-2 cell lines treated for 24 hours with these inhibitors. Heat maps (Figure 4.12) and Venn diagram analysis (Figure 4.13) of significantly modulated genes indicated a dominant role of sorafenib in changing gene expression levels, with less impact by perifosine, in all three cell lines.

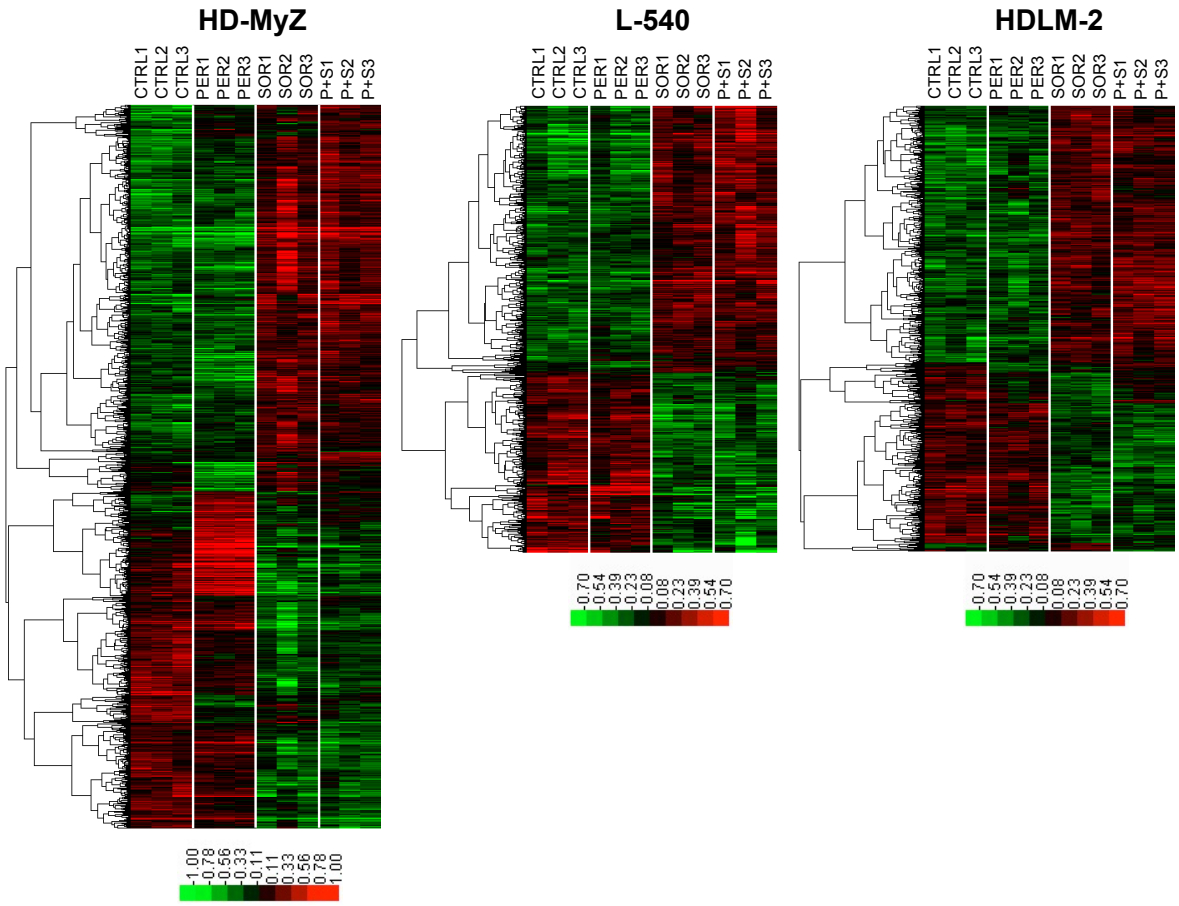

Figure 4.12: Modulation of gene expression in HL cell lines by perifosine, sorafenib or their combination. One way hierarchical clustering of genes (HD-MyZ: n=1242; L-540: n=778; HDLM-2: n=829) showing significant modulation (at P =.005 of the univariate F test) by perifosine and/or sorafenib treatment. Gene-wise median centered normalized intensities (in Log space) of untreated cells (CTRL1-3) and of cells treated with perifosine (PER1-3), sorafenib (SOR1-3) or the perifosine/sorafenib combination (P+S1-3) are shown. The heat map was clustered using centered correlation as distance metric and complete linkage clustering.

In fact, as shown by the Venn diagrams (Figure 4.13) sorafenib modulated a larger number of genes, compared to perifosine and most of the genes modulated by "sorafenib only" treatment, remained modulated even in the perifosine/sorafenib combination.

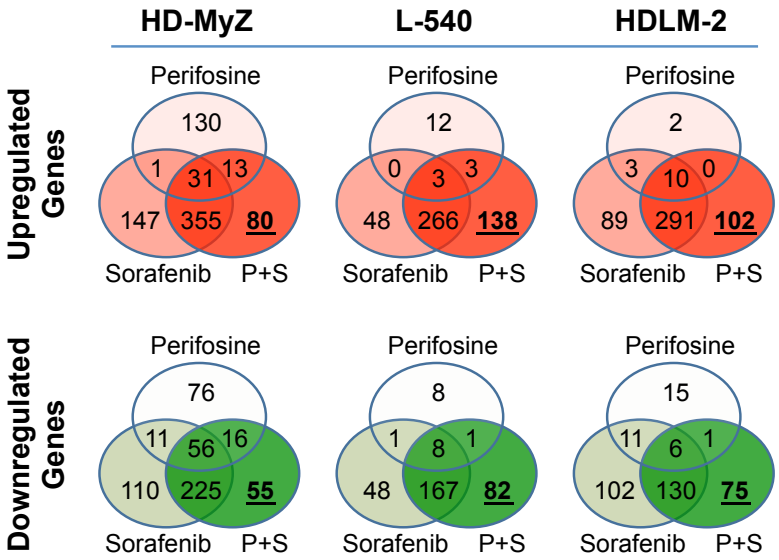

Figure 4.13: Venn diagram analysis of significantly modulated genes by perifosine, sorafenib or their combination in the three HL lines. Numbers indicated in bold underlined highlight genes significantly modulated only by the perifosine/sorafenib combination.

However, in all three cell lines, Venn diagram analysis identified also the genes significantly modulated by the perifosine/sorafenib combination (Figure 4.13 lower right circles in each Venn diagram and Supplementary Table 1A-C for the identity and fold change values of all significantly modulated genes). Volcano plots of the latter subsets of genes indicated that only a small group of these genes underwent a strong modulation (i.e. a fold change >1.5) by the perifosine/sorafenib treatment (Figure 4.14).

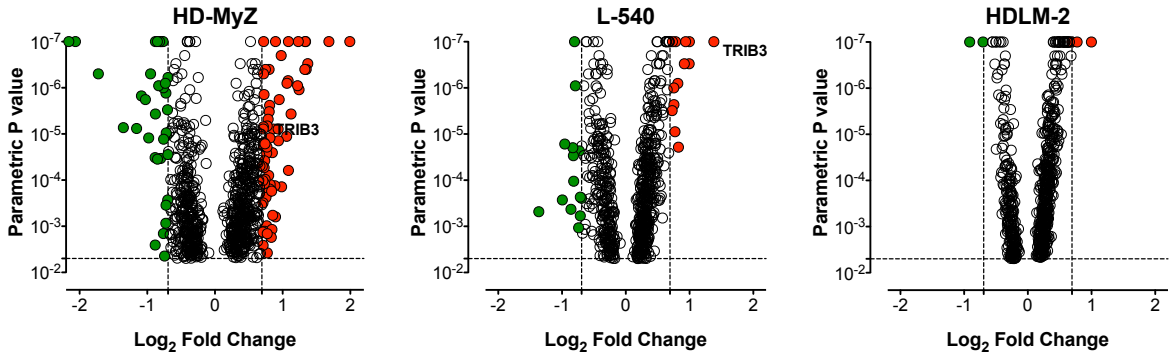

Figure 4.14: Volcano plots of all genes significantly modulated by the perifosine/sorafenib combination, showing extent of modulation (as Log_2 Fold Change) vs P value of the univariate F test. Vertical dotted bars: ± 1.5 fold changes. Horizontal dotted line identifies the P =.005 nominal significance value of the univariate F test.

We then carried out Ingenuity Pathway analysis of the genes significantly modulated by perifosine/sorafenib combination (Supplementary Table 2A-C) to classify them according to the most relevant networks of interaction, functional classes and canonical pathways. In the most

informative cell line (i.e. HD-MyZ, the line showing the largest number of genes modulated by the perifosine/sorafenib combination) we found that several of the most up- and down-modulated genes (indicated in bold red or green in Supplementary Table 2A, respectively), were part of interacting networks and/or had functions related to cellular movement, cell cycle and cell death, DNA replication, cellular growth and proliferation. In this cell line, genes inhibited by the perifosine/sorafenib combination were part of canonical pathways regulating cell cycle progression (Supplementary Table 2A). In the same cell line, we then looked for genes showing enhanced modulation by perifosine/sorafenib combined treatment compared to single agent. Some of these genes were validated by RT-PCR (Figure 4.15A) and, in-vivo in tumor bearing mice treated with inhibitors, by confocal microscopy (Figure 4.15B).

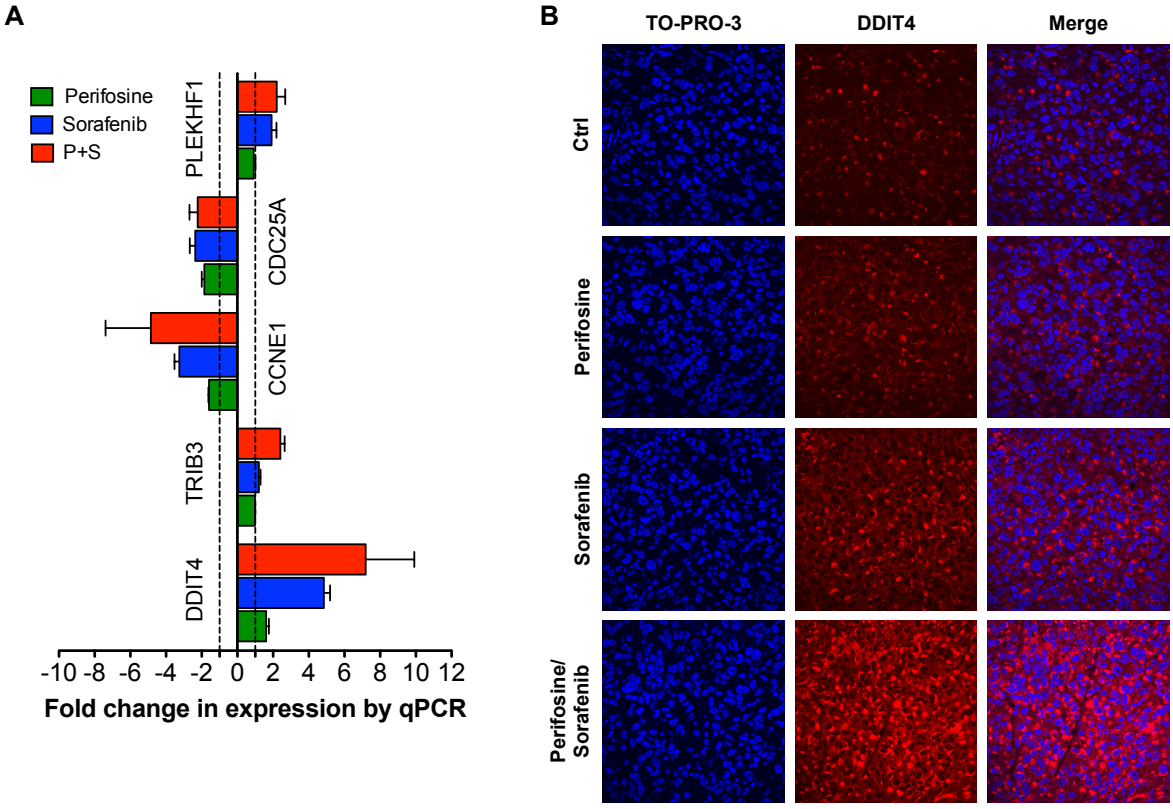

Figure 4.15: Validation of selected genes in HD-MyZ cell line treated with perifosine and/or sorafenib for 24 hours. (A) The bar chart shows the gene expression patterns (presented as fold change with respect to control levels) of selected significantly regulated genes calculated using real-time RT-PCR analysis. The down-regulated genes selected were CCNE1, and CDC25A while the up-regulated genes were TRIB3, DDIT4, and PLEKHF1. All PCR data were normalized to the intensity of β2-microglobulina as a housekeeping gene. Each statistical error bar (± SEM) represents three independent experiments. (B) NOD/SCID mice bearing HD-MyZ SC tumor nodules 100 mg in weigth were randomly assigned to receive perifosine (30 mg/kg/5die, PO) and/or sorafenib (90 mg/kg/5die, IP) or control vehicle. Representative confocal images of tumors from untreated and treated animals processed by double immunofluorescence staining. Cell nuclei (*blue*) were detected by TO-PRO-3; DDIT-4 expression (*red*) was detected by anti-DDIT-4 antibody and Alexa Fluor 568-conjugated secondary antibody. Objective lens, original magnification: 1.0 NA oil objective, 40x

4.6.1 Perifosine/sorafenib induces apoptosis requiring TRIB3 up-regulation

The experiments performed above highlighted many differences between HD-MyZ, L-540 and HDLM-2 cell types in response to perifosine/sorafenib. Interestingly, only one gene, tribbles homology 3 (TRIB3), was significantly modulated by the combined treatment in the two most responsive cell lines (HD-MyZ and L-540, Figure 4.14). Tribbles homology 3 (TRB3 or TRIB3) became of interest due to its array of binding partners such as mitogen-activated protein kinase family members[211] and AKT.[212] Furthermore, TRIB3 expression was enanched in HD-MyZ and L-540 tumor nodules after perifosine/sorafenib treatment (Figure 4.16), with no expression observed in HDLM-2 (Figure 4.16).

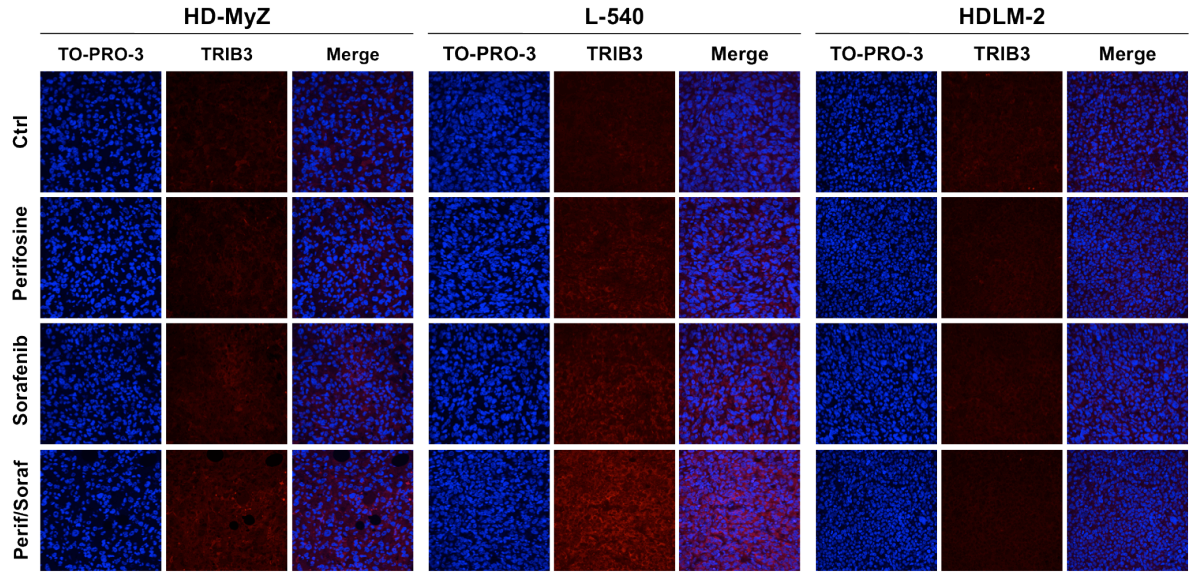

Figure 4.16: In vivo modulation of TRIB3 by perifosine/sorafenib treatment in HL cells. NOD/SCID mice bearing HD-MyZ, L-540 and HDLM-2 tumor nodules 100 mg in weigth were randomly assigned to receive perifosine (30 mg/kg/mouse, PO) or sorafenib (90 mg/kg/mouse, IP) (alone or in combination) or control vehicle. Representative confocal images of tumors from untreated and treated animals processed by double immunofluorescence staining. Cell nuclei (*blue*) were detected by TO-PRO-3; TRIB3 expression (*red*) was detected by anti-TRIB3 antibody and Alexa Fluor 568-conjugated secondary antibody. Objective lens, original magnification: 1.0 NA oil objective, 40x.

In order to define whether perifosine/sorafenib induces apoptosis requiring up-regulation of TRIB3, we silenced the expression of TRIB3 using TRIB3 siRNA and then examined cell sensitivity to perifosine/sorafenib combined treatment. By Western blotting, we detected substantially reduced levels of TRIB3 (43% reduction) in L-540 cells transfected with TRIB3 siRNA compared with those in control siRNA-transfected cells (Figure 4.17A), indicating successful TRIB3 knockdown. Accordingly, a 50% increase in cell viability was also enhanced in TRIB3 siRNA-transfected cells compared with control siRNA-transfected cells (Figure 4.17B). These results indicate that TRIB3 up-regulation is involved in perifosine/sorafenib-induced apoptosis.

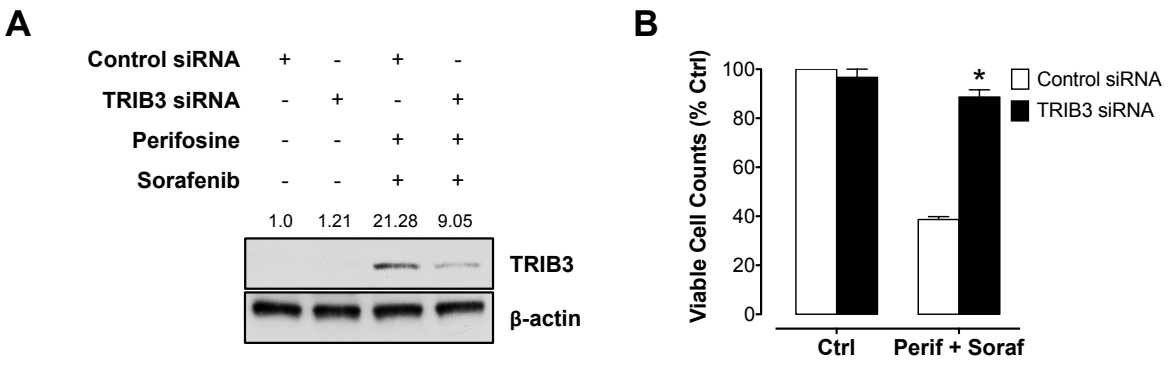

Figure 4.17: Demonstration of the role of TRIB3 induction in perifosine-induced apoptosis in HL cells. (**A-B**) TRIB3 siRNA (100 nM) and also with control siRNA (100 nM) were transfected in L-540 cells overnight. After transfection, the cells were treated with perifosine or sorafenib or in combination for 48 – 72 hours. (**A**) After 48 hours the efficiency of TRIB3 siRNA inhibition was analyzed by Western blotting using TRIB3-specific antibodies. Equal protein loading was confirmed by blotting for β-actin. Each lane were subjected to western immunoblot analysis as described under the Material and Methods section. Representative blots are shown. Experiments were repeated twice with similar results. (**B**) Viable cell counts were obtained as described in Materials and Methods. Mean (± SEM) values refer to three independent experiments. * P <.001 compared with control siRNA.

4.7 IN VIVO ACTIVITY OF PERIFOSINE AND SORAFENIB IN HL TUMOR MODELS

Six- to eight-week-old NOD/SCID mice with a body weight of 20 to 25 g were xenografted with HD-MyZ, L-540, or HDLM-2 cell lines. Mice were inoculated intravenously (IV) with HD-MyZ (1.8 x 10^6 cells/mouse). After 3 days HD-MyZ injection, mice were randomized in four groups (n=5/group, for a total of two different experiments) to receive per os (PO) injections of perifosine (7.5 mg/kg/mouse/5die/5weeks) and/or intraperitoneal (IP) injections of sorafenib (60 mg/kg/mouse/5die/5weeks), or control NaCl solution 0.9%. Endpoint of in vivo IV experiments was death.

HD-MyZ (5×10^6 cells/mouse), L-540 and HDLM-2 (25×10^6 cells/mouse) cells were inoculated subcutaneously (SC) in the right flank of each mouse. When tumor volume reached approximately 100 mg in weight (see Meterial and Methods for details), mice were randomly assigned to receive either a short- or long-term treatment with perifosine and/or sorafenib or control vehicle. The short-term treatment was used to assess necrotic and apoptotic areas, whereas the long-term treatment was used to assess tumor growth inhibition. Mice were checked twice weekly for tumor appearance, body weight measurements and toxicity. Each experiment was performed on at least two separate occasions, using five mice per treatment group.

4.7.1 Combining perifosine with sorafenib increases median surviaval of NOD/SCID mice xenografted with HL tumors

To determine whether the combined perifosine/sorafenib treatment could enhance the anti-lymphoma activity not only in vitro but also in vivo, a xenograft model of Hodgkin lymphoma was used. The antitumor activity of perifosine/sorafenib was investigated in NOD/SCID mice xenografted intavenously (IV) with HD-MyZ. HD-MyZ cell line was selected for in vivo studies due to its tumorigenic features which mimick disseminated tumor with infiltrative and destructive growth. NOD/SCID mice inoculated IV with 1.8 x 10^6 HD-MyZ cells, received a 25-day treatment with perifosine (7.5 mg/kg/day, 5 days per week for 5 weeks, PO), sorafenib (60 mg/kg/day, 5 days per week for 5 weeks, IP), the combined treatment or vehicle control. Drug treatment was started 3 days after tumor inoculation. No significant changes in weight or other signs of potential toxicity were observed during treatment with perifosine, sorafenib or the combined treatment (Figure 4.18).

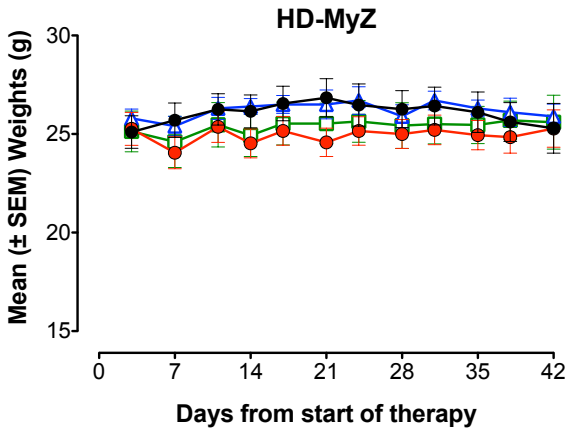

Figure 4.18: Mice weight of each group during the treatment. HD-MyZ cells line (1.8 × 10^6 cells/mouse) were injected IV into NOD/SCID mice. Mice received control vehicle (black circle), perifosine (7.5 mg/kg/mouse/5die/5weeks, PO, green square), sorafenib (60 mg/kg/mouse/5die/5weeks, IP, blue triangle) or the combined treatment (red circle). Treatment started at day 3 from tumor inoculation. Each treatment group contained 10 mice. The weights of treated mice did not significantly change over the course of treatment with perifosine and/or sorafenib. Points, average mouse weight; bars, SEM.

Using Kaplan-Meier curves and log-rank analysis, there was no statistically significant difference in the mean overall survival of mice treated with perifosine over controls, whereas a modest increase of median survival over controls was detected in sorafenib-treated mice (45 vs 54 days, P <.03) (Figure 4.19). In contrast, the combined treatment with perifosine plus sorafenib resulted in a significant increase of median survival as compared to controls (45 vs 81 days, P <.0001) as well as mice receiving perifosine (49 vs 81, P <.03) or sorafenib alone (54 vs 81, P <.007) (Figure 4.19). The significant enhancement of therapeutic activity of the combined perifosine/sorafenib treatment over single drug-treatment was further supported by an increase up to 25% of animals being alive and well at the end of the 200-day observation period (Figure 4.19).

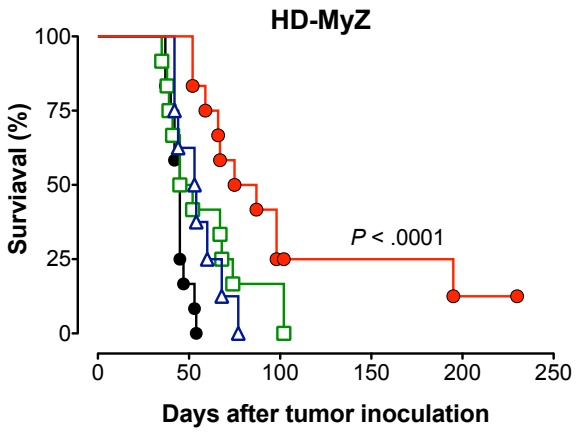

Figure 4.19: Perifosine in combination with sorafenib produces robust efficacy against HL xenografts in NOD/SCID mice. HD-MyZ cells line (1.8 × 10^6 cells/mouse) were injected IV into NOD/SCID mice. Mice received control vehicle (black circle), perifosine (7.5 mg/kg/mouse/5die/5weeks, PO, green square), sorafenib (60 mg/kg/mouse/5die/5weeks, IP, blue triangle) or the combined treatment (red circle). Treatment started at day 3 from tumor inoculation. Each treatment group contained 10 mice. Kaplan-Meyer estimates of overall survival of NOD/SCID mice xenografted with HD-MyZ cell line. Survival was measured from the day of xenografting. * P <.0001 compared to controls.

4.7.2 In vivo tumor growth inhibition by perifosine in combination with sorafenib

The in vivo antitumor activity of perifosine in combination with sorafenib was investigated in NOD/SCID mice bearing subcutaneous L-540 and HDLM-2 tumor nodules. Treatments with perifosine without and with sorafenib were started when tumor volume reached approximately 100 mg in weight and tumor size was monitored until mice were sacrificed due to extensive disease. The tumors were measured with calipers, and their weights were calculated using the formula: $(a \times b^2)/2$, where a and b represented the longest and shortest diameters, respectively. Antitumor efficacy was measured as tumor growth inhibition (TGI) defined as [1 - (T/C) × 100], where T and C are the mean tumor weight in the treated and untreated control groups, respectively. Each experiment was performed on at least two separate occasions, using five mice per treatment group.

In contrast with in vitro experiments showing significant levels of perifosine and sorafenib activity against the responsive L-540 cell line, in vivo perifosine and sorafenib as single treatments failed to affect the subcutaneous growth of L-540 nodules, as compared to vehicle-treated controls (2 ± 0.2 vs 2.4 ± 0.1 g and 2.6 ± 0.4 vs 2.4 ± 0.1 g, P >0.5, respectively) (Figure 4.20). Notwithstanding their lack of activity when used as single treatments, combination of perifosine with sorafenib significantly reduced the growth of L-540 nodules by 42% over controls (1.5 ± 0.5 vs 2.6 ± 0.4 g, P <.0001), 35% over perifosine alone (1.5 ± 0.5 vs 2.3 ± 0.7 g, P <.0001), and 46% over sorafenib alone (1.5 ± 0.5 vs 2.8 ± 0.7 g, P <.0001) (Figure 4.20).

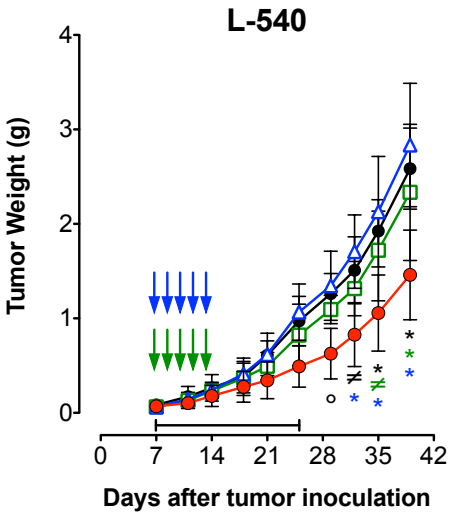

Figure 4.20: Perifosine plus sorafenib inhibits L-540 cell growth in vivo. NOD/SCID mice were SC inoculated with L-540 tumor cells (25 x 10^6 cells/mouse). Treatments were initiated on day 7, when all groups had tumor nodules reached approximately 100 mg in weight. Control vehicle (black circle), perifosine (15 mg/kg/die, 5 days per 3 weeks, PO, green square), sorafenib (30 mg/kg/die, 5 days per 3 weeks, IP, blue triangle) and the combined treatment (red circle). Mice were checked twice weekly for tumor appearance, tumor dimensions, body weight, and toxicity. Each experiment was performed on at least two separate occasions, using 5 mice per treatment group. Green arrows indicate perifosine treatment administration; blue arrows indicate sorafenib treatment administration. Treatment duration is indicated by horizontal capped black lines (days 7 – 25 for L-540 xenograft). Mean (± SD) tumor weight data are shown. * P <.0001 compared to controls and sorafenib, ° P <.01 compared to sorafenib and ≠ P <.05 compared to perifosine.

The growth of perifosine-resistent HDLM-2 tumor nodules was uneffected by both perifosine or sorafenib alone as compared to controls (0.7 ± 0.2 vs 0.8 ± 0.2 g and 0.8 ± 0.2 vs 0.8 ± 0.2 g, P >0.5, respectively) (Figure 4.21). Furthermore, the combined treatment perifosine/sorafenib did not reduced the growth of HDLM-2 tumor nodules as compared to controls (0.8 ± 0.2 vs 0.8 ± 0.2 g, P >0.5) (Figure 4.21).

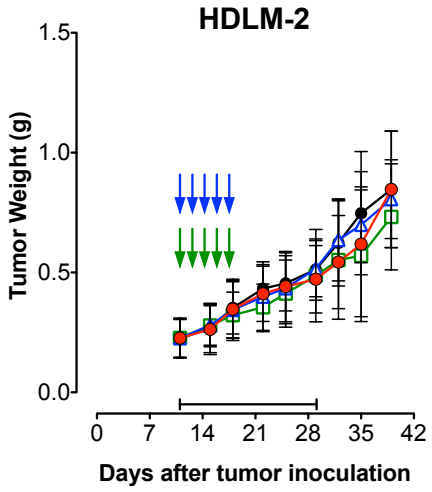

Figure 4.21: Perifosine plus sorafenib doesn't affect HDLM-2 cell growth in vivo. NOD/SCID mice were SC inoculated with HDLM-2 tumor cells (25 x 10^6 cells/mouse). Treatments were initiated on day 11, when all groups had tumor nodules reached approximately 100 mg in weight. Control vehicle (black circle), perifosine

(15 mg/kg/die, 5 days per 3 weeks, PO, green square), sorafenib (30 mg/kg/die, 5 days per 3 weeks, IP, blue triangle) and the combined treatment (red circle). Mice were checked twice weekly for tumor appearance, tumor dimensions, body weight, and toxicity. Each experiment was performed on at least two separate occasions, using 5 mice per treatment group. Green arrows indicate perifosine treatment administration; blue arrows indicate sorafenib treatment administration. Treatment duration is indicated by horizontal capped black lines (days 11 – 29 for HDLM-2 xenograft). Mean (± SD) tumor weight data are shown.

4.7.3 In vivo perifosine/sorafenib combined treatment induces necrosis events

To elucidate the mechanism(s) of perifosine/sorafenib-induced anti-lymphoma activity, tumor-bearing mice were treated for 5 days with vehicle control, perifosine (30 mg/kg/day), and sorafenib (90 mg/kg/day), used alone or in combination. Treatment was started when tumor volumes reached approximately 100 mg in weight (i.e., 10 days after tumor inoculation) and three hours after the last treatment, nodules were excised and appropriately stained. Hematoxylin and eosin and TUNEL staining of both HD-MyZ and L-540, but not HDLM-2 tumors excised from mice receiving perifosine in combination with sorafenib showed the presence of extensive necrotic areas within tumor tissue, which were much more widespread as compared to tumors from untreated, perifosine- or sorafenib-treated mice (Figure 4.22).

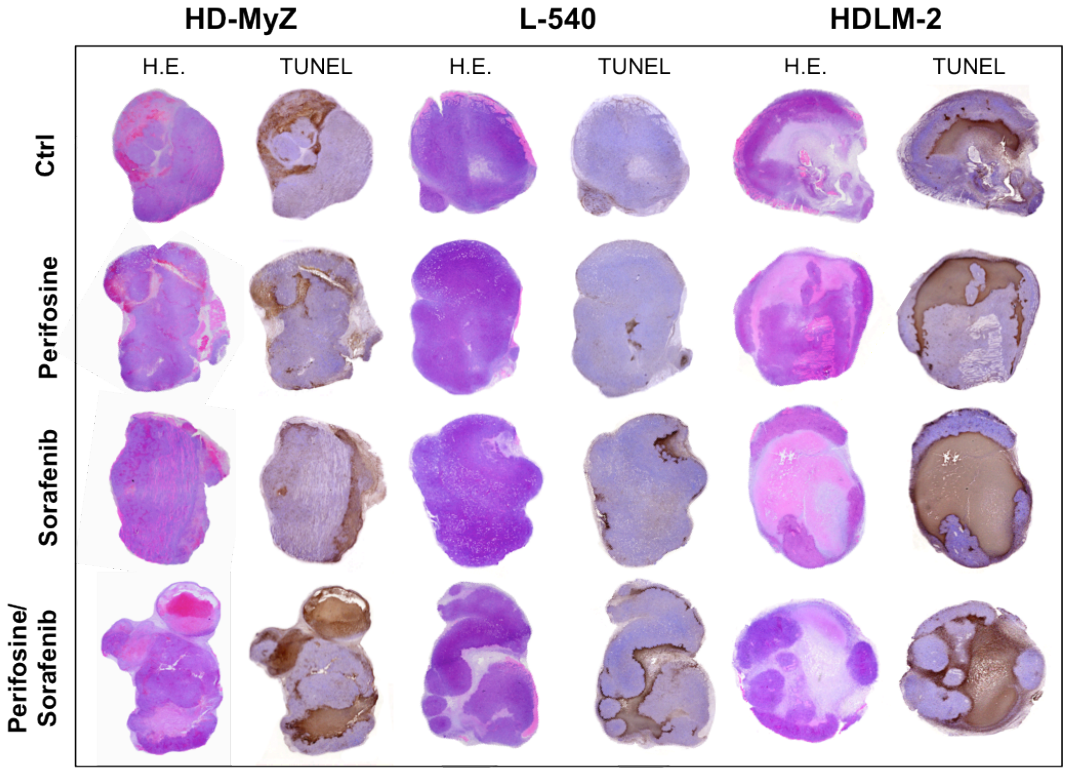

Figure 4.22: Quantification of tumor necrosis within entire tumor sections. NOD/SCID mice bearing SC tumor nodules 100 mg in weight were randomly assigned to receive a 5-day treatment with perifosine (30 mg/kg/die, PO) and/or sorafenib (90 mg/kg/die, IP), or control vehicle. Representative histological images of entire tumors sections from mice receving the different treatments are shown. Tumor tissue morphology were detected by hematoxylin and eosin (H&E) staining. Tumor necrotic areas were detected by TUNEL staining

and revealed as brown areas using 3,3'-diaminobenzidine for light microscopy analysis. Objective lens, original magnification: 0.08 NA dry objective, 2x.

An objective quantification of tumor necrosis in entire tumor sections following TUNEL staining was achieved by a computer-aided imaging analysis using ImageJ software (Figure 4.23-25). HD-MyZ tumors from mice treated with perifosine or sorafenib alone was not able to induce significant tumor necrosis over controls (20.4 ± 2.6% vs 20.7 ± 4.4% vs 20.8 ± 3.1%, $P > .05$) (Figure 4.23), whereas the combined treatment resulted in a 2-fold increase in tumor necrosis compared to single treatments (38.8 ± 9.7% vs 20.4 ± 2.6% vs 20.7 ± 4.4%, $P < .0001$) (Figure 4.23).

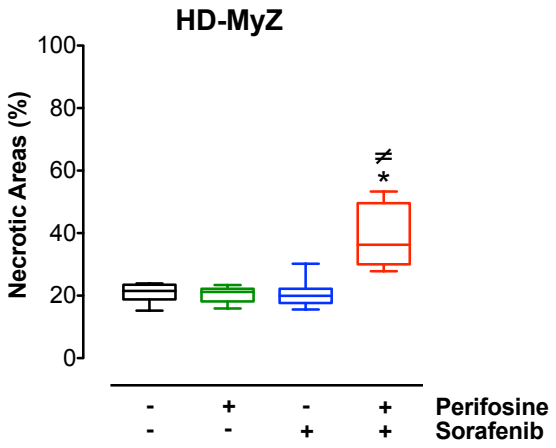

Figure 4.23: Quantification of tumor necrosis within entire HD-MyZ tumor sections. NOD/SCID mice bearing SC tumor nodules 100 mg in weight were randomly assigned to receive a 5-day treatment with perifosine (30 mg/kg/die, PO) and/or sorafenib (90 mg/kg/die, IP), or control vehicle. After counterstaining with hematoxylin, sections were analyzed using ImageJ for quantification of tumor necrosis percentage. Quantification of HD-MyZ necrotic areas by ImageJ analysis on digitally acquired tissue sections stained with TUNEL. At least three sections from different animals were analyzed per treatment group. The boxes extend from the 25th to the 75th percentile, the lines indicate the median values and the wiskers indicate the range of values. * $P < .0001$ compared to controls, and ≠ $P < .0001$ compared to single treatments.

In addition, TUNEL staining of L-540 tumor sections from untreated, and perifosine-treated mice revealed a homogeneous mass of viable cells with necrotic areas accounting only for 2.7 ± 0.6%, and 3.9 ± 1.9% of total tissue, respectively (Figure 4.24). In contrast, tumors from sorafenib-treated mice displayed a significant increase of necrotic areas as compared to controls (7 ± 1.3% vs 2.7 ± 0.6%, $P < .01$) (Figure 4.24). After perifosine/sorafenib-tretment, the percentages of necrotic areas per tissue section ranged from 17% to 27%, resulting in a mean 8-fold increase over controls (22.2 ± 3.9% vs 2.7 ± 0.6%, $P < .0001$), and a 1.4 to 2.6-fold increase over perifosine or sorafenib-treated mice, respectively (22.2 ± 3.9% vs 3.9 ± 1.9% vs 7 ± 1.3%, $P < .0001$) (Figure 4.24).

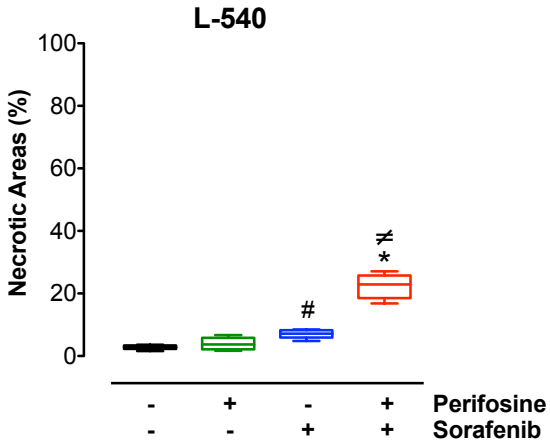

Figure 4.24: Quantification of tumor necrosis within entire L-540 tumor sections. NOD/SCID mice bearing SC tumor nodules 100 mg in weight were randomly assigned to receive a 5-day treatment with perifosine (30 mg/kg/die, PO) and/or sorafenib (90 mg/kg/die, IP), or control vehicle. After counterstaining with hematoxylin, sections were analyzed using ImageJ for quantification of tumor necrosis percentage. Quantification L-540 necrotic areas by ImageJ analysis on digitally acquired tissue sections stained with TUNEL. At least three sections from different animals were analyzed per treatment group. The boxes extend from the 25th to the 75th percentile, the lines indicate the median values and the wiskers indicate the range of values. * P <.0001 and # P <.01, compared to controls. ≠ P <.0001 compared to single treatments.

In accordance with the absence of in vitro responce, treatment with perifosine in mice bearing perifosine-resistant HDLM-2 tumors failed to induced any significant increase in tumor necrosis compared to untreated controls (28.9 ± 3.9% vs 26.2 ± 12%, P >.05) (Figure 4.25). Interestingly, HDLM-2 tumors treated with sorafenib showed a significant increase in tumor necrosis as compared to controls (68.9 ± 7.6% vs 26.2 ± 12%, P <.0001) (Figure 4.25). Similarly, HDLM-2 tumors from mice receiving perifosine in combination with sorafenib resulted in a 2-fold increase in tumor necrosis compared to controls (52.9 ± 3.7% vs 26.2 ± 12%, P <.0001) (Figure 4.25), but failed to show any increase in tumor necrosis over sorafenib-treated mice (52.9 ± 3.7% vs 68.9 ± 7.6%, P >.05) (Figure 4.25).

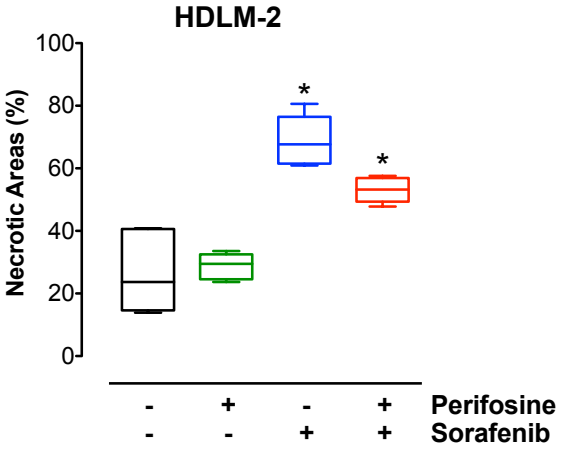

Figure 4.25: Quantification of tumor necrosis within entire HDLM-2 tumor sections. NOD/SCID mice bearing SC tumor nodules 100 mg in weight were randomly assigned to receive a 5-day treatment with perifosine (30 mg/kg/die, PO) and/or sorafenib (90 mg/kg/die, IP), or control vehicle. After counterstaining with

hematoxylin, sections were analyzed using ImageJ for quantification of tumor necrosis percentage. Quantification of HDLM-2 necrotic areas by ImageJ analysis on digitally acquired tissue sections stained with TUNEL. At least three sections from different animals were analyzed per treatment group. The boxes extend from the 25th to the 75th percentile, the lines indicate the median values and the wiskers indicate the range of values. * P <.0001 compared to controls.

4.7.4 Perifosine and sorafenib combined treatment enhances direct tumor cell killing in HL xenograft tumors

Besides a significant increase of necrotic areas, TUNEL staining of both HD-MyZ and L-540 tumors from mice treated with perifosine and sorafenib also revealed a strong increase of tumor cell death (TUNEL+ cells) as compared with single treatments as well as control animals (Figure 4.26). Quantification of tumor cell death within entire tumor sections was performed using ImageJ software (Figure 4.27-29).

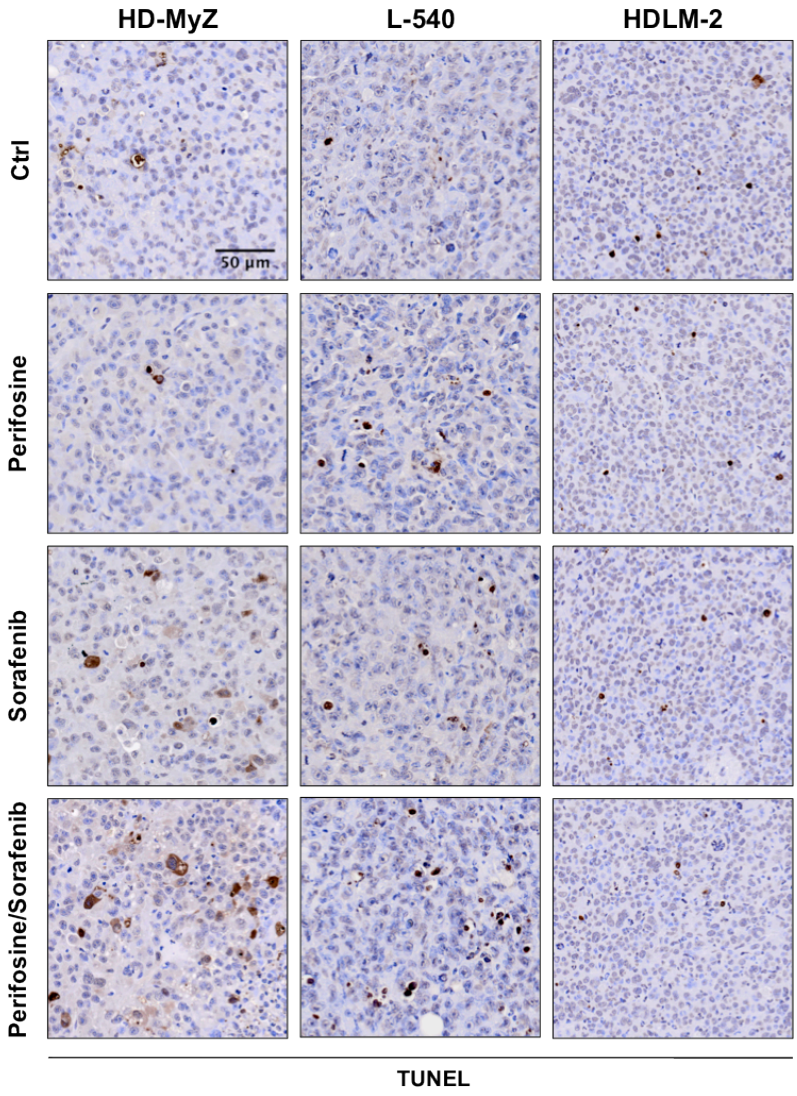

Figure 4.26: Perifosine in combination with sorafenib results in direct tumor cell killing in vivo. NOD/SCID mice bearing SC tumor nodules 100 mg in weight were randomly assigned to receive a 5-day treatment with

perifosine (30 mg/kg/die, PO) and/or sorafenib (90 mg/kg/die, IP), or control vehicle. Three hours after the last treatment tumor nodules were harvested and analyzed for tumor apoptosis. Tumor apoptotic cells were detected by TUNEL staining and revealed as brown nuclei using 3,3'-diaminobenzidine for light microscopy analysis. Objective lens, original magnification: 0.75 NA dry objective, 20x.

TUNEL staining of HD-MyZ nodules treated with perifosine failed to show any rise in tumor cell death over controls (0.9 ± 0.6% vs 1.1 ± 0.7%, P >.05) (Figure 4.27). By contrast, sorafenib alone or combined with perifosine increased TUNEL+ cells over controls by 1.6- and 2.3-fold, respectively (1.7 ± 1.1% vs 1.1 ± 0.7%, P <.0001; 2.2 ± 1.7% vs 1.1 ± 0.7%, P <.0001) (Figure 4.27).

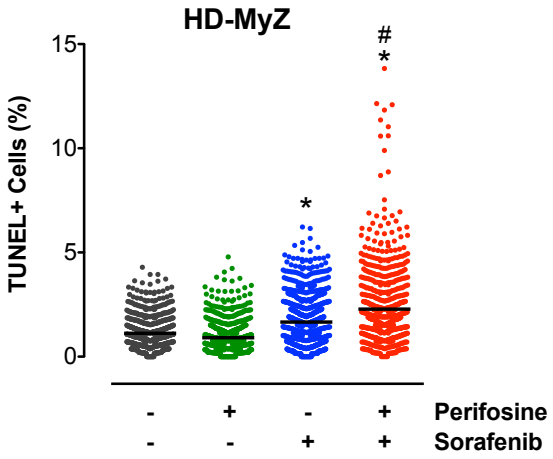

Figure 4.27: Perifosine in combination with sorafenib results in direct HD-MyZ tumor cell killing in vivo. NOD/SCID mice bearing SC tumor nodules 100 mg in weight were randomly assigned to receive a 5-day treatment with perifosine (30 mg/kg/die, PO) and/or sorafenib (90 mg/kg/die, IP), or control vehicle. Three hours after the last treatment tumor nodules were harvested and analyzed for tumor apoptosis. After counterstaining with hematoxylin, sections were analyzed using ImageJ for quantification of apoptotic tumor cells percentage. Quantification of HD-MyZ apoptotic cells by ImageJ analysis on digitally acquired tissue sections stained with TUNEL. At least three sections from different animals were analyzed. Each dot represents the value obtained from the analysis of a single tissue field and the lines indicate the mean values. * P <.0001 compared to controls. # P <.0001 compared to single treatments.

In L-540 tumors, perifosine or sorafenib as single agents produced respectively a 1.6- (1.6 ± 0.7% vs 1 ± 0.5%, P <.0001) and 1.4-fold increase (1.4 ± 0.8% vs 1 ± 0.5%, P <.0001) of TUNEL+ cells over controls (Figure 4.28). Perifosine/sorafenib combined treatment enhanced the anti-tumor activity of single agents, causing a 2-fold increase of L-540 cell death over controls (2 ± 0.9% vs 1 ± 0.5%, P <.0001) (Figure 4.28).

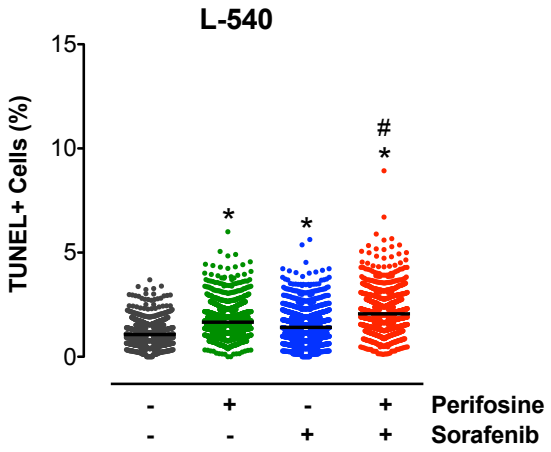

Figure 4.28: Perifosine in combination with sorafenib results in direct L-540 tumor cell killing in vivo. NOD/SCID mice bearing SC tumor nodules 100 mg in weight were randomly assigned to receive a 5-day treatment with perifosine (30 mg/kg/die, PO) and/or sorafenib (90 mg/kg/die, IP), or control vehicle. Three hours after the last treatment tumor nodules were harvested and analyzed for tumor apoptosis. After counterstaining with hematoxylin, sections were analyzed using ImageJ for quantification of apoptotic tumor cells percentage. Quantification of L-540 apoptotic cells by ImageJ analysis on digitally acquired tissue sections stained with TUNEL. At least three sections from different animals were analyzed. Each dot represents the value obtained from the analysis of a single tissue field and the lines indicate the mean values. * P <.0001 compared to controls. # P <.0001 compared to single treatments.

In accordance with all results described above, TUNEL staining of HDLM-2 nodules treated with perifosine didn't show any rise in tumor cell death over controls (0.9 ± 0.4% vs 0.9 ± 0.5%, P >.05) (Figure 4.29). In addition, both sorafenib used as single agent (0.8 ± 0.4% vs 0.9 ± 0.5%, P >.05) and the combined-treatment (0.8 ± 0.5% vs 0.9 ± 0.5%, P >.05) failed to potentiate anti-tumor activity over controls (Figure 4.29).

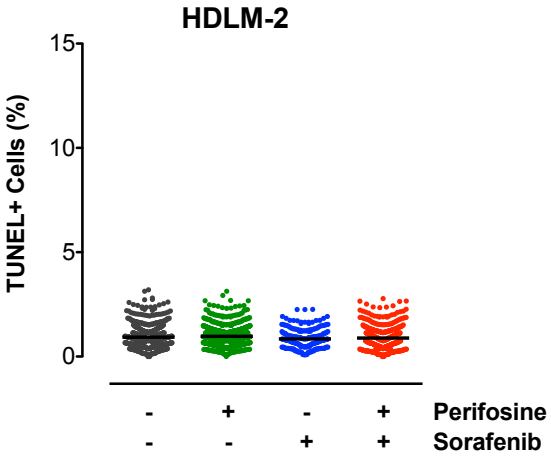

Figure 4.29: Perifosine in combination with sorafenib doesn't induce HDLM-2 tumor cell killing in vivo. NOD/SCID mice bearing SC tumor nodules 100 mg in weight were randomly assigned to receive a 5-day treatment with perifosine (30 mg/kg/die, PO) and/or sorafenib (90 mg/kg/die, IP), or control vehicle. Three hours after the last treatment tumor nodules were harvested and analyzed for tumor apoptosis. After counterstaining with hematoxylin, sections were analyzed using ImageJ for quantification of apoptotic tumor

cells percentage. Quantification of HDLM-2 apoptotic cells by ImageJ analysis on digitally acquired tissue sections stained with TUNEL. At least three sections from different animals were analyzed. Each dot represents the value obtained from the analysis of a single tissue field and the lines indicate the mean values.

Taken together, these data suggest that although perifosine and sorafenib alone exhibit modest anti-HL effects in vitro, they are only marginally effective as monotherapy in vivo. However, combining perifosine with sorafenib results in significant HL tumor growth inhibition in vivo, an observation of potential clinical utility.

5. DISCUSSION

The generally cytoprotective role played by the MEK/ERK1/2 and PI3-K/Akt signaling cascades has focused attention on the use of MEK and PI3-K/Akt inhibitors to enhance the activity of conventional cytotoxic agents.[213] However, it has been shown that simultaneous interruption of two complementary signaling pathways potently induces apoptosis in transformed cells.[214] In this context, concomitant interruption of the MEK/ERK1/2 (i.e., by sorafenib) and PI3-K/Akt (i.e., by perifosine) pathways represents an effective treatment option in Hodgkin lymphoma. The resulting data provide compelling evidence that combining perifosine with sorafenib produces an effective cytotoxic and cytostatic combination, both in vitro and in vivo. We therefore propose that additional exploration of this combination in clinical trials is warranted.

The present findings indicate that coadministration of clinically relevant perifosine and sorafenib results in a striking increase in mitochondrial injury, gene expression changes, apoptosis, and in a marked reduction of the viability, supported by decreased S-phase fraction, in HL responsive cells. These events are associated with multiple perturbations of diverse cell signaling pathways including inactivation of Akt and MEK/ERK1/2, inactivation of Mcl-1, an increase in cytochrome c and apoptosis-inducing factor (AIF) release, and a marked conformational change in Bax accompanied by translocation to the mitochondrial membrane. Such findings are consistent with the results of several recent reports indicating that a variety of agents that perturb signal transduction pathways, including proteasome, HDAC, and RAF/MAPK inhibitors are able to enhance PI3-K/Akt inhibitors-mediated lethality, culminating in marked anti-tumor synergism.[215-217] However, this study identified a putative role for TRIB3, an endogenous inhibitor of Akt, in mediating perifosine- and sorafenib-potentiated apoptosis.

The effects of perifosine/sorafenib combined treatment was evaluated in vitro and in vivo using three well established Hodgkin lymphoma cell lines (HD-MyZ, L-540, HDLM-2). Despite the close resemblance in immunophenotype, these cell lines are not generally accepted as being truly derived from H or RS cells in all instances. Indeed, HD-MyZ cell line differs strikingly from in situ HRS cells as it expresses the macrophage associated CD68 antigen and lacks expression of CD30 and CD15 as well as rearrangement of immunoglobulin or TCR genes.[218] Due to the fact that H or RS cells account only for a minority of cells within the bystander cells in Hodgkin disease (HD) tissue and that many attempts to cultivate H or RS cells failed, one has to bear in mind that these cell lines, which were successfully derived from HD, might only reflect a certain aspect of the disease.

The Akt pathway plays an important anti-apoptotic role; furthermore, disruption of the PI3-K/Akt cascade has been implicated in perifosine-mediated lethality in various tumor cells.[146,219] Consistent with these results, exposure to perifosine inactivated Akt and reduced phosphorylation of some of its downstream targets (eg, S6) in HL cells; however, low expression of Akt significantly diminished perifosine-mediated lethality in HDLM-2 cells. Interestingly, low activation of Akt failed to attenuate sorafenib-mediated lethality despite dramatically reducing apoptosis induced by perifosine or the perifosine/sorafenib regimen in HDLM-2 cells. Such observations are consistent with previous findings demonstrating a connection between perifosine efficacy and PI3-K/Akt

pathway activation.[220] It is tempting to speculate that HL cells, particularly those exhibiting Akt dysregulation, may be addicted to these pathways, thus accounting for their susceptibility to this regimen. However, it is clear that larger cell lines number will be necessary to define the relationship between susceptibility to the perifosine/sorafenib regimen and both the basal signaling status. Furthermore, PI3-K/Akt and MEK/ERK1/2 pathways activation status may allow baseline selection of patients most likely to respond to perifosine and sorafenib alone or in combination with other therapies.

In several recent studies perifosine and sorafenib have been shown to be potent inhibitors of the MAPK-pathway.[221,222] Overall, perifosine in combination with sorafenib significantly affected the MAPK signaling pathway in the HD-MyZ and L-540 sensitive cell lines, whereas the HDLM-2 cell line was substantially unaffected by perifosine/sorafenib treatment. Although coadministration of sorafenib did not abrogate MAPK activation in cells exposed to a low, minimally toxic concentration of perifosine, it did reduce activation to levels well below those observed in cells exposed to perifosine alone, suggesting that diminution in MAPK activation by sorafenib promotes perifosine lethality by blocking a cytoprotective response.

Another controversial point is the mechanism of perifosine and sorafenib-mediated cell death. Studies demonstrating either dependent or independent CD95-mediated apoptotic effects[150,223] have been reported, along with studies describing autophagy[224,225] as well as caspase-dependence[226] or caspase-independence[219,227] of perifosine and sorafenib-mediated cell death. The controversial role of these events in molecular targeted drugs-induced cell death might be due to the use in different studies of different cell models. Perifosine and sorafenib, either alone or in combination, failed to induce any processing of the caspases-3, 8, and 9, as well as PARP, which is typical of caspase-dependent apoptosis, in HL cells. In addition, we did not detect any effect of the pan-caspase inhibitor Z-VADfmk on perifosine/sorafenib-induced cell death suggesting the involvement of caspase-independent pathways. It has been shown that a conformational change in Bax is required for its proapoptotic activity, manifested by the translocation of cytochrome c, Smac/DIABLO, and AIF from the mitochondria to the cytosol.[228] The present studies showed that combined exposure of L-540 cells to perifosine and sorafenib resulted in a marked increase in Bax conformational change, accompanied by extensive translocation of Bax to the mitochondria and conseguent marked cell death. It is also notable that we did not observe induction of apoptosis or activation of cleaved caspase in response to perifosine and sorafenib used as single-agents or in combination in HD-MyZ cell line, suggesting that the mechanism of action of perifosine and sorafenib in HD-MyZ is predominantly cytostatic and not cytotoxic and may be mediated by G2 arrest. It is currently thought that the anti-apoptotic activity of Mcl-1 primarily involves interactions with Bak.[229] In the present study, the anti-apoptotic Bcl-2 family member Mcl-1 downregulation in all likelihood plays an important functional role in synergistic induction of HL cell death by simultaneous interruption of the MEK/ERK1/2 and PI3-K/Akt pathways, in responsive cell lines. Mcl-1 expression is regulated by ERK1/2 at the transcriptional level and at the posttranslational level through direct phosphorylation on threonine 163, which attenuates Mcl-1 degradation.[230] Conversely, GSK-3, a

kinase inactivated by Akt, phosphorylates Mcl-1 on serine 159, an event that promotes Mcl-1 degradation.[231] Consequently, both transcriptional and posttranscriptional mechanisms may be involved in Mcl-1 down-regulation after perifosine/sorafenib exposure.

Perifosine and sorafenib trigger mediators of endoplasmic reticulum (ER) stress-induced apoptosis in HL cells, consistent with previous reports.[216,232] A potential mechanism for increased expression of TRIB3 is ER stress.[233] Further investigation highlighted the importance of TRIB3 in mediating HL cell survival. Significantly greater amounts of TRIB3 were detected in HL cells relative to perifosine/sorafenib exposure both in vitro and in vivo. Consistent with this, downregulation of TRIB3 with siRNA significantly reduced perifosine/sorafenib-induced anti-lymphoma effects, indicating that the activation of the pseudokinase exerts a major role in the mechanism of action of perifosine and sorafenib combined treatment. It has been reported that TRIB3 appears necessary for MAP kinase pathway function and is inhibitory at high levels,[211] in addition TRIB3 binds Akt preventing its phosphorylation and activation.[212] We can speculate that TRIB3, once overexpressed by perifosine/sorafenib treatment, could enhances perifosine and sorafenib single agent-activity by simultaneous interruption of the PI3-K/Akt and MEK/ERK1/2 pathways leading to a pronounced Akt, ERK and Mcl-1 inactivation and a striking increase in mitochondrial dysfunction (Figure 5.1). Together, such findings show that two caspase-independent apoptotic pathways, one from the mitochondrion and one from the endoplasmic reticulum, are coactivated during perifosine/sorafenib treatment and cooperate to trigger Hodgkin lymphoma cell death.

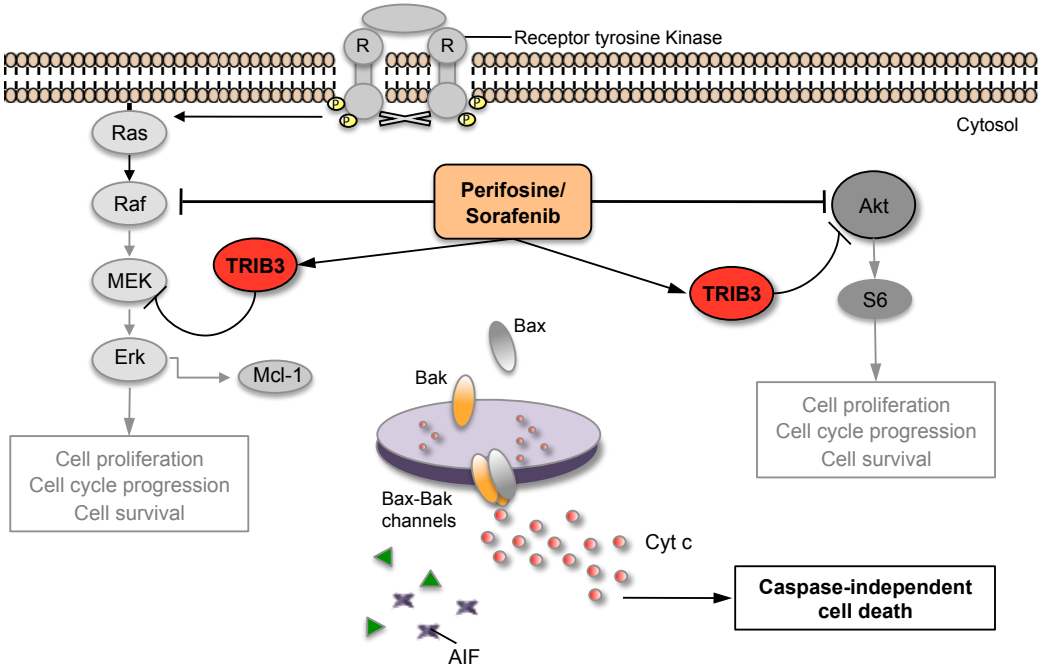

Figure 5.1: Proposed mechanistic model by which dual disruption of PI3-K/Akt and MEK/ERK1/2 pathways induces apoptosis in HL cells. Dual disruption of the MEK/ERK1/2 and PI3-K/Akt pathways results in TRIB3 accumulation, most likely through caspase-idependent cell death. In addition, this treatment also diminishes Akt, ERK and Mcl-1 phosphorilated protein levels, leading to Bax confomational change and activation, mitochondrial outer membrane permeabilization, release of cytochrome c, and AIF.

Based on the promising in vitro data, perifosine/sorafenib combined treatment also showed potent in vivo tumoricidal efficacy. Perifosine and sorafenib showed minimal efficacy in vivo when used as single agents. However, the combination resulted in improved efficacy; survival was significantly prolonged in HD-MyZ tumor-bearing mice, and a substantial percentage remained tumor free at the end of the 200-day observation period. Moreover, perifosine/sorafenib reduced L-540 tumor growth (by 42%), but not HDLM-2 resistent xenograft model. Lymphoma growth inhibition developed slowly and progressively, usually reaching the level of objective regression after three weeks of dosing. While a 5-day treatment with perifosine/sorafenib resulted in early induction of extensive tumor necrosis (2 to 8-fold) only in responsive HD-MyZ and L-540 xenograft models. In vitro perifosine and sorafenib single agents-activity partially correlated with in vivo effects, likely due to a much more complex scenario occurring in xenograft models which essentially involves an active role of microenvironmental cells in modulating tumor cell growth.

HL results in approximately 1,300 deaths per year in the United States.[234] Owing to the limitations of the available therapy, there is an urgent need for new therapeutic options for relapsed HL patients. The signaling pathways that we examined are the two pathways most commonly activated in HL. The drugs that we employed to target these pathways are in active clinical development. The preclinical activity that we observed justifies further investigation and lays groundwork for phase I-II studies combining perifosine and sorafenib in HL.

6. CONCLUSIONS

The proposed project was aimed at investigating in vitro and in vivo the activity and mechanism(s) of action of perifosine in combination with sorafenib by using three HL cell lines (HD-MyZ, L-540, HDLM-2). Despite perifosine and sorafenib used as single agents had modest effects on HL cells, perifosine/sorafenib combination resulted in potent anti-HL activity both in vitro and in vivo.

In 2 of 3 HL cell lines, the combined perfosine/sorafenib treatment induced potent antitumor effects in vitro:

- Synergistic cell growth inhibition and cell death induction in HD-MyZ and L-540 cell lines, but not in HDLM-2 cell line
- Blocking cell cycle
- Down-modulating MAPK and PI3K/Akt pathways
- Caspase-independent apoptosis associated with severe mitochondrial dysfunction
- Modulating genes involved in amino acid metabolism, cell cycle, DNA replication and cell death
- Overexpressing tribbles homologues 3 (TRIB3)

Effects of the combined perifosine/sorafenib treatment in vivo:

- HD-MyZ – Significant increase of survival (45 vs 81 days, as compared to controls)
- HD-MyZ – 25% tumor-free mice at the end of the 200-day observation period
- No significant changes in weight or other signs of potential toxicity during perifosine and/or sorafenib treatments
- L-540 – Reduction of tumor volumes as compared to controls (by 42%), perifosine (by 35%) or sorafenib (by 46%) alone
- HD-MyZ and L-540 but not HDLM-2:
  - Tumor necrosis (2- to 8-fold, $P \leq .0001$)
  - Tumor apoptosis (2- to 2.5-fold, $P \leq .0001$)

Based on these preclinical data, a phase II trial exploring the clinical activity of perifosine/sorafenib in HL is currently ongoing.

BIBLIOGRAPHY

1. Jemal, A., Siegel, R., Xu, J. & Ward, E. Cancer statistics, 2010. *CA Cancer J Clin* **60**, 277-300 (2010).
2. Carbone, P.P., Kaplan, H.S., Musshoff, K., Smithers, D.W. & Tubiana, M. Report of the Committee on Hodgkin's Disease Staging Classification. *Cancer Res* **31**, 1860-1861 (1971).
3. Lister, T.A., *et al.* Report of a committee convened to discuss the evaluation and staging of patients with Hodgkin's disease: Cotswolds meeting. *J Clin Oncol* **7**, 1630-1636 (1989).
4. Josting, A., Wolf, J. & Diehl, V. Hodgkin disease: prognostic factors and treatment strategies. *Curr Opin Oncol* **12**, 403-411 (2000).
5. Pavone, V., Guarini, A. & Liso, V. Early autologous stem cell transplantation in Hodgkin disease in partial remission or in relapse. *Haematologica* **82**, 638-639 (1997).
6. Buglio, D., Georgakis, G. & Younes, A. Novel small-molecule therapy of Hodgkin lymphoma. *Expert Rev Anticancer Ther* **7**, 735-740 (2007).
7. Klimm, B., Schnell, R., Diehl, V. & Engert, A. Current treatment and immunotherapy of Hodgkin's lymphoma. *Haematologica* **90**, 1680-1692 (2005).
8. Pileri, S.A., *et al.* Hodgkin's lymphoma: the pathologist's viewpoint. *J Clin Pathol* **55**, 162-176 (2002).
9. Gruss, H.J. & Kadin, M.E. Pathophysiology of Hodgkin's disease: functional and molecular aspects. *Baillieres Clin Haematol* **9**, 417-446 (1996).
10. Cossman, J., Messineo, C. & Bagg, A. Reed-Sternberg cell: survival in a hostile sea. *Lab Invest* **78**, 229-235 (1998).
11. Skinnider, B.F. & Mak, T.W. The role of cytokines in classical Hodgkin lymphoma. *Blood* **99**, 4283-4297 (2002).
12. Khan, G. Epstein-Barr virus, cytokines, and inflammation: a cocktail for the pathogenesis of Hodgkin's lymphoma? *Exp Hematol* **34**, 399-406 (2006).
13. Teruya-Feldstein, J., Tosato, G. & Jaffe, E.S. The role of chemokines in Hodgkin's disease. *Leuk Lymphoma* **38**, 363-371 (2000).
14. Lukes, R.J. & Butler, J.J. The pathology and nomenclature of Hodgkin's disease. *Cancer Res* **26**, 1063-1083 (1966).
15. Harris, N.L., *et al.* A revised European-American classification of lymphoid neoplasms: a proposal from the International Lymphoma Study Group. *Blood* **84**, 1361-1392 (1994).
16. Harris, N.L., *et al.* The World Health Organization classification of neoplastic diseases of the haematopoietic and lymphoid tissues: Report of the Clinical Advisory Committee Meeting, Airlie House, Virginia, November 1997. *Histopathology* **36**, 69-86 (2000).
17. Nogova, L., Rudiger, T. & Engert, A. Biology, clinical course and management of nodular lymphocyte-predominant hodgkin lymphoma. *Hematology Am Soc Hematol Educ Program*, 266-272 (2006).
18. Schmid, C., Pan, L., Diss, T. & Isaacson, P.G. Expression of B-cell antigens by Hodgkin's and Reed-Sternberg cells. *Am J Pathol* **139**, 701-707 (1991).
19. Anagnostopoulos, I., *et al.* European Task Force on Lymphoma project on lymphocyte predominance Hodgkin disease: histologic and immunohistologic analysis of submitted cases reveals 2 types of Hodgkin disease with a nodular growth pattern and abundant lymphocytes. *Blood* **96**, 1889-1899 (2000).
20. Drexler, H.G. Recent results on the biology of Hodgkin and Reed-Sternberg cells. II. Continuous cell lines. *Leuk Lymphoma* **9**, 1-25 (1993).
21. Drexler, H.G., Dirks, W.G. & MacLeod, R.A. False human hematopoietic cell lines: cross-contaminations and misinterpretations. *Leukemia* **13**, 1601-1607 (1999).
22. Kanzler, H., *et al.* Molecular single cell analysis demonstrates the derivation of a peripheral blood-derived cell line (L1236) from the Hodgkin/Reed-Sternberg cells of a Hodgkin's lymphoma patient. *Blood* **87**, 3429-3436 (1996).
23. Kanzler, H., Kuppers, R., Hansmann, M.L. & Rajewsky, K. Hodgkin and Reed-Sternberg cells in Hodgkin's disease represent the outgrowth of a dominant tumor clone derived from (crippled) germinal center B cells. *J Exp Med* **184**, 1495-1505 (1996).
24. Kuppers, R., *et al.* Hodgkin disease: Hodgkin and Reed-Sternberg cells picked from histological sections show clonal immunoglobulin gene rearrangements and appear to be derived from B cells at various stages of development. *Proc Natl Acad Sci U S A* **91**, 10962-10966 (1994).
25. Marafioti, T., *et al.* Hodgkin and reed-sternberg cells represent an expansion of a single clone originating from a germinal center B-cell with functional immunoglobulin gene rearrangements but defective immunoglobulin transcription. *Blood* **95**, 1443-1450 (2000).
26. Thorbecke, G.J., Amin, A.R. & Tsiagbe, V.K. Biology of germinal centers in lymphoid tissue. *FASEB J* **8**, 832-840 (1994).
27. Muschen, M., *et al.* Rare occurrence of classical Hodgkin's disease as a T cell lymphoma. *J Exp Med* **191**, 387-394 (2000).
28. Seitz, V., *et al.* Detection of clonal T-cell receptor gamma-chain gene rearrangements in Reed-Sternberg cells of classic Hodgkin disease. *Blood* **95**, 3020-3024 (2000).
29. Muschen, M., *et al.* Somatic mutations of the CD95 gene in Hodgkin and Reed-Sternberg cells. *Cancer Res* **60**, 5640-5643 (2000).
30. Kuppers, R. & Hansmann, M.L. The Hodgkin and Reed/Sternberg cell. *Int J Biochem Cell Biol* **37**, 511-517 (2005).

31. Kuppers, R., *et al.* Evidence that Hodgkin and Reed-Sternberg cells in Hodgkin disease do not represent cell fusions. *Blood* **97**, 818-821 (2001).
32. Schwering, I., *et al.* Loss of the B-lineage-specific gene expression program in Hodgkin and Reed-Sternberg cells of Hodgkin lymphoma. *Blood* **101**, 1505-1512 (2003).
33. Adjei, A.A. & Hidalgo, M. Intracellular signal transduction pathway proteins as targets for cancer therapy. *J Clin Oncol* **23**, 5386-5403 (2005).
34. Bargou, R.C., *et al.* High-level nuclear NF-kappa B and Oct-2 is a common feature of cultured Hodgkin/Reed-Sternberg cells. *Blood* **87**, 4340-4347 (1996).
35. Bargou, R.C., *et al.* Constitutive nuclear factor-kappaB-RelA activation is required for proliferation and survival of Hodgkin's disease tumor cells. *J Clin Invest* **100**, 2961-2969 (1997).
36. Hinz, M., *et al.* Constitutive NF-kappaB maintains high expression of a characteristic gene network, including CD40, CD86, and a set of antiapoptotic genes in Hodgkin/Reed-Sternberg cells. *Blood* **97**, 2798-2807 (2001).
37. Joos, S., *et al.* Classical Hodgkin lymphoma is characterized by recurrent copy number gains of the short arm of chromosome 2. *Blood* **99**, 1381-1387 (2002).
38. Martin-Subero, J.I., *et al.* Recurrent involvement of the REL and BCL11A loci in classical Hodgkin lymphoma. *Blood* **99**, 1474-1477 (2002).
39. Horie, R., *et al.* Ligand-independent signaling by overexpressed CD30 drives NF-kappaB activation in Hodgkin-Reed-Sternberg cells. *Oncogene* **21**, 2493-2503 (2002).
40. Annunziata, C.M., Safiran, Y.J., Irving, S.G., Kasid, U.N. & Cossman, J. Hodgkin disease: pharmacologic intervention of the CD40-NF kappa B pathway by a protease inhibitor. *Blood* **96**, 2841-2848 (2000).
41. Fiumara, P., *et al.* Functional expression of receptor activator of nuclear factor kappaB in Hodgkin disease cell lines. *Blood* **98**, 2784-2790 (2001).
42. Jundt, F., *et al.* Activated Notch1 signaling promotes tumor cell proliferation and survival in Hodgkin and anaplastic large cell lymphoma. *Blood* **99**, 3398-3403 (2002).
43. Rodig, S.J., *et al.* TRAF1 expression and c-Rel activation are useful adjuncts in distinguishing classical Hodgkin lymphoma from a subset of morphologically or immunophenotypically similar lymphomas. *Am J Surg Pathol* **29**, 196-203 (2005).
44. Zheng, B., *et al.* MEK/ERK pathway is aberrantly active in Hodgkin disease: a signaling pathway shared by CD30, CD40, and RANK that regulates cell proliferation and survival. *Blood* **102**, 1019-1027 (2003).
45. Nonaka, M., *et al.* Aberrant NF-kappaB2/p52 expression in Hodgkin/Reed-Sternberg cells and CD30-transformed rat fibroblasts. *Oncogene* **24**, 3976-3986 (2005).
46. Nagel, S., *et al.* HLXB9 activates IL6 in Hodgkin lymphoma cell lines and is regulated by PI3K signalling involving E2F3. *Leukemia* **19**, 841-846 (2005).
47. Georgakis, G.V., *et al.* Inhibition of the phosphatidylinositol-3 kinase/Akt promotes G1 cell cycle arrest and apoptosis in Hodgkin lymphoma. *Br J Haematol* **132**, 503-511 (2006).
48. Mathas, S., *et al.* Aberrantly expressed c-Jun and JunB are a hallmark of Hodgkin lymphoma cells, stimulate proliferation and synergize with NF-kappa B. *EMBO J* **21**, 4104-4113 (2002).
49. Radtke, F., Wilson, A., Mancini, S.J. & MacDonald, H.R. Notch regulation of lymphocyte development and function. *Nat Immunol* **5**, 247-253 (2004).
50. Zweidler-McKay, P.A., *et al.* Notch signaling is a potent inducer of growth arrest and apoptosis in a wide range of B-cell malignancies. *Blood* **106**, 3898-3906 (2005).
51. Hinz, M., *et al.* Nuclear factor kappaB-dependent gene expression profiling of Hodgkin's disease tumor cells, pathogenetic significance, and link to constitutive signal transducer and activator of transcription 5a activity. *J Exp Med* **196**, 605-617 (2002).
52. Skinnider, B.F., *et al.* Signal transducer and activator of transcription 6 is frequently activated in Hodgkin and Reed-Sternberg cells of Hodgkin lymphoma. *Blood* **99**, 618-626 (2002).
53. Baus, D. & Pfitzner, E. Specific function of STAT3, SOCS1, and SOCS3 in the regulation of proliferation and survival of classical Hodgkin lymphoma cells. *Int J Cancer* **118**, 1404-1413 (2006).
54. Holtick, U., *et al.* STAT3 is essential for Hodgkin lymphoma cell proliferation and is a target of tyrphostin AG17 which confers sensitization for apoptosis. *Leukemia* **19**, 936-944 (2005).
55. Renne, C., Willenbrock, K., Kuppers, R., Hansmann, M.L. & Brauninger, A. Autocrine- and paracrine-activated receptor tyrosine kinases in classic Hodgkin lymphoma. *Blood* **105**, 4051-4059 (2005).
56. Wymann, M.P. & Pirola, L. Structure and function of phosphoinositide 3-kinases. *Biochim Biophys Acta* **1436**, 127-150 (1998).
57. Marone, R., Cmiljanovic, V., Giese, B. & Wymann, M.P. Targeting phosphoinositide 3-kinase: moving towards therapy. *Biochim Biophys Acta* **1784**, 159-185 (2008).
58. Vanhaesebroeck, B., *et al.* Synthesis and function of 3-phosphorylated inositol lipids. *Annu Rev Biochem* **70**, 535-602 (2001).
59. Cantley, L.C. The phosphoinositide 3-kinase pathway. *Science* **296**, 1655-1657 (2002).
60. Wymann, M.P., Zvelebil, M. & Laffargue, M. Phosphoinositide 3-kinase signalling--which way to target? *Trends Pharmacol Sci* **24**, 366-376 (2003).
61. Falasca, M. & Maffucci, T. Role of class II phosphoinositide 3-kinase in cell signalling. *Biochem Soc Trans* **35**, 211-214 (2007).
62. Domin, J., Gaidarov, I., Smith, M.E., Keen, J.H. & Waterfield, M.D. The class II phosphoinositide 3-kinase PI3K-C2alpha is concentrated in the trans-Golgi network and present in clathrin-coated vesicles. *J Biol Chem* **275**, 11943-11950 (2000).

63. Gaidarov, I., Smith, M.E., Domin, J. & Keen, J.H. The class II phosphoinositide 3-kinase C2alpha is activated by clathrin and regulates clathrin-mediated membrane trafficking. *Mol Cell* **7**, 443-449 (2001).
64. Maffucci, T., *et al.* Class II phosphoinositide 3-kinase defines a novel signaling pathway in cell migration. *J Cell Biol* **169**, 789-799 (2005).
65. Schu, P.V., *et al.* Phosphatidylinositol 3-kinase encoded by yeast VPS34 gene essential for protein sorting. *Science* **260**, 88-91 (1993).
66. Herman, P.K., Stack, J.H. & Emr, S.D. An essential role for a protein and lipid kinase complex in secretory protein sorting. *Trends Cell Biol* **2**, 363-368 (1992).
67. Murray, J.T., Panaretou, C., Stenmark, H., Miaczynska, M. & Backer, J.M. Role of Rab5 in the recruitment of hVps34/p150 to the early endosome. *Traffic* **3**, 416-427 (2002).
68. Kihara, A., Noda, T., Ishihara, N. & Ohsumi, Y. Two distinct Vps34 phosphatidylinositol 3-kinase complexes function in autophagy and carboxypeptidase Y sorting in Saccharomyces cerevisiae. *J Cell Biol* **152**, 519-530 (2001).
69. Kihara, A., Kabeya, Y., Ohsumi, Y. & Yoshimori, T. Beclin-phosphatidylinositol 3-kinase complex functions at the trans-Golgi network. *EMBO Rep* **2**, 330-335 (2001).
70. Qu, X., *et al.* Promotion of tumorigenesis by heterozygous disruption of the beclin 1 autophagy gene. *J Clin Invest* **112**, 1809-1820 (2003).
71. Nobukuni, T., Kozma, S.C. & Thomas, G. hvps34, an ancient player, enters a growing game: mTOR Complex1/S6K1 signaling. *Curr Opin Cell Biol* **19**, 135-141 (2007).
72. Samuels, Y., *et al.* High frequency of mutations of the PIK3CA gene in human cancers. *Science* **304**, 554 (2004).
73. Samuels, Y., *et al.* Mutant PIK3CA promotes cell growth and invasion of human cancer cells. *Cancer Cell* **7**, 561-573 (2005).
74. Philp, A.J., *et al.* The phosphatidylinositol 3'-kinase p85alpha gene is an oncogene in human ovarian and colon tumors. *Cancer Res* **61**, 7426-7429 (2001).
75. Mizoguchi, M., Nutt, C.L., Mohapatra, G. & Louis, D.N. Genetic alterations of phosphoinositide 3-kinase subunit genes in human glioblastomas. *Brain Pathol* **14**, 372-377 (2004).
76. Li, J., *et al.* PTEN, a putative protein tyrosine phosphatase gene mutated in human brain, breast, and prostate cancer. *Science* **275**, 1943-1947 (1997).
77. Hawkins, P.T., Anderson, K.E., Davidson, K. & Stephens, L.R. Signalling through Class I PI3Ks in mammalian cells. *Biochem Soc Trans* **34**, 647-662 (2006).
78. Manning, B.D. & Cantley, L.C. AKT/PKB signaling: navigating downstream. *Cell* **129**, 1261-1274 (2007).
79. Feng, J., Park, J., Cron, P., Hess, D. & Hemmings, B.A. Identification of a PKB/Akt hydrophobic motif Ser-473 kinase as DNA-dependent protein kinase. *J Biol Chem* **279**, 41189-41196 (2004).
80. Hanada, M., Feng, J. & Hemmings, B.A. Structure, regulation and function of PKB/AKT--a major therapeutic target. *Biochim Biophys Acta* **1697**, 3-16 (2004).
81. Brazil, D.P., Park, J. & Hemmings, B.A. PKB binding proteins. Getting in on the Akt. *Cell* **111**, 293-303 (2002).
82. Rohrschneider, L.R., Fuller, J.F., Wolf, I., Liu, Y. & Lucas, D.M. Structure, function, and biology of SHIP proteins. *Genes Dev* **14**, 505-520 (2000).
83. Kalesnikoff, J., *et al.* The role of SHIP in cytokine-induced signaling. *Rev Physiol Biochem Pharmacol* **149**, 87-103 (2003).
84. Stambolic, V., *et al.* Negative regulation of PKB/Akt-dependent cell survival by the tumor suppressor PTEN. *Cell* **95**, 29-39 (1998).
85. Cully, M., You, H., Levine, A.J. & Mak, T.W. Beyond PTEN mutations: the PI3K pathway as an integrator of multiple inputs during tumorigenesis. *Nat Rev Cancer* **6**, 184-192 (2006).
86. Vivanco, I. & Sawyers, C.L. The phosphatidylinositol 3-Kinase AKT pathway in human cancer. *Nat Rev Cancer* **2**, 489-501 (2002).
87. Liang, J. & Slingerland, J.M. Multiple roles of the PI3K/PKB (Akt) pathway in cell cycle progression. *Cell Cycle* **2**, 339-345 (2003).
88. Blume-Jensen, P. & Hunter, T. Oncogenic kinase signalling. *Nature* **411**, 355-365 (2001).
89. Blagosklonny, M.V. & Pardee, A.B. The restriction point of the cell cycle. *Cell Cycle* **1**, 103-110 (2002).
90. Alt, J.R., Cleveland, J.L., Hannink, M. & Diehl, J.A. Phosphorylation-dependent regulation of cyclin D1 nuclear export and cyclin D1-dependent cellular transformation. *Genes Dev* **14**, 3102-3114 (2000).
91. Diehl, J.A., Cheng, M., Roussel, M.F. & Sherr, C.J. Glycogen synthase kinase-3beta regulates cyclin D1 proteolysis and subcellular localization. *Genes Dev* **12**, 3499-3511 (1998).
92. Medema, R.H., Kops, G.J., Bos, J.L. & Burgering, B.M. AFX-like Forkhead transcription factors mediate cell-cycle regulation by Ras and PKB through p27kip1. *Nature* **404**, 782-787 (2000).
93. Liang, J., *et al.* PKB/Akt phosphorylates p27, impairs nuclear import of p27 and opposes p27-mediated G1 arrest. *Nat Med* **8**, 1153-1160 (2002).
94. Narita, Y., *et al.* Mutant epidermal growth factor receptor signaling down-regulates p27 through activation of the phosphatidylinositol 3-kinase/Akt pathway in glioblastomas. *Cancer Res* **62**, 6764-6769 (2002).
95. Mamillapalli, R., *et al.* PTEN regulates the ubiquitin-dependent degradation of the CDK inhibitor p27(KIP1) through the ubiquitin E3 ligase SCF(SKP2). *Curr Biol* **11**, 263-267 (2001).
96. Pene, F., *et al.* Role of the phosphatidylinositol 3-kinase/Akt and mTOR/P70S6-kinase pathways in the proliferation and apoptosis in multiple myeloma. *Oncogene* **21**, 6587-6597 (2002).

97. Li, Y., Dowbenko, D. & Lasky, L.A. AKT/PKB phosphorylation of p21Cip/WAF1 enhances protein stability of p21Cip/WAF1 and promotes cell survival. *J Biol Chem* **277**, 11352-11361 (2002).
98. Zhou, B.P., *et al.* Cytoplasmic localization of p21Cip1/WAF1 by Akt-induced phosphorylation in HER-2/neu-overexpressing cells. *Nat Cell Biol* **3**, 245-252 (2001).
99. Shin, I., *et al.* PKB/Akt mediates cell-cycle progression by phosphorylation of p27(Kip1) at threonine 157 and modulation of its cellular localization. *Nat Med* **8**, 1145-1152 (2002).
100. Levine, A.J. p53, the cellular gatekeeper for growth and division. *Cell* **88**, 323-331 (1997).
101. Mayo, L.D. & Donner, D.B. The PTEN, Mdm2, p53 tumor suppressor-oncoprotein network. *Trends Biochem Sci* **27**, 462-467 (2002).
102. Zhou, B.P., *et al.* HER-2/neu induces p53 ubiquitination via Akt-mediated MDM2 phosphorylation. *Nat Cell Biol* **3**, 973-982 (2001).
103. Cardone, M.H., *et al.* Regulation of cell death protease caspase-9 by phosphorylation. *Science* **282**, 1318-1321 (1998).
104. Datta, S.R., *et al.* Akt phosphorylation of BAD couples survival signals to the cell-intrinsic death machinery. *Cell* **91**, 231-241 (1997).
105. Ozes, O.N., *et al.* NF-kappaB activation by tumour necrosis factor requires the Akt serine-threonine kinase. *Nature* **401**, 82-85 (1999).
106. Schmelzle, T. & Hall, M.N. TOR, a central controller of cell growth. *Cell* **103**, 253-262 (2000).
107. Wendel, H.G., *et al.* Survival signalling by Akt and eIF4E in oncogenesis and cancer therapy. *Nature* **428**, 332-337 (2004).
108. Inoki, K., Li, Y., Zhu, T., Wu, J. & Guan, K.L. TSC2 is phosphorylated and inhibited by Akt and suppresses mTOR signalling. *Nat Cell Biol* **4**, 648-657 (2002).
109. Manning, B.D., Tee, A.R., Logsdon, M.N., Blenis, J. & Cantley, L.C. Identification of the tuberous sclerosis complex-2 tumor suppressor gene product tuberin as a target of the phosphoinositide 3-kinase/akt pathway. *Mol Cell* **10**, 151-162 (2002).
110. Potter, C.J., Pedraza, L.G. & Xu, T. Akt regulates growth by directly phosphorylating Tsc2. *Nat Cell Biol* **4**, 658-665 (2002).
111. Bjornsti, M.A. & Houghton, P.J. The TOR pathway: a target for cancer therapy. *Nat Rev Cancer* **4**, 335-348 (2004).
112. Sarbassov, D.D., Guertin, D.A., Ali, S.M. & Sabatini, D.M. Phosphorylation and regulation of Akt/PKB by the rictor-mTOR complex. *Science* **307**, 1098-1101 (2005).
113. Gerber, H.P., *et al.* Vascular endothelial growth factor regulates endothelial cell survival through the phosphatidylinositol 3'-kinase/Akt signal transduction pathway. Requirement for Flk-1/KDR activation. *J Biol Chem* **273**, 30336-30343 (1998).
114. Dimmeler, S., Dernbach, E. & Zeiher, A.M. Phosphorylation of the endothelial nitric oxide synthase at ser-1177 is required for VEGF-induced endothelial cell migration. *FEBS Lett* **477**, 258-262 (2000).
115. Jiang, B.H., Zheng, J.Z., Aoki, M. & Vogt, P.K. Phosphatidylinositol 3-kinase signaling mediates angiogenesis and expression of vascular endothelial growth factor in endothelial cells. *Proc Natl Acad Sci U S A* **97**, 1749-1753 (2000).
116. Forsythe, J.A., *et al.* Activation of vascular endothelial growth factor gene transcription by hypoxia-inducible factor 1. *Mol Cell Biol* **16**, 4604-4613 (1996).
117. Skinner, H.D., Zheng, J.Z., Fang, J., Agani, F. & Jiang, B.H. Vascular endothelial growth factor transcriptional activation is mediated by hypoxia-inducible factor 1alpha, HDM2, and p70S6K1 in response to phosphatidylinositol 3-kinase/AKT signaling. *J Biol Chem* **279**, 45643-45651 (2004).
118. Gort, E.H., *et al.* Hypoxia-inducible factor-1alpha expression requires PI 3-kinase activity and correlates with Akt1 phosphorylation in invasive breast carcinomas. *Oncogene* **25**, 6123-6127 (2006).
119. Li, Y.M., *et al.* A hypoxia-independent hypoxia-inducible factor-1 activation pathway induced by phosphatidylinositol-3 kinase/Akt in HER2 overexpressing cells. *Cancer Res* **65**, 3257-3263 (2005).
120. Altomare, D.A. & Testa, J.R. Perturbations of the AKT signaling pathway in human cancer. *Oncogene* **24**, 7455-7464 (2005).
121. Shayesteh, L., *et al.* PIK3CA is implicated as an oncogene in ovarian cancer. *Nat Genet* **21**, 99-102 (1999).
122. Byun, D.S., *et al.* Frequent monoallelic deletion of PTEN and its reciprocal associatioin with PIK3CA amplification in gastric carcinoma. *Int J Cancer* **104**, 318-327 (2003).
123. Pedrero, J.M., *et al.* Frequent genetic and biochemical alterations of the PI 3-K/AKT/PTEN pathway in head and neck squamous cell carcinoma. *Int J Cancer* **114**, 242-248 (2005).
124. Bertelsen, B.I., Steine, S.J., Sandvei, R., Molven, A. & Laerum, O.D. Molecular analysis of the PI3K-AKT pathway in uterine cervical neoplasia: frequent PIK3CA amplification and AKT phosphorylation. *Int J Cancer* **118**, 1877-1883 (2006).
125. Bachman, K.E., *et al.* The PIK3CA gene is mutated with high frequency in human breast cancers. *Cancer Biol Ther* **3**, 772-775 (2004).
126. Jucker, M., *et al.* Expression of a mutated form of the p85alpha regulatory subunit of phosphatidylinositol 3-kinase in a Hodgkin's lymphoma-derived cell line (CO). *Leukemia* **16**, 894-901 (2002).
127. Hennessy, B.T., Smith, D.L., Ram, P.T., Lu, Y. & Mills, G.B. Exploiting the PI3K/AKT pathway for cancer drug discovery. *Nat Rev Drug Discov* **4**, 988-1004 (2005).
128. Shoman, N., *et al.* Reduced PTEN expression predicts relapse in patients with breast carcinoma treated by tamoxifen. *Mod Pathol* **18**, 250-259 (2005).
129. Oki, E., *et al.* Akt phosphorylation associates with LOH of PTEN and leads to chemoresistance for gastric cancer. *Int J Cancer* **117**, 376-380 (2005).

130. Tokunaga, E., *et al.* Coexistence of the loss of heterozygosity at the PTEN locus and HER2 overexpression enhances the Akt activity thus leading to a negative progesterone receptor expression in breast carcinoma. *Breast Cancer Res Treat* **101**, 249-257 (2007).
131. Nakayama, K., *et al.* Sequence mutations and amplification of PIK3CA and AKT2 genes in purified ovarian serous neoplasms. *Cancer Biol Ther* **5**, 779-785 (2006).
132. Ruggeri, B.A., Huang, L., Wood, M., Cheng, J.Q. & Testa, J.R. Amplification and overexpression of the AKT2 oncogene in a subset of human pancreatic ductal adenocarcinomas. *Mol Carcinog* **21**, 81-86 (1998).
133. Knobbe, C.B. & Reifenberger, G. Genetic alterations and aberrant expression of genes related to the phosphatidyl-inositol-3'-kinase/protein kinase B (Akt) signal transduction pathway in glioblastomas. *Brain Pathol* **13**, 507-518 (2003).
134. Stal, O., *et al.* Akt kinases in breast cancer and the results of adjuvant therapy. *Breast Cancer Res* **5**, R37-44 (2003).
135. Roy, H.K., *et al.* AKT proto-oncogene overexpression is an early event during sporadic colon carcinogenesis. *Carcinogenesis* **23**, 201-205 (2002).
136. West, K.A., Castillo, S.S. & Dennis, P.A. Activation of the PI3K/Akt pathway and chemotherapeutic resistance. *Drug Resist Updat* **5**, 234-248 (2002).
137. Asselin, E., Mills, G.B. & Tsang, B.K. XIAP regulates Akt activity and caspase-3-dependent cleavage during cisplatin-induced apoptosis in human ovarian epithelial cancer cells. *Cancer Res* **61**, 1862-1868 (2001).
138. Hayakawa, J., *et al.* Regulation of the PRL promoter by Akt through cAMP response element binding protein. *Endocrinology* **143**, 13-22 (2002).
139. Jiang, B.H. & Liu, L.Z. Role of mTOR in anticancer drug resistance: perspectives for improved drug treatment. *Drug Resist Updat* **11**, 63-76 (2008).
140. Wolpin, B.M., *et al.* Oral mTOR inhibitor everolimus in patients with gemcitabine-refractory metastatic pancreatic cancer. *J Clin Oncol* **27**, 193-198 (2009).
141. Ghayad, S.E., *et al.* mTOR inhibition reverses acquired endocrine therapy resistance of breast cancer cells at the cell proliferation and gene-expression levels. *Cancer Sci* **99**, 1992-2003 (2008).
142. LoPiccolo, J., Granville, C.A., Gills, J.J. & Dennis, P.A. Targeting Akt in cancer therapy. *Anticancer Drugs* **18**, 861-874 (2007).
143. Crul, M., *et al.* Phase I and pharmacological study of daily oral administration of perifosine (D-21266) in patients with advanced solid tumours. *Eur J Cancer* **38**, 1615-1621 (2002).
144. Kondapaka, S.B., Singh, S.S., Dasmahapatra, G.P., Sausville, E.A. & Roy, K.K. Perifosine, a novel alkylphospholipid, inhibits protein kinase B activation. *Mol Cancer Ther* **2**, 1093-1103 (2003).
145. Nyakern, M., Cappellini, A., Mantovani, I. & Martelli, A.M. Synergistic induction of apoptosis in human leukemia T cells by the Akt inhibitor perifosine and etoposide through activation of intrinsic and Fas-mediated extrinsic cell death pathways. *Mol Cancer Ther* **5**, 1559-1570 (2006).
146. Hideshima, T., *et al.* Perifosine, an oral bioactive novel alkylphospholipid, inhibits Akt and induces in vitro and in vivo cytotoxicity in human multiple myeloma cells. *Blood* **107**, 4053-4062 (2006).
147. Momota, H., Nerio, E. & Holland, E.C. Perifosine inhibits multiple signaling pathways in glial progenitors and cooperates with temozolomide to arrest cell proliferation in gliomas in vivo. *Cancer Res* **65**, 7429-7435 (2005).
148. Caron, R.W., *et al.* Activated forms of H-RAS and K-RAS differentially regulate membrane association of PI3K, PDK-1, and AKT and the effect of therapeutic kinase inhibitors on cell survival. *Mol Cancer Ther* **4**, 257-270 (2005).
149. Ruiter, G.A., Zerp, S.F., Bartelink, H., van Blitterswijk, W.J. & Verheij, M. Alkyl-lysophospholipids activate the SAPK/JNK pathway and enhance radiation-induced apoptosis. *Cancer Res* **59**, 2457-2463 (1999).
150. Gills, J.J. & Dennis, P.A. Perifosine: update on a novel Akt inhibitor. *Curr Oncol Rep* **11**, 102-110 (2009).
151. Jakubowiak, A., *et al.* A multiple myeloma research consortium (MMRC) Multicenter phase I trial of perifosine (KRX-0401) in combination with lenalidomide and dexamethasone in patients with Relapsed/Refractory multiple myeloma (MM): Updated results. *Blood* **110**, 354A-354A (2007).
152. Vink, S.R., *et al.* Phase I and pharmacokinetic study of combined treatment with perifosine and radiation in patients with advanced solid tumours. *Radiother Oncol* **80**, 207-213 (2006).
153. Breslin, E.M., White, P.C., Shore, A.M., Clement, M. & Brennan, P. LY294002 and rapamycin co-operate to inhibit T-cell proliferation. *Br J Pharmacol* **144**, 791-800 (2005).
154. Sun, S.Y., *et al.* Activation of Akt and eIF4E survival pathways by rapamycin-mediated mammalian target of rapamycin inhibition. *Cancer Res* **65**, 7052-7058 (2005).
155. Takeuchi, H., *et al.* Synergistic augmentation of rapamycin-induced autophagy in malignant glioma cells by phosphatidylinositol 3-kinase/protein kinase B inhibitors. *Cancer Res* **65**, 3336-3346 (2005).
156. Fan, Q.W., *et al.* A dual PI3 kinase/mTOR inhibitor reveals emergent efficacy in glioma. *Cancer Cell* **9**, 341-349 (2006).
157. Tortora, G., *et al.* Overcoming resistance to molecularly targeted anticancer therapies: Rational drug combinations based on EGFR and MAPK inhibition for solid tumours and haematologic malignancies. *Drug Resist Updat* **10**, 81-100 (2007).
158. She, Q.B., *et al.* The BAD protein integrates survival signaling by EGFR/MAPK and PI3K/Akt kinase pathways in PTEN-deficient tumor cells. *Cancer Cell* **8**, 287-297 (2005).
159. Landis-Piwowar, K.R., *et al.* The proteasome as a potential target for novel anticancer drugs and chemosensitizers. *Drug Resist Updat* **9**, 263-273 (2006).

160. Hanahan, D. & Weinberg, R.A. The hallmarks of cancer. *Cell* **100**, 57-70 (2000).
161. Johnson, G.L. & Lapadat, R. Mitogen-activated protein kinase pathways mediated by ERK, JNK, and p38 protein kinases. *Science* **298**, 1911-1912 (2002).
162. Raman, M., Chen, W. & Cobb, M.H. Differential regulation and properties of MAPKs. *Oncogene* **26**, 3100-3112 (2007).
163. Yoon, S. & Seger, R. The extracellular signal-regulated kinase: multiple substrates regulate diverse cellular functions. *Growth Factors* **24**, 21-44 (2006).
164. Meloche, S. & Pouyssegur, J. The ERK1/2 mitogen-activated protein kinase pathway as a master regulator of the G1- to S-phase transition. *Oncogene* **26**, 3227-3239 (2007).
165. Meloche, S., Pages, G. & Pouyssegur, J. Functional expression and growth factor activation of an epitope-tagged p44 mitogen-activated protein kinase, p44mapk. *Mol Biol Cell* **3**, 63-71 (1992).
166. Liu, X., Yan, S., Zhou, T., Terada, Y. & Erikson, R.L. The MAP kinase pathway is required for entry into mitosis and cell survival. *Oncogene* **23**, 763-776 (2004).
167. Lefloch, R., Pouyssegur, J. & Lenormand, P. Single and combined silencing of ERK1 and ERK2 reveals their positive contribution to growth signaling depending on their expression levels. *Mol Cell Biol* **28**, 511-527 (2008).
168. Sebolt-Leopold, J.S., *et al.* Blockade of the MAP kinase pathway suppresses growth of colon tumors in vivo. *Nat Med* **5**, 810-816 (1999).
169. Brunet, A., Pages, G. & Pouyssegur, J. Constitutively active mutants of MAP kinase kinase (MEK1) induce growth factor-relaxation and oncogenicity when expressed in fibroblasts. *Oncogene* **9**, 3379-3387 (1994).
170. Roovers, K. & Assoian, R.K. Integrating the MAP kinase signal into the G1 phase cell cycle machinery. *Bioessays* **22**, 818-826 (2000).
171. Lavoie, J.N., L'Allemain, G., Brunet, A., Muller, R. & Pouyssegur, J. Cyclin D1 expression is regulated positively by the p42/p44MAPK and negatively by the p38/HOGMAPK pathway. *J Biol Chem* **271**, 20608-20616 (1996).
172. Sears, R., *et al.* Multiple Ras-dependent phosphorylation pathways regulate Myc protein stability. *Genes Dev* **14**, 2501-2514 (2000).
173. Yamamoto, T., *et al.* Continuous ERK activation downregulates antiproliferative genes throughout G1 phase to allow cell-cycle progression. *Curr Biol* **16**, 1171-1182 (2006).
174. Yang, J.Y., *et al.* ERK promotes tumorigenesis by inhibiting FOXO3a via MDM2-mediated degradation. *Nat Cell Biol* **10**, 138-148 (2008).
175. Hwang, C.Y., Lee, C. & Kwon, K.S. Extracellular signal-regulated kinase 2-dependent phosphorylation induces cytoplasmic localization and degradation of p21Cip1. *Mol Cell Biol* **29**, 3379-3389 (2009).
176. Chambard, J.C., Lefloch, R., Pouyssegur, J. & Lenormand, P. ERK implication in cell cycle regulation. *Biochim Biophys Acta* **1773**, 1299-1310 (2007).
177. Roux, P.P., Ballif, B.A., Anjum, R., Gygi, S.P. & Blenis, J. Tumor-promoting phorbol esters and activated Ras inactivate the tuberous sclerosis tumor suppressor complex via p90 ribosomal S6 kinase. *Proc Natl Acad Sci U S A* **101**, 13489-13494 (2004).
178. Ballif, B.A. & Blenis, J. Molecular mechanisms mediating mammalian mitogen-activated protein kinase (MAPK) kinase (MEK)-MAPK cell survival signals. *Cell Growth Differ* **12**, 397-408 (2001).
179. Balmanno, K. & Cook, S.J. Tumour cell survival signalling by the ERK1/2 pathway. *Cell Death Differ* **16**, 368-377 (2009).
180. Xia, Z., Dickens, M., Raingeaud, J., Davis, R.J. & Greenberg, M.E. Opposing effects of ERK and JNK-p38 MAP kinases on apoptosis. *Science* **270**, 1326-1331 (1995).
181. Erhardt, P., Schremser, E.J. & Cooper, G.M. B-Raf inhibits programmed cell death downstream of cytochrome c release from mitochondria by activating the MEK/Erk pathway. *Mol Cell Biol* **19**, 5308-5315 (1999).
182. Scholl, F.A., *et al.* Mek1/2 MAPK kinases are essential for Mammalian development, homeostasis, and Raf-induced hyperplasia. *Dev Cell* **12**, 615-629 (2007).
183. Grandis, J.R. & Sok, J.C. Signaling through the epidermal growth factor receptor during the development of malignancy. *Pharmacol Ther* **102**, 37-46 (2004).
184. Schubbert, S., Shannon, K. & Bollag, G. Hyperactive Ras in developmental disorders and cancer. *Nat Rev Cancer* **7**, 295-308 (2007).
185. Davies, H., *et al.* Mutations of the BRAF gene in human cancer. *Nature* **417**, 949-954 (2002).
186. Garnett, M.J. & Marais, R. Guilty as charged: B-RAF is a human oncogene. *Cancer Cell* **6**, 313-319 (2004).
187. Marks, J.L., *et al.* Novel MEK1 mutation identified by mutational analysis of epidermal growth factor receptor signaling pathway genes in lung adenocarcinoma. *Cancer Res* **68**, 5524-5528 (2008).
188. Murugan, A.K., Dong, J., Xie, J. & Xing, M. MEK1 mutations, but not ERK2 mutations, occur in melanomas and colon carcinomas, but none in thyroid carcinomas. *Cell Cycle* **8**, 2122-2124 (2009).
189. Hoshino, R., *et al.* Constitutive activation of the 41-/43-kDa mitogen-activated protein kinase signaling pathway in human tumors. *Oncogene* **18**, 813-822 (1999).
190. Sebolt-Leopold, J.S. & Herrera, R. Targeting the mitogen-activated protein kinase cascade to treat cancer. *Nat Rev Cancer* **4**, 937-947 (2004).
191. Milella, M., *et al.* Therapeutic targeting of the MEK/MAPK signal transduction module in acute myeloid leukemia. *J Clin Invest* **108**, 851-859 (2001).
192. Collisson, E.A., De, A., Suzuki, H., Gambhir, S.S. & Kolodney, M.S. Treatment of metastatic melanoma with an orally available inhibitor of the Ras-Raf-MAPK cascade. *Cancer Res* **63**, 5669-5673 (2003).

193. Maloney, A. & Workman, P. HSP90 as a new therapeutic target for cancer therapy: the story unfolds. *Expert Opin Biol Ther* **2**, 3-24 (2002).
194. Shelton, J.G., *et al.* Differential effects of kinase cascade inhibitors on neoplastic and cytokine-mediated cell proliferation. *Leukemia* **17**, 1765-1782 (2003).
195. Lackey, K., *et al.* The discovery of potent cRaf1 kinase inhibitors. *Bioorg Med Chem Lett* **10**, 223-226 (2000).
196. Smith, R.A., Dumas, J., Adnane, L. & Wilhelm, S.M. Recent advances in the research and development of RAF kinase inhibitors. *Curr Top Med Chem* **6**, 1071-1089 (2006).
197. Lyons, J.F., Wilhelm, S., Hibner, B. & Bollag, G. Discovery of a novel Raf kinase inhibitor. *Endocr Relat Cancer* **8**, 219-225 (2001).
198. Wan, P.T., *et al.* Mechanism of activation of the RAF-ERK signaling pathway by oncogenic mutations of B-RAF. *Cell* **116**, 855-867 (2004).
199. Wilhelm, S.M., *et al.* BAY 43-9006 exhibits broad spectrum oral antitumor activity and targets the RAF/MEK/ERK pathway and receptor tyrosine kinases involved in tumor progression and angiogenesis. *Cancer Res* **64**, 7099-7109 (2004).
200. Awada, A., *et al.* Phase I safety and pharmacokinetics of BAY 43-9006 administered for 21 days on/7 days off in patients with advanced, refractory solid tumours. *Br J Cancer* **92**, 1855-1861 (2005).
201. Hahn, O. & Stadler, W. Sorafenib. *Curr Opin Oncol* **18**, 615-621 (2006).
202. Eisen, T., *et al.* Sorafenib in advanced melanoma: a Phase II randomised discontinuation trial analysis. *Br J Cancer* **95**, 581-586 (2006).
203. Sebolt-Leopold, J.S. & English, J.M. Mechanisms of drug inhibition of signalling molecules. *Nature* **441**, 457-462 (2006).
204. O'Reilly, C.M., Fogarty, K.E., Drummond, R.M., Tuft, R.A. & Walsh, J.V., Jr. Quantitative analysis of spontaneous mitochondrial depolarizations. *Biophys J* **85**, 3350-3357 (2003).
205. Scaduto, R.C., Jr. & Grotyohann, L.W. Measurement of mitochondrial membrane potential using fluorescent rhodamine derivatives. *Biophys J* **76**, 469-477 (1999).
206. Strumberg, D., *et al.* Phase I clinical and pharmacokinetic study of the Novel Raf kinase and vascular endothelial growth factor receptor inhibitor BAY 43-9006 in patients with advanced refractory solid tumors. *J Clin Oncol* **23**, 965-972 (2005).
207. Yu, C., *et al.* The role of Mcl-1 downregulation in the proapoptotic activity of the multikinase inhibitor BAY 43-9006. *Oncogene* **24**, 6861-6869 (2005).
208. Schmidt-Hieber, M., *et al.* In vitro cytotoxicity of the novel antimyeloma agents perifosine, bortezomib and lenalidomide against different cell lines. *Invest New Drugs* (2010).
209. Panka, D.J., Wang, W., Atkins, M.B. & Mier, J.W. The Raf inhibitor BAY 43-9006 (Sorafenib) induces caspase-independent apoptosis in melanoma cells. *Cancer Res* **66**, 1611-1619 (2006).
210. Wolter, K.G., *et al.* Movement of Bax from the cytosol to mitochondria during apoptosis. *J Cell Biol* **139**, 1281-1292 (1997).
211. Kiss-Toth, E., *et al.* Human tribbles, a protein family controlling mitogen-activated protein kinase cascades. *J Biol Chem* **279**, 42703-42708 (2004).
212. Du, K., Herzig, S., Kulkarni, R.N. & Montminy, M. TRB3: a tribbles homolog that inhibits Akt/PKB activation by insulin in liver. *Science* **300**, 1574-1577 (2003).
213. Teachey, D.T., Grupp, S.A. & Brown, V.I. Mammalian target of rapamycin inhibitors and their potential role in therapy in leukaemia and other haematological malignancies. *Br J Haematol* **145**, 569-580 (2009).
214. Stommel, J.M., *et al.* Coactivation of receptor tyrosine kinases affects the response of tumor cells to targeted therapies. *Science* **318**, 287-290 (2007).
215. Leleu, X., *et al.* Targeting NF-kappaB in Waldenstrom macroglobulinemia. *Blood* **111**, 5068-5077 (2008).
216. Rahmani, M., *et al.* Coadministration of histone deacetylase inhibitors and perifosine synergistically induces apoptosis in human leukemia cells through Akt and ERK1/2 inactivation and the generation of ceramide and reactive oxygen species. *Cancer Res* **65**, 2422-2432 (2005).
217. Hoeflich, K.P., *et al.* In vivo antitumor activity of MEK and phosphatidylinositol 3-kinase inhibitors in basal-like breast cancer models. *Clin Cancer Res* **15**, 4649-4664 (2009).
218. Bargou, R.C., *et al.* Characterization of a novel Hodgkin cell line, HD-MyZ, with myelomonocytic features mimicking Hodgkin's disease in severe combined immunodeficient mice. *J Exp Med* **177**, 1257-1268 (1993).
219. Floryk, D. & Thompson, T.C. Perifosine induces differentiation and cell death in prostate cancer cells. *Cancer Lett* **266**, 216-226 (2008).
220. Hennessy, B.T., *et al.* Pharmacodynamic markers of perifosine efficacy. *Clin Cancer Res* **13**, 7421-7431 (2007).
221. Vink, S.R., van Blitterswijk, W.J., Schellens, J.H. & Verheij, M. Rationale and clinical application of alkylphospholipid analogues in combination with radiotherapy. *Cancer Treat Rev* **33**, 191-202 (2007).
222. Nguyen, T.K., *et al.* Inhibition of MEK/ERK1/2 sensitizes lymphoma cells to sorafenib-induced apoptosis. *Leuk Res* **34**, 379-386 (2010).
223. Walker, T., *et al.* Sorafenib and vorinostat kill colon cancer cells by CD95-dependent and -independent mechanisms. *Mol Pharmacol* **76**, 342-355 (2009).
224. Fu, L., *et al.* Perifosine inhibits mammalian target of rapamycin signaling through facilitating degradation of major components in the mTOR axis and induces autophagy. *Cancer Res* **69**, 8967-8976 (2009).

225. Bareford, M.D., *et al.* Sorafenib enhances pemetrexed cytotoxicity through an autophagy-dependent mechanism in cancer cells. *Cancer Res* **71**, 4955-4967 (2011).
226. Chiarini, F., *et al.* The novel Akt inhibitor, perifosine, induces caspase-dependent apoptosis and downregulates P-glycoprotein expression in multidrug-resistant human T-acute leukemia cells by a JNK-dependent mechanism. *Leukemia* **22**, 1106-1116 (2008).
227. Liu, L., *et al.* Sorafenib blocks the RAF/MEK/ERK pathway, inhibits tumor angiogenesis, and induces tumor cell apoptosis in hepatocellular carcinoma model PLC/PRF/5. *Cancer Res* **66**, 11851-11858 (2006).
228. Kroemer, G., Galluzzi, L. & Brenner, C. Mitochondrial membrane permeabilization in cell death. *Physiol Rev* **87**, 99-163 (2007).
229. Zhuang, J. & Brady, H.J. Emerging role of Mcl-1 in actively counteracting BH3-only proteins in apoptosis. *Cell Death Differ* **13**, 1263-1267 (2006).
230. Domina, A.M., Vrana, J.A., Gregory, M.A., Hann, S.R. & Craig, R.W. MCL1 is phosphorylated in the PEST region and stabilized upon ERK activation in viable cells, and at additional sites with cytotoxic okadaic acid or taxol. *Oncogene* **23**, 5301-5315 (2004).
231. Maurer, U., Charvet, C., Wagman, A.S., Dejardin, E. & Green, D.R. Glycogen synthase kinase-3 regulates mitochondrial outer membrane permeabilization and apoptosis by destabilization of MCL-1. *Mol Cell* **21**, 749-760 (2006).
232. Rahmani, M., *et al.* The kinase inhibitor sorafenib induces cell death through a process involving induction of endoplasmic reticulum stress. *Mol Cell Biol* **27**, 5499-5513 (2007).
233. Ohoka, N., Yoshii, S., Hattori, T., Onozaki, K. & Hayashi, H. TRB3, a novel ER stress-inducible gene, is induced via ATF4-CHOP pathway and is involved in cell death. *EMBO J* **24**, 1243-1255 (2005).
234. Siegel, R., Ward, E., Brawley, O. & Jemal, A. Cancer statistics, 2011: the impact of eliminating socioeconomic and racial disparities on premature cancer deaths. *CA Cancer J Clin* **61**, 212-236 (2011).

SUPPLEMENTARY TABLES

ACKNOWLEDGEMENTS

First of all I would like to express my sincere gratitude to Professor Carmelo Carlo-Stella who has been my supervisor since the beginning of my study. He provided me with many helpful suggestions, important advice and constant encouragement during the course of this work.

I also wish to express my appreciation to Professor Alessandro M. Gianni for allowing me the opportunity to undertake this degree.

Special thanks are due to Dr. Andrea Anichini for taking intense interest in this study as well as providing valuable suggestions that improved the quality of this study.

Sincere thanks are extended to Loredana Cleris and Dr. Michele Magni, for devoting their precious time and made many valuable suggestions which indeed helped improve of this thesis.

The completion of this investigation would not have been possible without the assistance of my colleagues. I would particularly like to thank Dr. Paolo Longoni, Dr. Arianna Giacomini, Dr. Roberta Zappasodi, and Marco Milanesi for their invaluable support.

On a special note I would like to thank my colleagues Drs. Alessandra Cavanè and Giusi Ruggiero for helping me get through the difficult times, and for all the emotional support, comaraderie, entertainment, and caring they provided.

My special appreciation goes to my parents, who always kept me away from family responsibilities and encouraged me to concentrate on my study.

I would like to express special thanks to Francesco. He helped me to concentrate on completing this dissertation and supported mentally during the course of this work. He has provided encouragement, support, sustenance and laughter.

Finally, I would like to thank everybody who was important to the successful realization of this thesis, as well as expressing my apology that I could not mention personally one by one.